

Statistical Methods for Image Reconstruction

Jeffrey A. Fessler

EECS Department
The University of Michigan

Johns Hopkins University: “Short” Course

May 11, 2007

Image Reconstruction Methods

(Simplified View)

Analytical

(FBP)

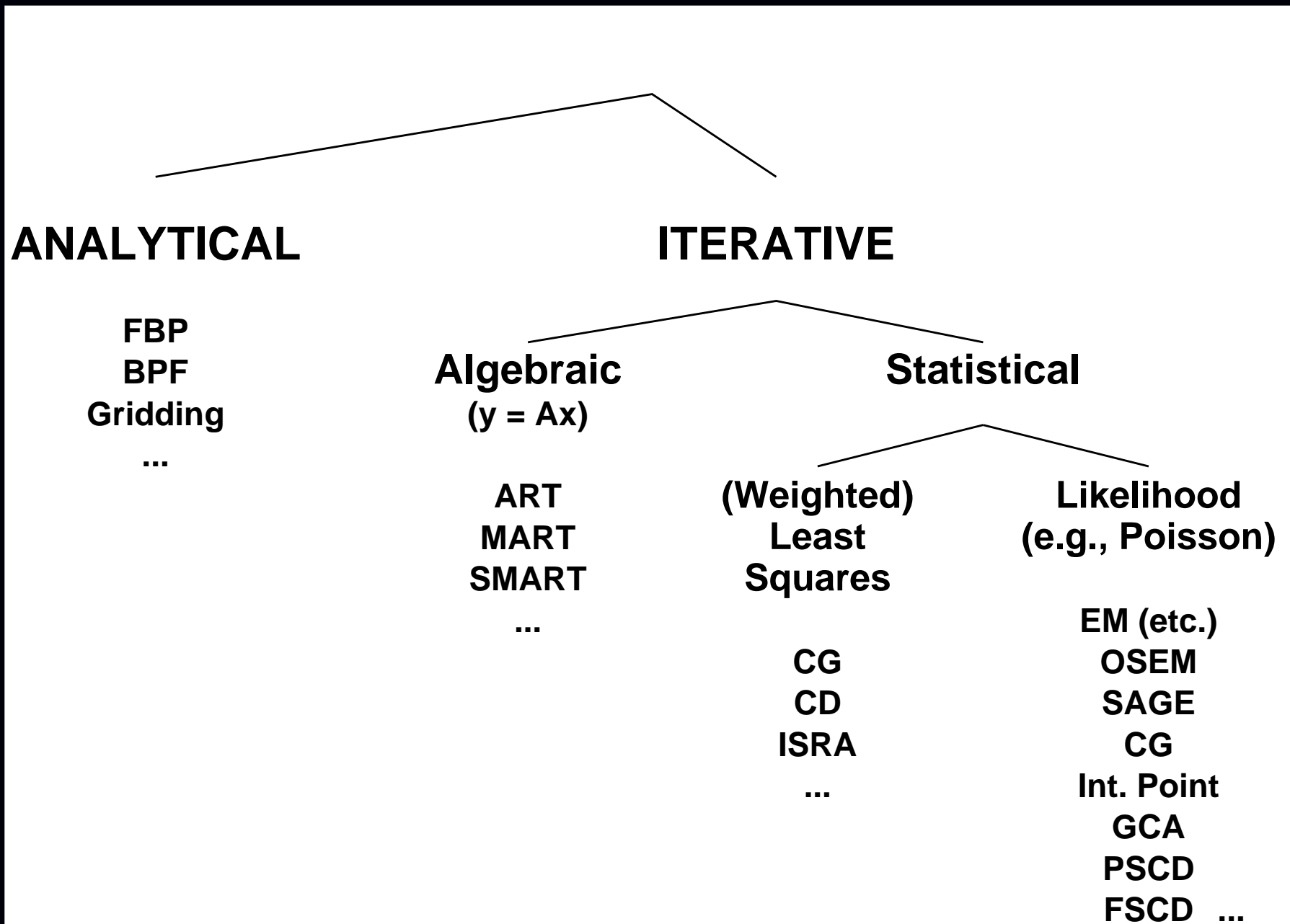
(MR: iFFT)

Iterative

(OSEM?)

(MR: CG?)

Image Reconstruction Methods / Algorithms



Outline

Part 0: Introduction / Overview / Examples

Part 1: Problem Statements

- Continuous-discrete vs continuous-continuous vs discrete-discrete

Part 2: Four of Five Choices for Statistical Image Reconstruction

- Object parameterization
- System physical modeling
- Statistical modeling of measurements
- Cost functions and regularization

Part 3: Fifth Choice: Iterative algorithms

- Classical optimization methods
- Considerations: nonnegativity, convergence rate, ...
- Optimization transfer: EM etc.
- Ordered subsets / block iterative / incremental gradient methods

Part 4: Performance Analysis

- Spatial resolution properties
- Noise properties
- Detection performance

History

- Successive substitution method vs direct Fourier (Bracewell, 1956)
- Iterative method for X-ray CT (Hounsfield, 1968)
- ART for tomography (Gordon, Bender, Herman, JTB, 1970)
- Richardson/Lucy iteration for image restoration (1972, 1974)
- Weighted least squares for 3D SPECT (Goitein, NIM, 1972)
- Proposals to use Poisson likelihood for emission and transmission tomography
Emission: (Rockmore and Macovski, TNS, 1976)
Transmission: (Rockmore and Macovski, TNS, 1977)
- Expectation-maximization (EM) algorithms for Poisson model
Emission: (Shepp and Vardi, TMI, 1982)
Transmission: (Lange and Carson, JCAT, 1984)
- Regularized (aka Bayesian) Poisson emission reconstruction (Geman and McClure, ASA, 1985)
- Ordered-subsets EM algorithm (Hudson and Larkin, TMI, 1994)
- Commercial introduction of OSEM for PET scanners circa 1997

Why Statistical Methods?

- Object constraints (e.g., nonnegativity, object support)
- Accurate physical models (less bias \implies improved quantitative accuracy) (e.g., nonuniform attenuation in SPECT)
improved spatial resolution?
- Appropriate statistical models (less variance \implies lower image noise) (FBP treats all rays equally)
- Side information (e.g., MRI or CT boundaries)
- Nonstandard geometries (e.g., irregular sampling or “missing” data)

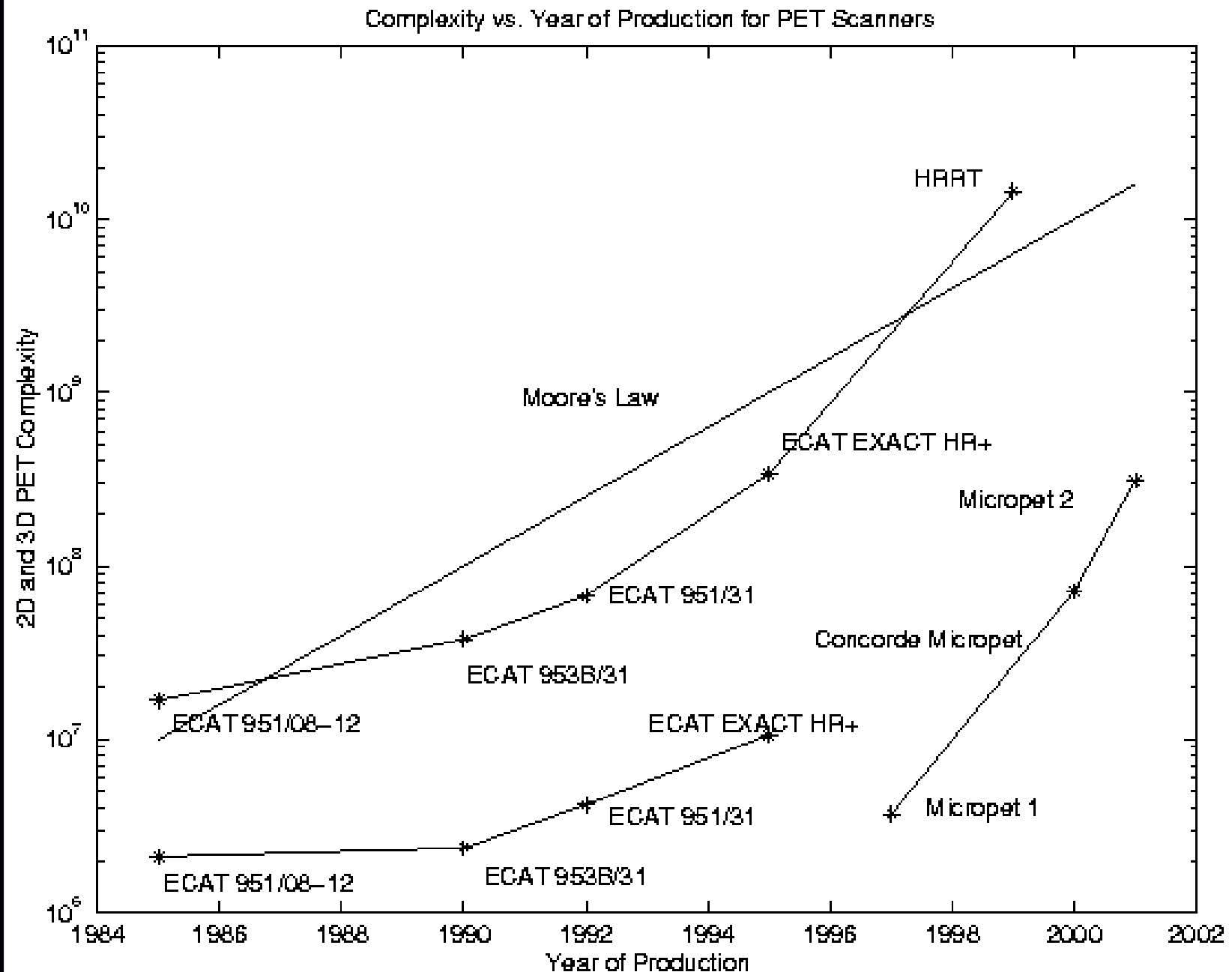
Disadvantages?

- Computation time
- Model complexity
- Software complexity

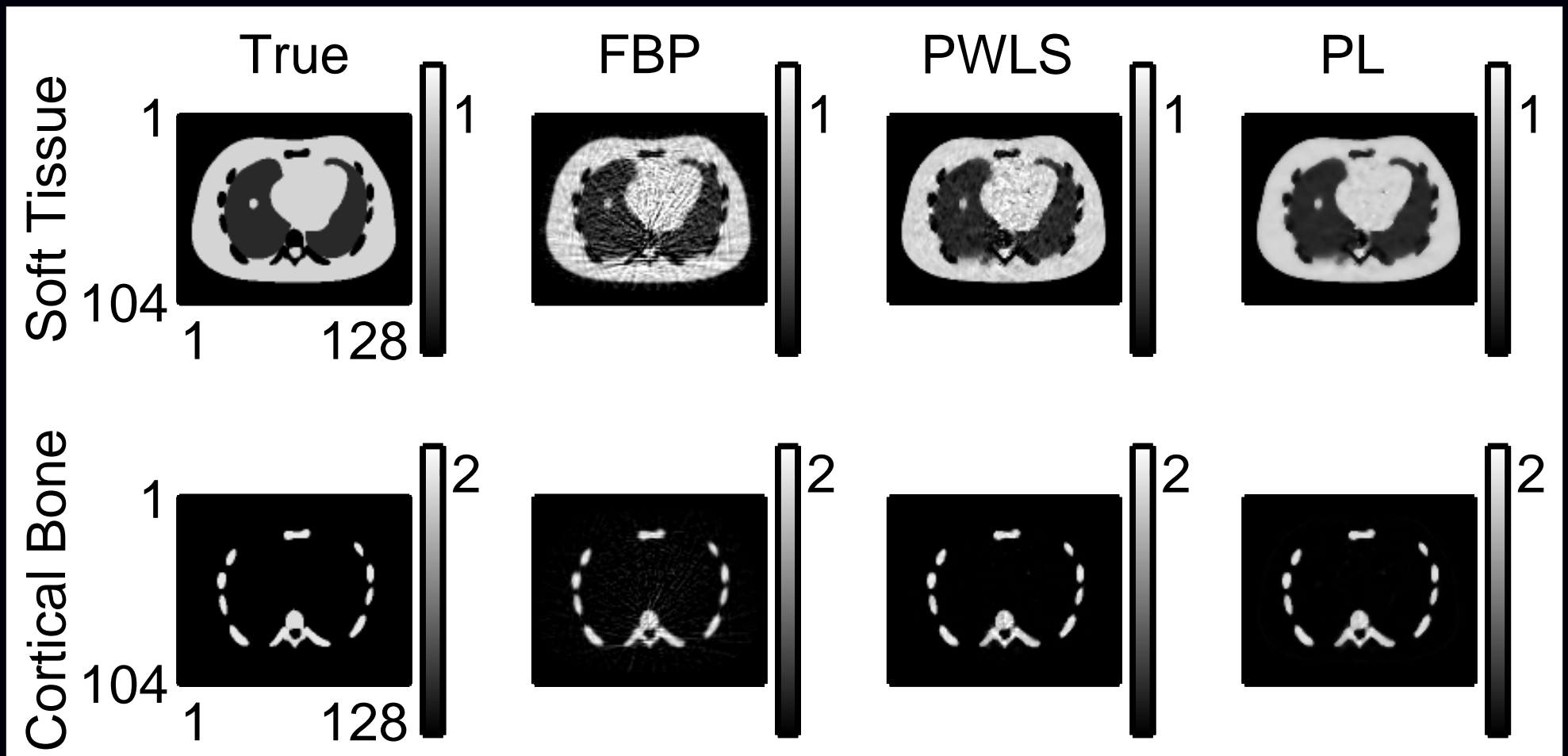
Analytical methods (a different short course!)

- Idealized mathematical model
 - Usually geometry only, greatly over-simplified physics
 - Continuum measurements (discretize/sample *after* solving)
- No statistical model
- Easier analysis of properties (due to linearity)
e.g., Huesman (1984) FBP ROI variance for kinetic fitting

What about Moore's Law?



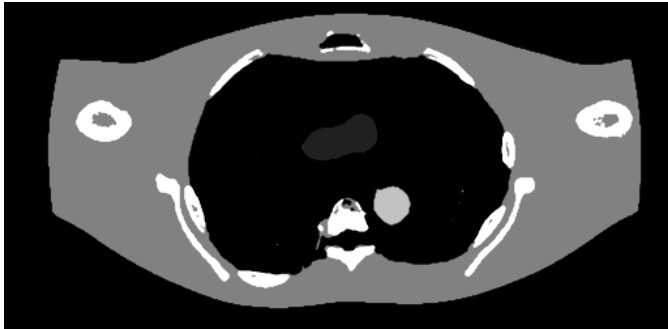
Benefit Example: Statistical Models



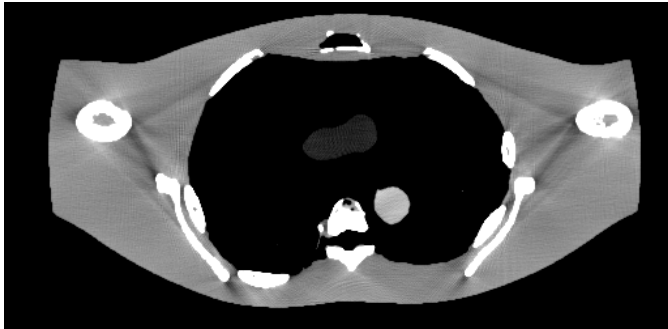
Method	NRMS Error	
	Soft Tissue	Cortical Bone
FBP	22.7%	29.6%
PWLS	13.6%	16.2%
PL	11.8%	15.8%

Benefit Example: Physical Models

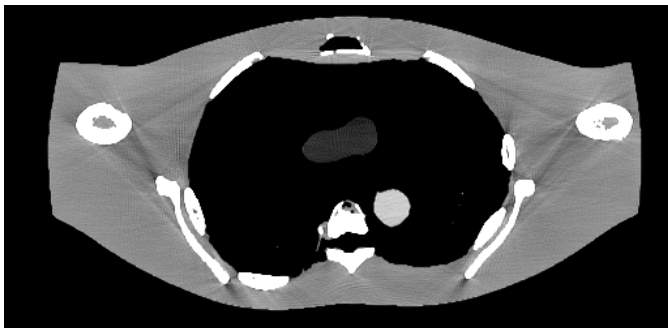
a. True object



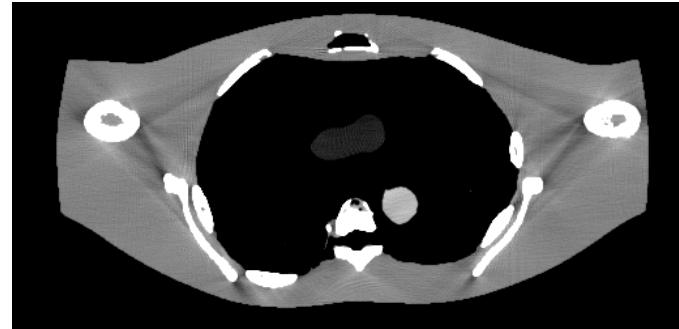
b. Unocorrected FBP



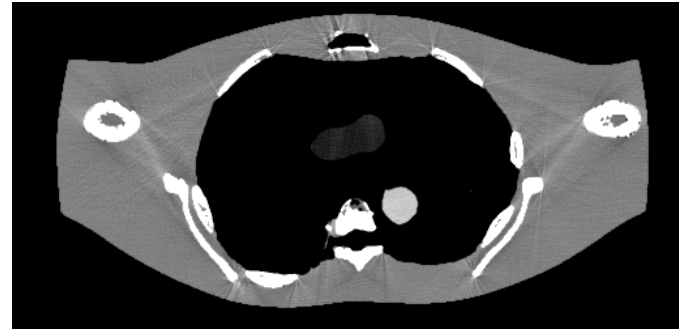
c. Monoenergetic statistical reconstruction



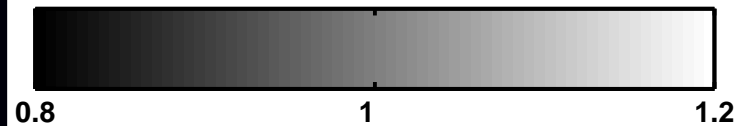
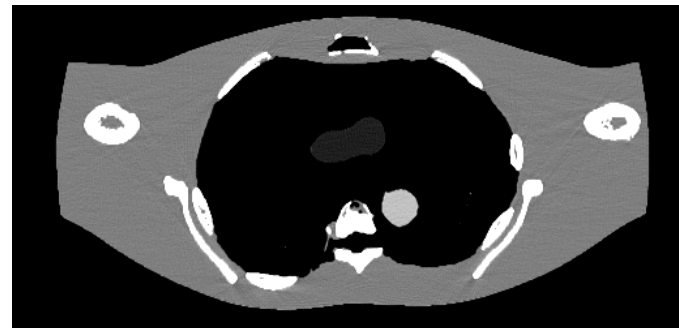
a. Soft-tissue corrected FBP



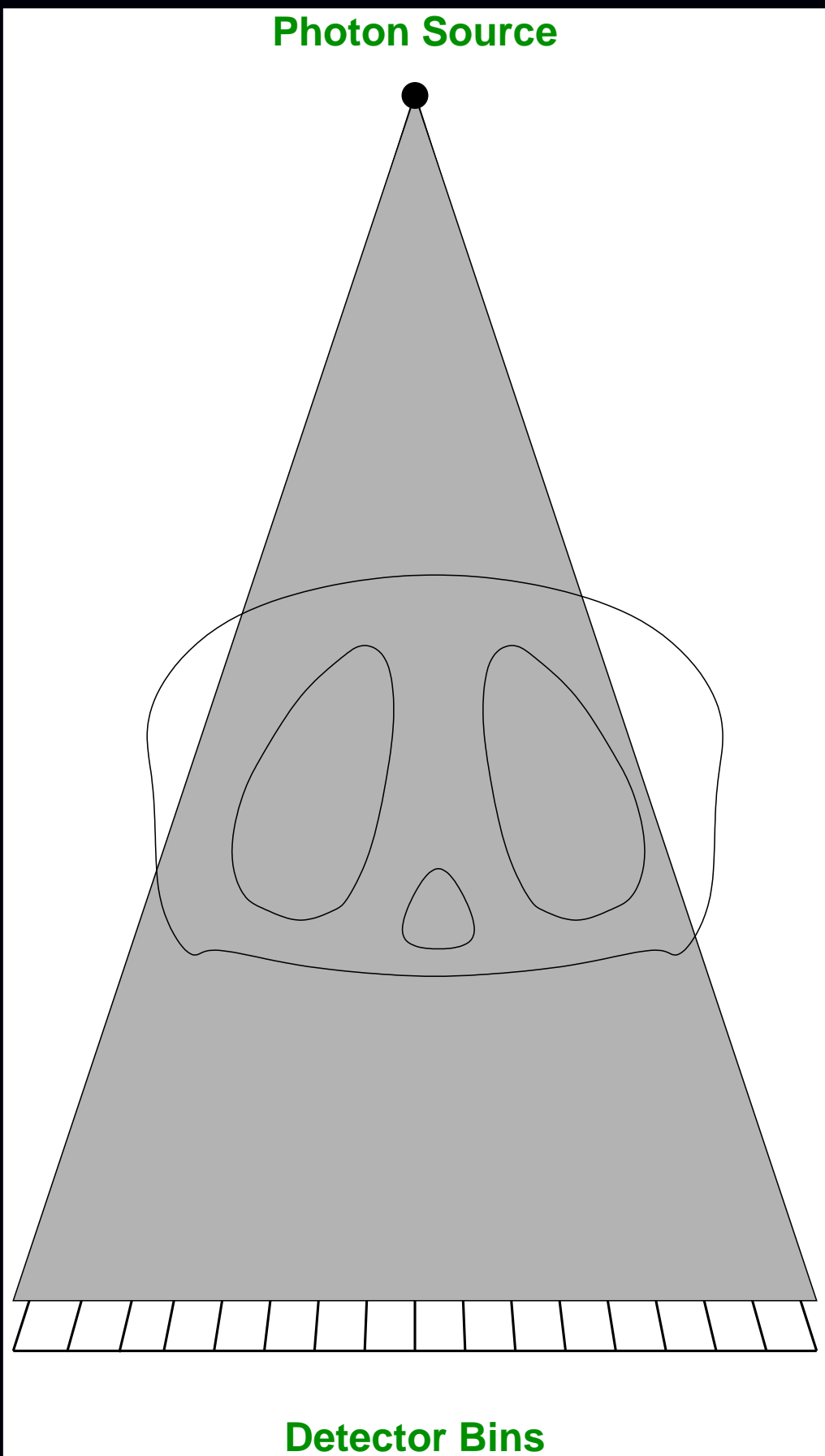
b. JS corrected FBP



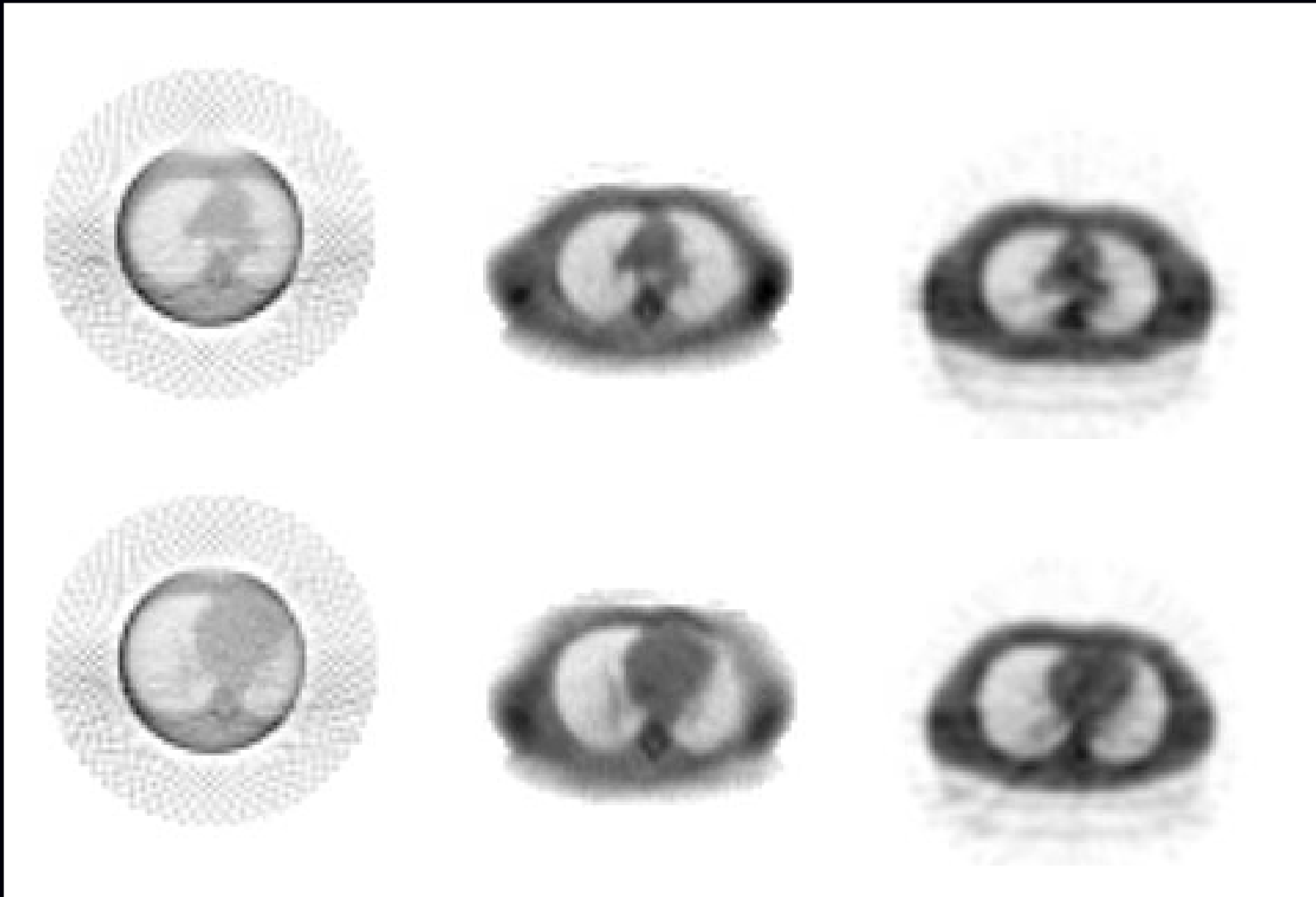
c. Polyenergetic Statistical Reconstruction



Benefit Example: Nonstandard Geometries



Truncated Fan-Beam SPECT Transmission Scan

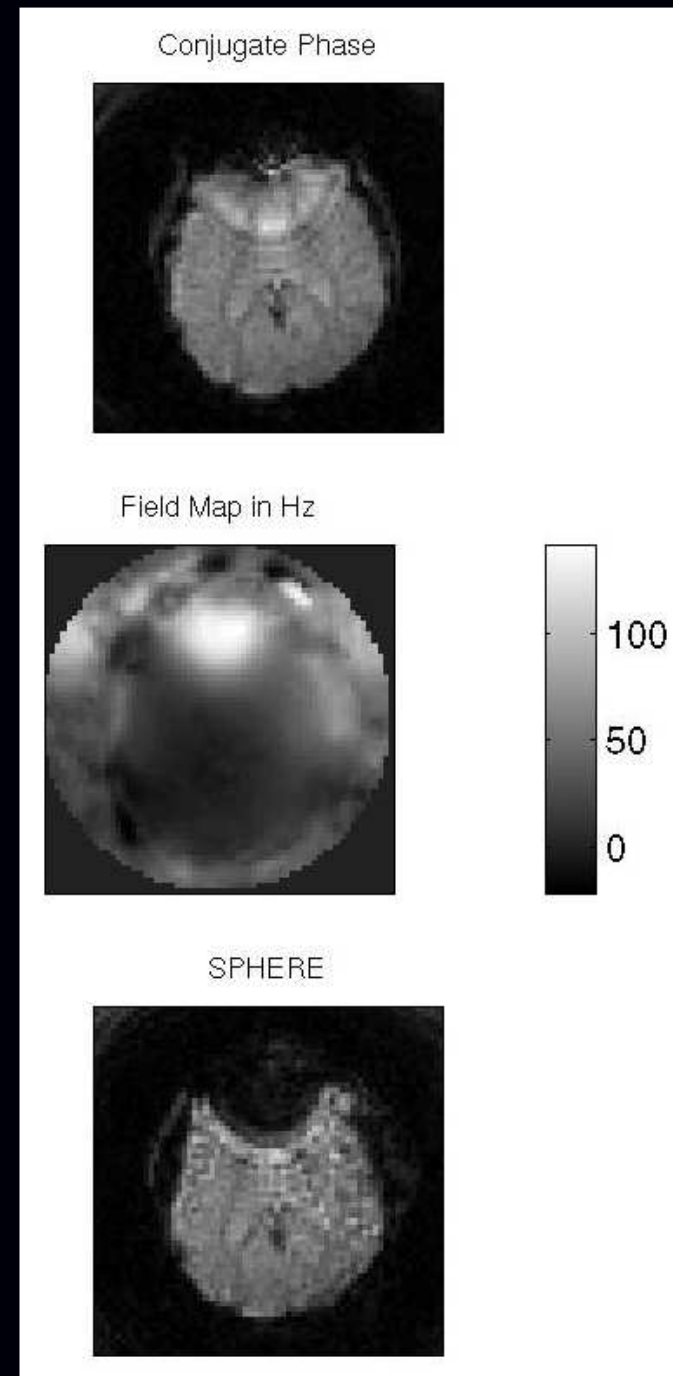
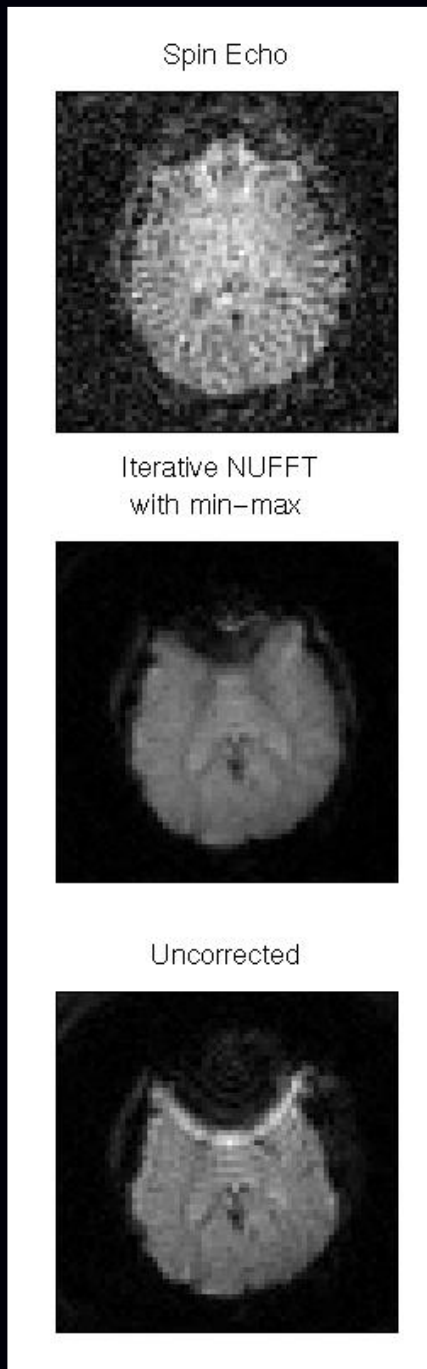


Truncated
FBP

Truncated
PWLS

Untruncated
FBP

One Final Advertisement: Iterative MR Reconstruction



Part 1: From Physics to Statistics

or

“What quantity is reconstructed?”
(in emission tomography)

Outline

- Decay phenomena and fundamental assumptions
- Idealized detectors
- Random phenomena
- Poisson measurement statistics
- State emission tomography reconstruction problem

What Object is Reconstructed?

In *emission imaging*, our aim is to image the *radiotracer distribution*.

The what?

At time $t = 0$ we inject the patient with some *radiotracer*, containing a “large” number N of metastable atoms of some radionuclide.

Let $\vec{X}_k(t) \in \mathbb{R}^3$ denote the position of the k th *tracer atom* at time t .

These positions are influenced by blood flow, patient physiology, and other unpredictable phenomena such as Brownian motion.

The ultimate imaging device would provide an exact list of the spatial locations $\vec{X}_1(t), \dots, \vec{X}_N(t)$ of all tracer atoms for the entire scan.

Would this be enough?

Atom Positions or Statistical Distribution?

Repeating a scan would yield different tracer atom sample paths $\left\{ \vec{X}_k(t) \right\}_{k=1}^N$.

\therefore statistical formulation

Assumption 1. The spatial locations of individual tracer atoms at any time $t \geq 0$ are *independent* random variables that are all *identically distributed* according to a common probability density function (pdf) $p_t(\vec{x})$.

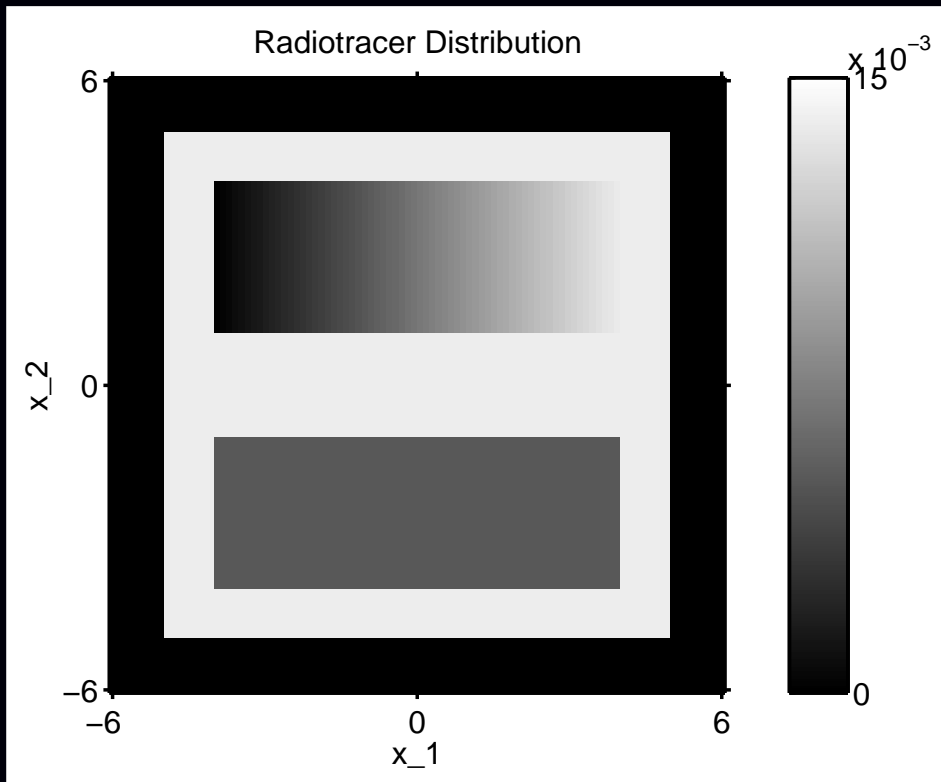
This pdf is determined by patient physiology and tracer properties.

Larger values of $p_t(\vec{x})$ correspond to “hot spots” where the tracer atoms tend to be located at time t . Units: inverse volume, e.g., atoms per cubic centimeter.

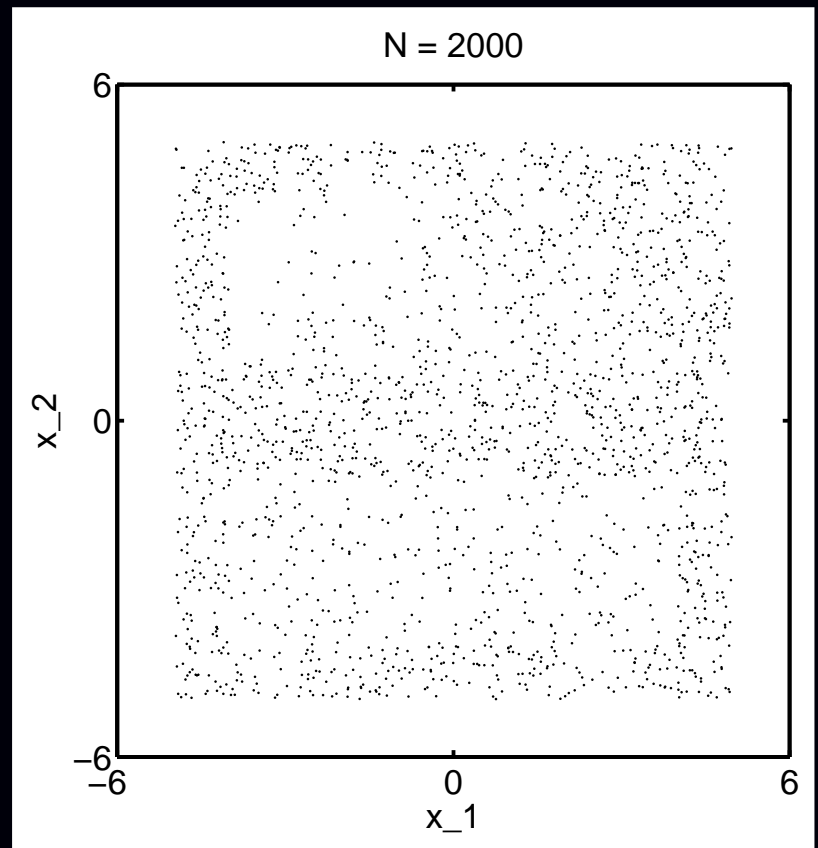
The *radiotracer distribution* $p_t(\vec{x})$ is the quantity of interest.

(Not $\left\{ \vec{X}_k(t) \right\}_{k=1}^N$!)

Example: Perfect Detector



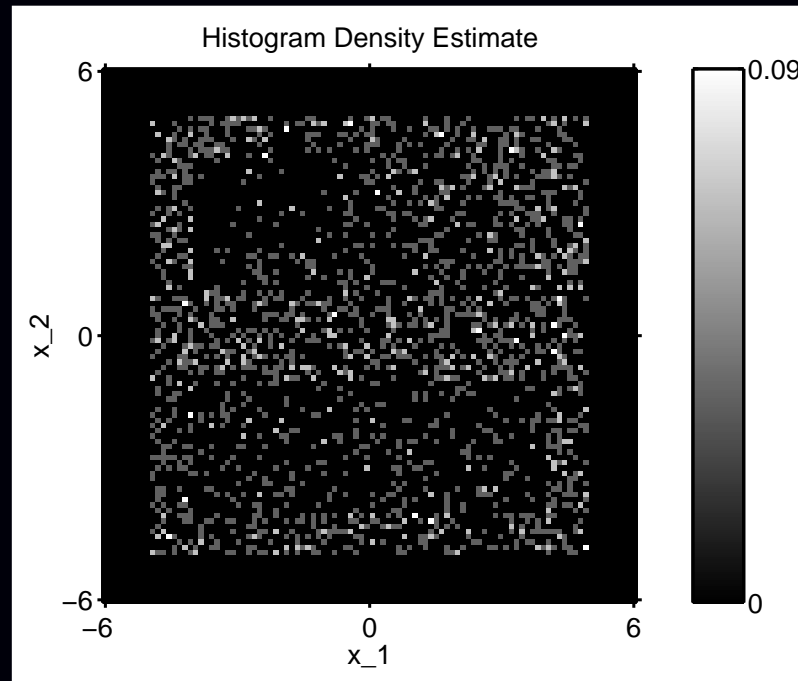
True radiotracer distribution $p_t(\vec{x})$
at some time t .



A realization of $N = 2000$ i.i.d.
atom positions (dots) recorded
“exactly.”

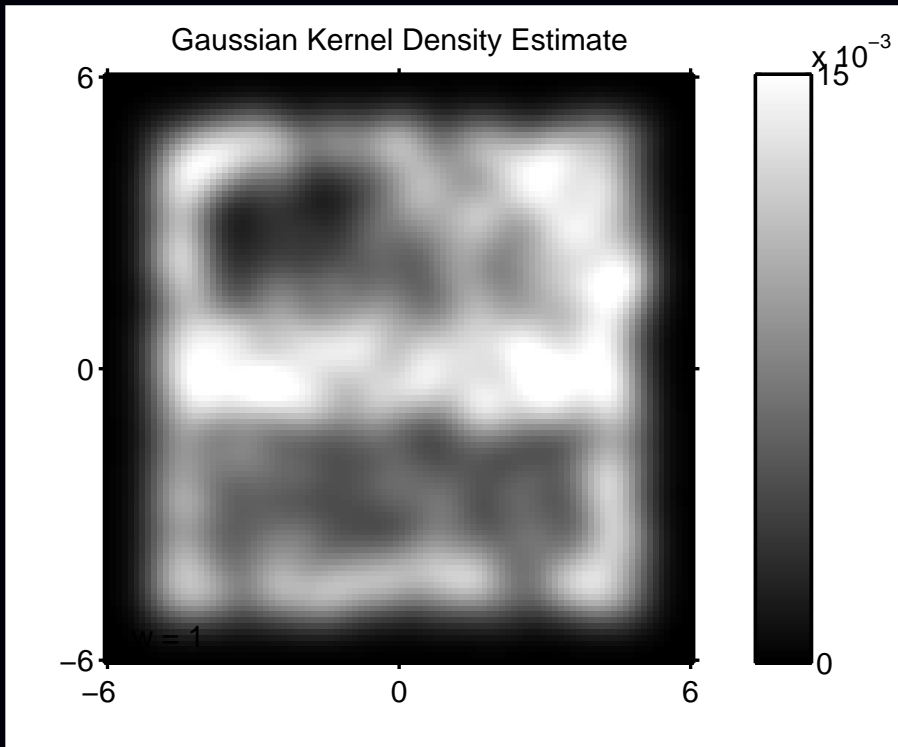
Little similarity!

Binning/Histogram Density Estimator

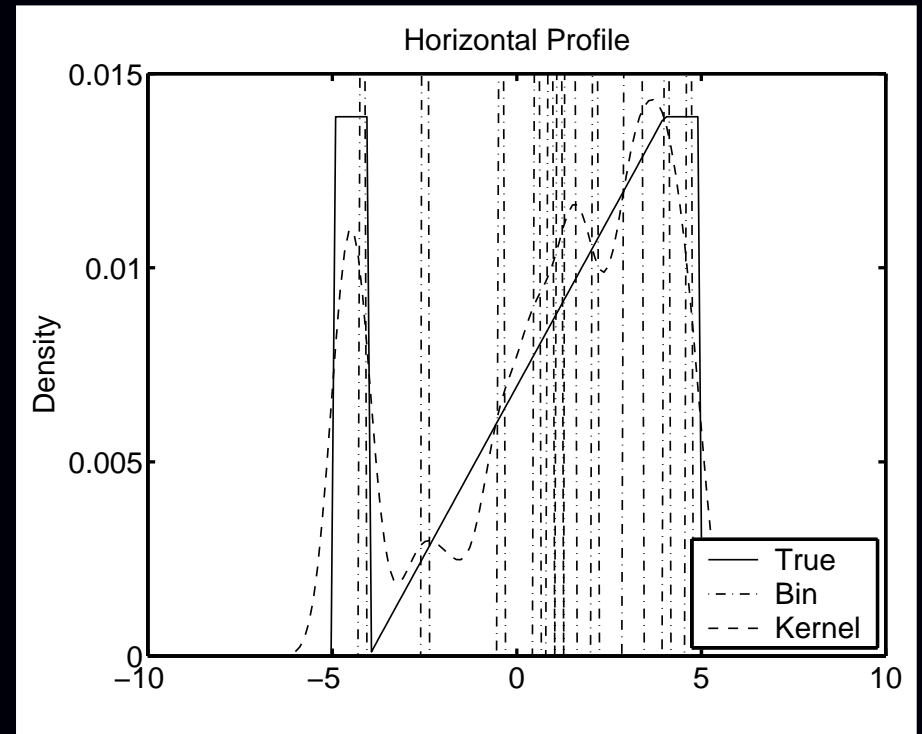


Estimate of $p_t(\vec{x})$ formed by histogram binning of $N = 2000$ points.
Ramp remains difficult to visualize.

Kernel Density Estimator



Gaussian kernel density estimator for $p_t(\vec{x})$ from $N = 2000$ points.



Horizontal profiles at $x_2 = 3$ through density estimates.

Poisson Spatial Point Process

Assumption 2. The number of administered tracer atoms N has a Poisson distribution with some mean

$$\mu_N \triangleq E[N] = \sum_{n=0}^{\infty} n P\{N = n\}.$$

Let $N_t(\mathcal{B})$ denote the number of tracer atoms that have spatial locations in any set $\mathcal{B} \subset \mathbb{R}^3$ (VOI) at time t after injection.

$N_t(\cdot)$ is called a *Poisson spatial point process*.

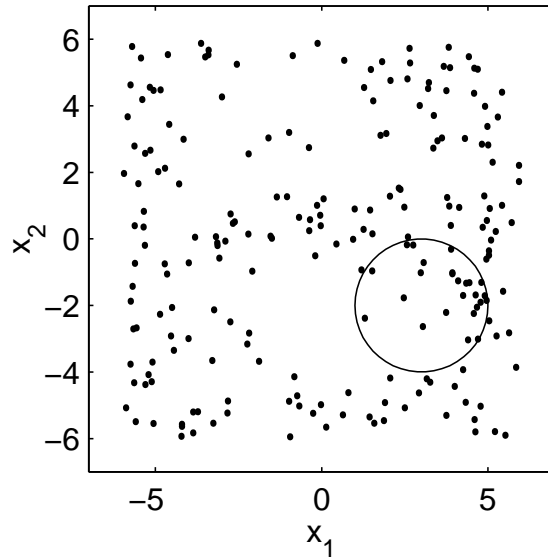
Fact. For any set \mathcal{B} , $N_t(\mathcal{B})$ is Poisson distributed with mean:

$$E[N_t(\mathcal{B})] = E[N] P\left\{\vec{X}_k(t) \in \mathcal{B}\right\} = \mu_N \int_{\mathcal{B}} p_t(\vec{x}) d\vec{x}.$$

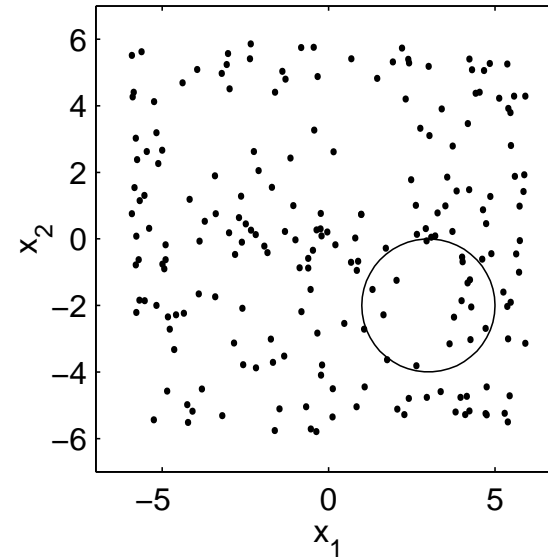
Poisson N injected atoms + i.i.d. locations \implies Poisson point process

Illustration of Point Process ($\mu_N = 200$)

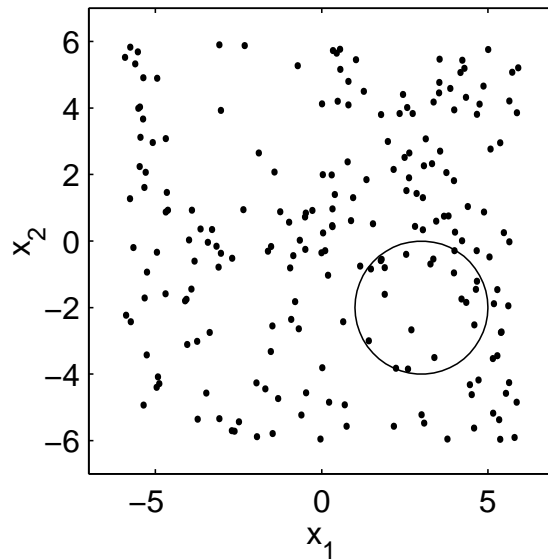
25 points within ROI



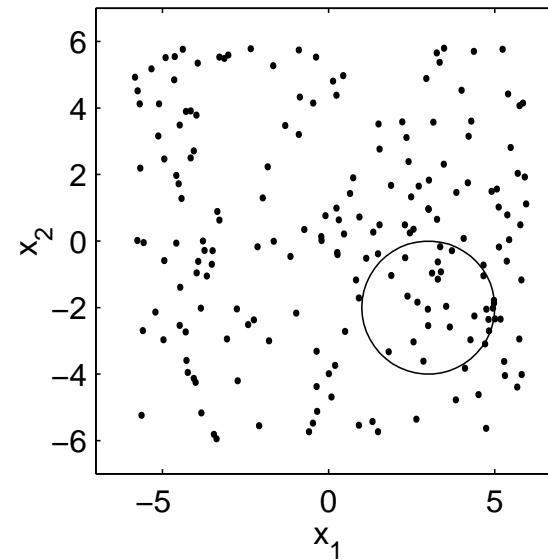
15 points within ROI



20 points within ROI



26 points within ROI



Radionuclide Decay

Preceding quantities are all unobservable.

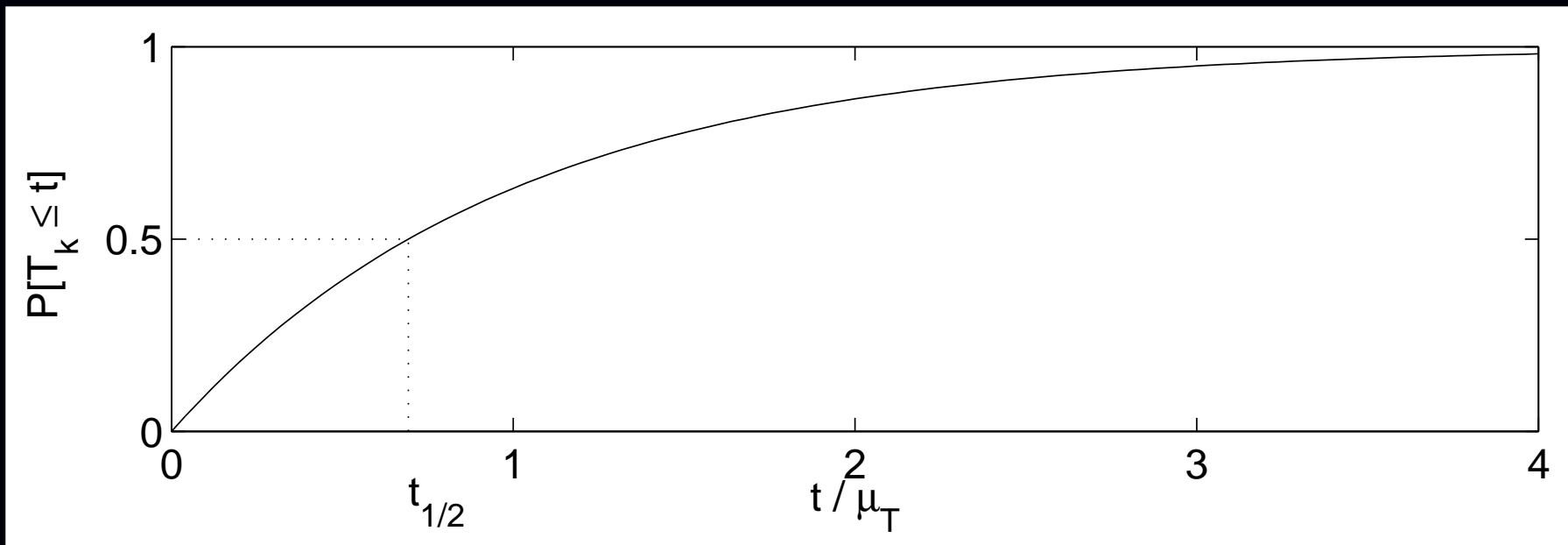
We “observe” a tracer atom only when it decays and emits photon(s).

The time that the k th tracer atom decays is a random variable T_k .

Assumption 3. The T_k 's are statistically *independent* random variables, and are independent of the (random) spatial location.

Assumption 4. Each T_k has an exponential distribution with mean $\mu_T = t_{1/2}/\ln 2$.

Cumulative distribution function: $P\{T_k \leq t\} = 1 - \exp(-t/\mu_T)$



Statistics of an Ideal Decay Counter

Let $K_t(\mathcal{B})$ denote the number of tracer atoms that decay by time t , and that were located in the VOI $\mathcal{B} \subset \mathbb{R}^3$ at the time of decay.

Fact. $K_t(\mathcal{B})$ is a *Poisson counting process* with mean

$$E[K_t(\mathcal{B})] = \int_0^t \int_{\mathcal{B}} \lambda(\vec{x}, \tau) d\vec{x} d\tau,$$

where the (nonuniform) *emission rate density* is given by

$$\lambda(\vec{x}, t) \triangleq \mu_N \frac{e^{-t/\mu_T}}{\mu_T} \cdot p_t(\vec{x}).$$

Ingredients: “dose,” “decay,” “distribution”

Units: “counts” per unit time per unit volume, e.g., $\mu\text{Ci/cc}$.

“Photon emission is a Poisson process”

What about the actual measurement statistics?

Idealized Detector Units

A nuclear imaging system consists of n_d conceptual *detector units*.

Assumption 5. Each decay of a tracer atom produces a recorded count in at most one detector unit.

Let $S_k \in \{0, 1, \dots, n_d\}$ denote the index of the incremented detector unit for decay of k th tracer atom. ($S_k = 0$ if decay is undetected.)

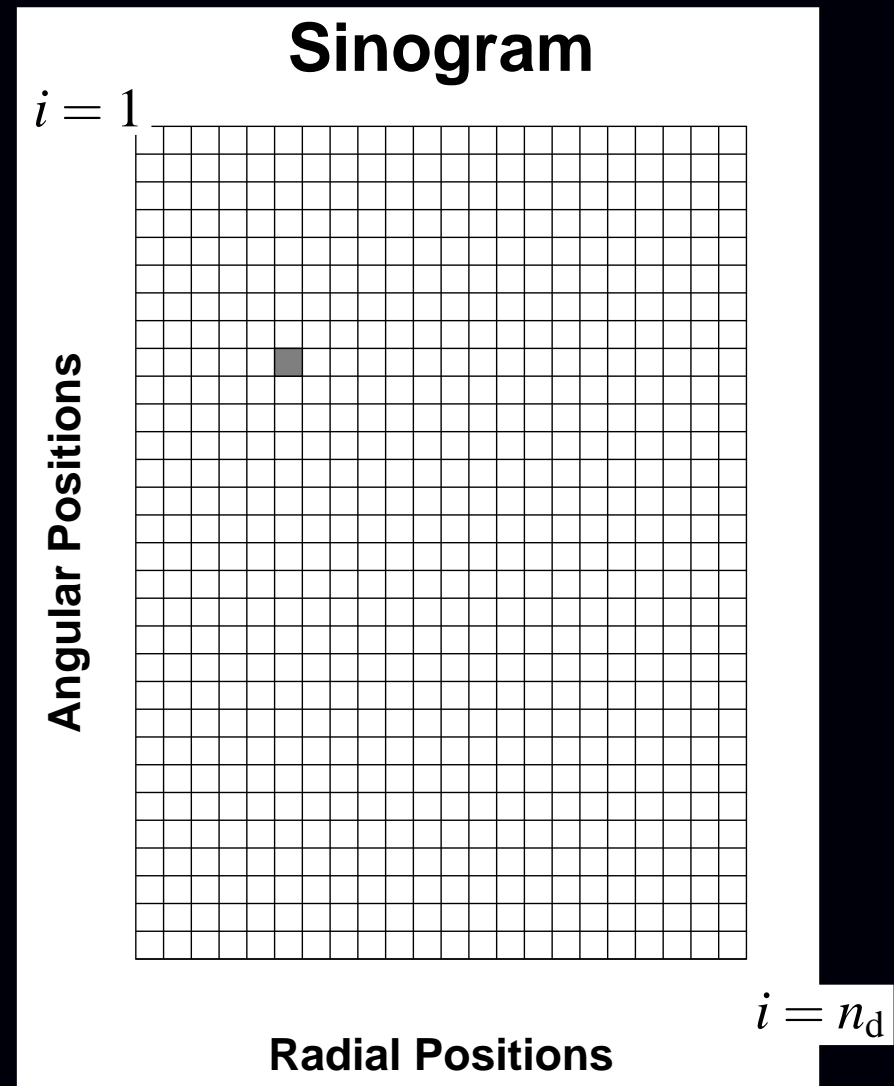
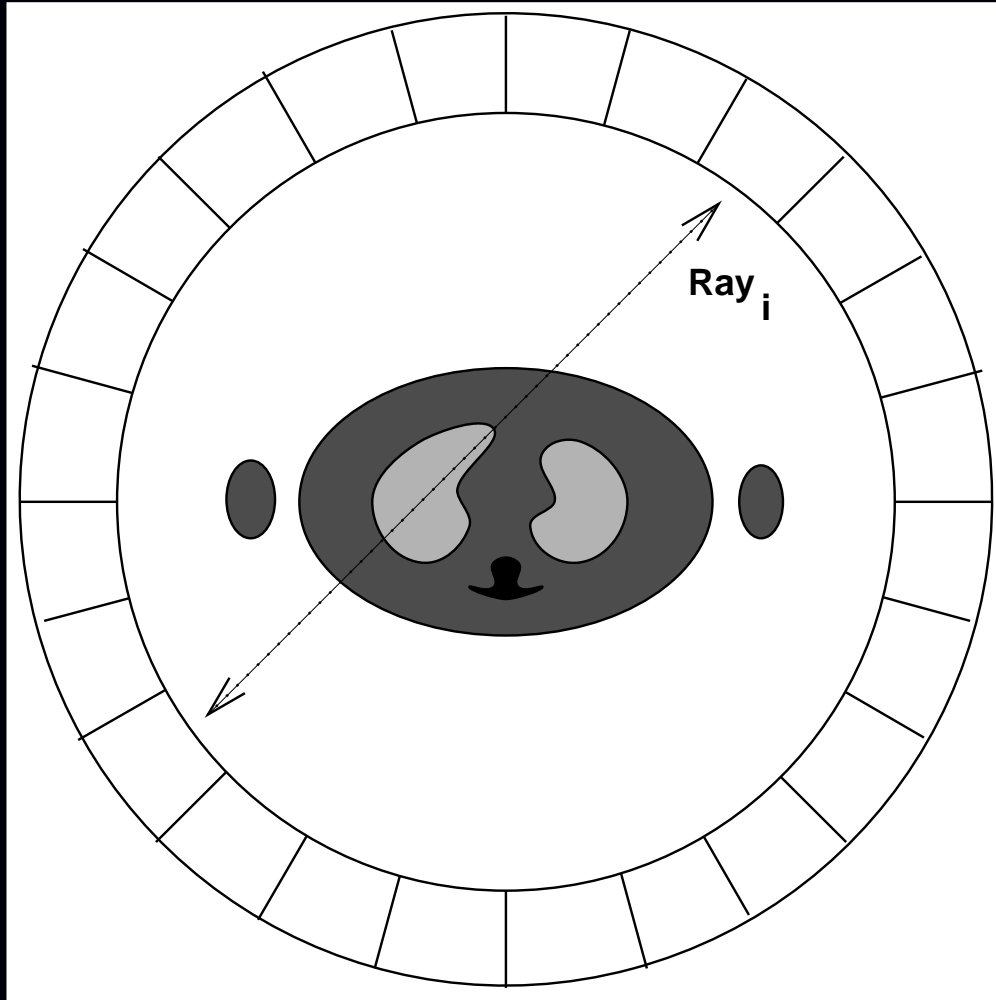
Assumption 6. The S_k 's satisfy the following conditional independence:

$$P\left\{S_1, \dots, S_N \mid N, T_1, \dots, T_N, \vec{X}_1(\cdot), \dots, \vec{X}_N(\cdot)\right\} = \prod_{k=1}^N P\left\{S_k \mid \vec{X}_k(T_k)\right\}.$$

The recorded bin for the k th tracer atom's decay depends only on its position when it decays, and is independent of all other tracer atoms.

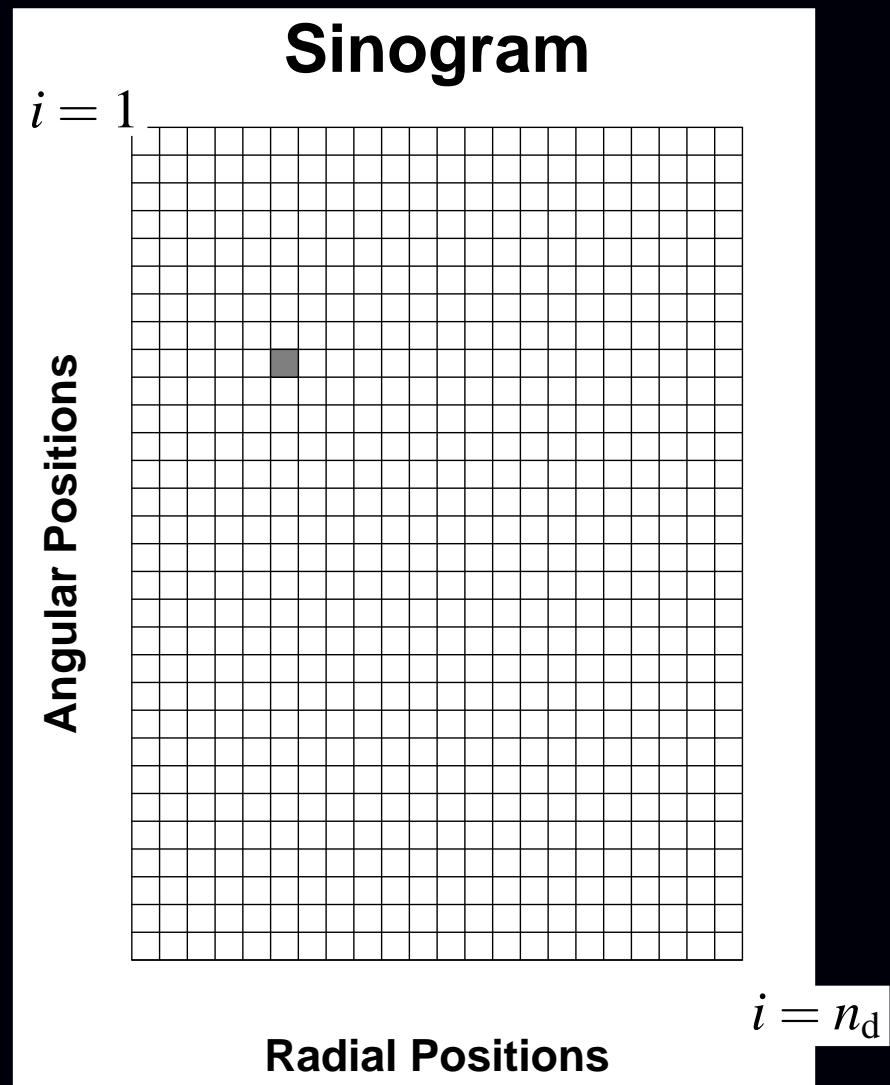
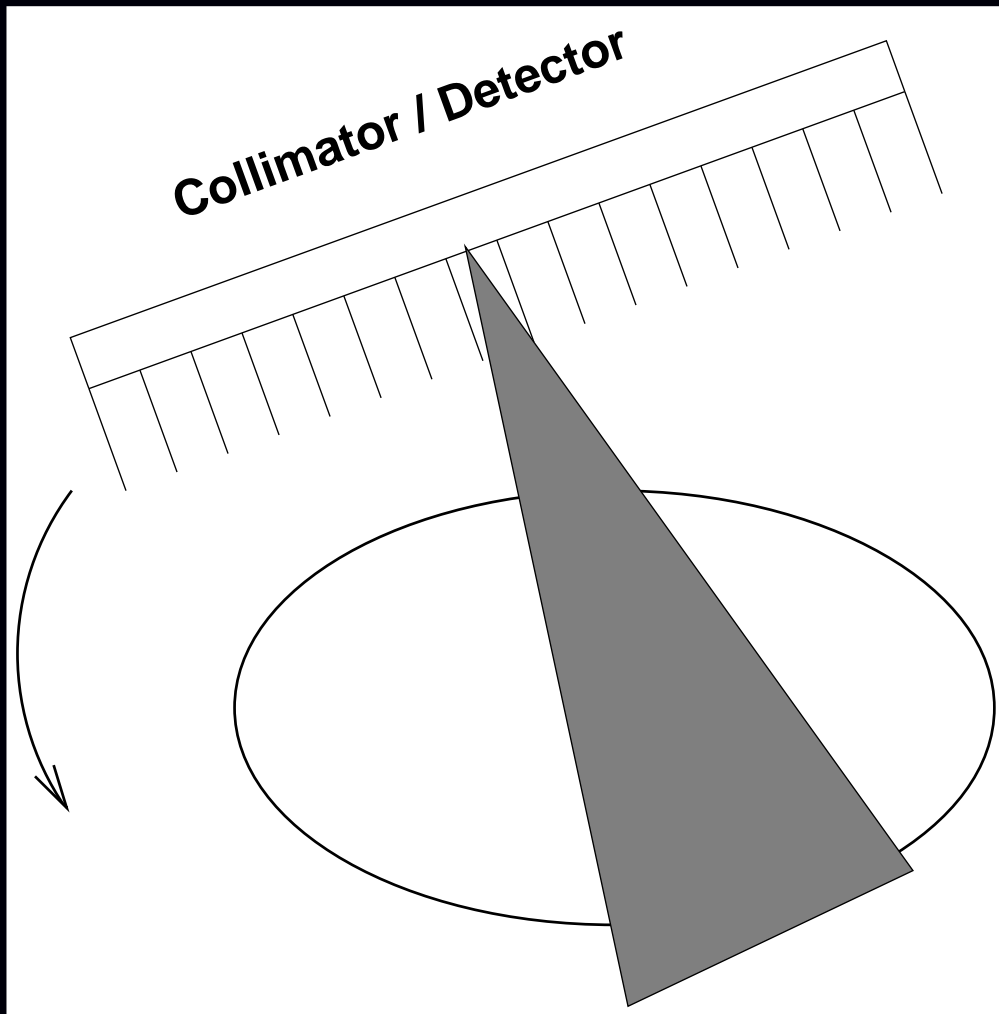
(No event pileup; no deadtime losses.)

PET Example



$$n_d \leq (n_{\text{crystals}} - 1) \cdot n_{\text{crystals}} / 2$$

SPECT Example



$$n_d = n_{\text{radial_bins}} \cdot n_{\text{angular_steps}}$$

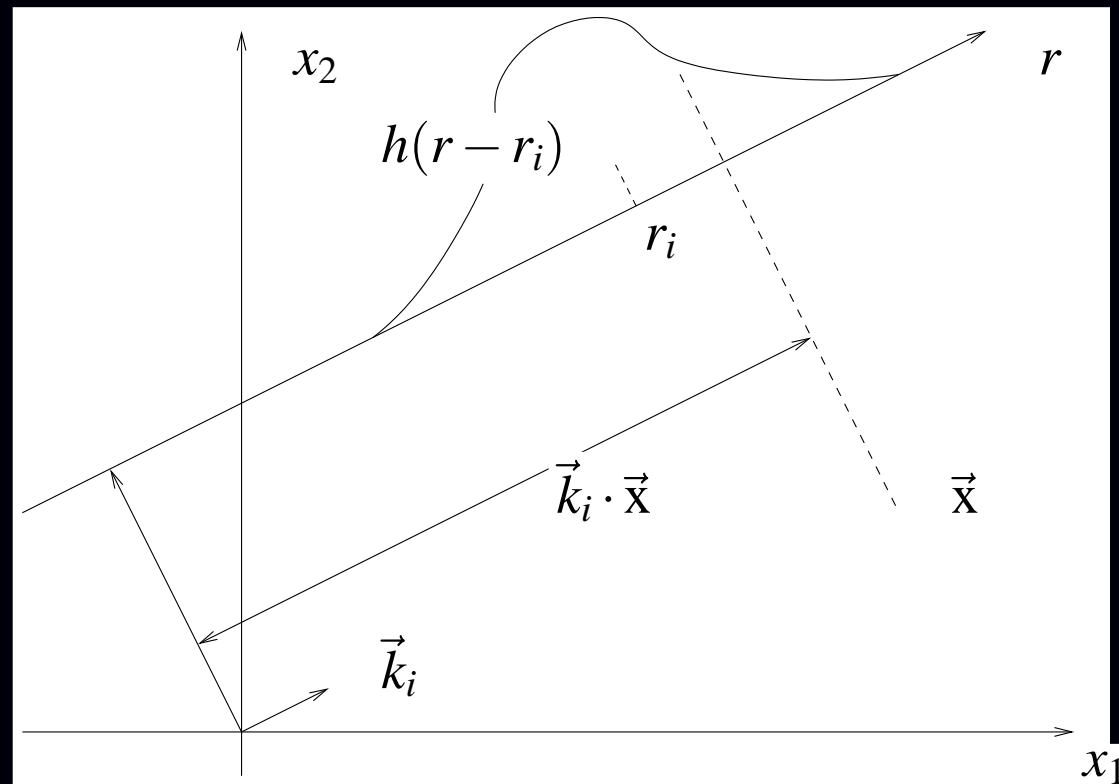
Detector Unit Sensitivity Patterns

Spatial localization:

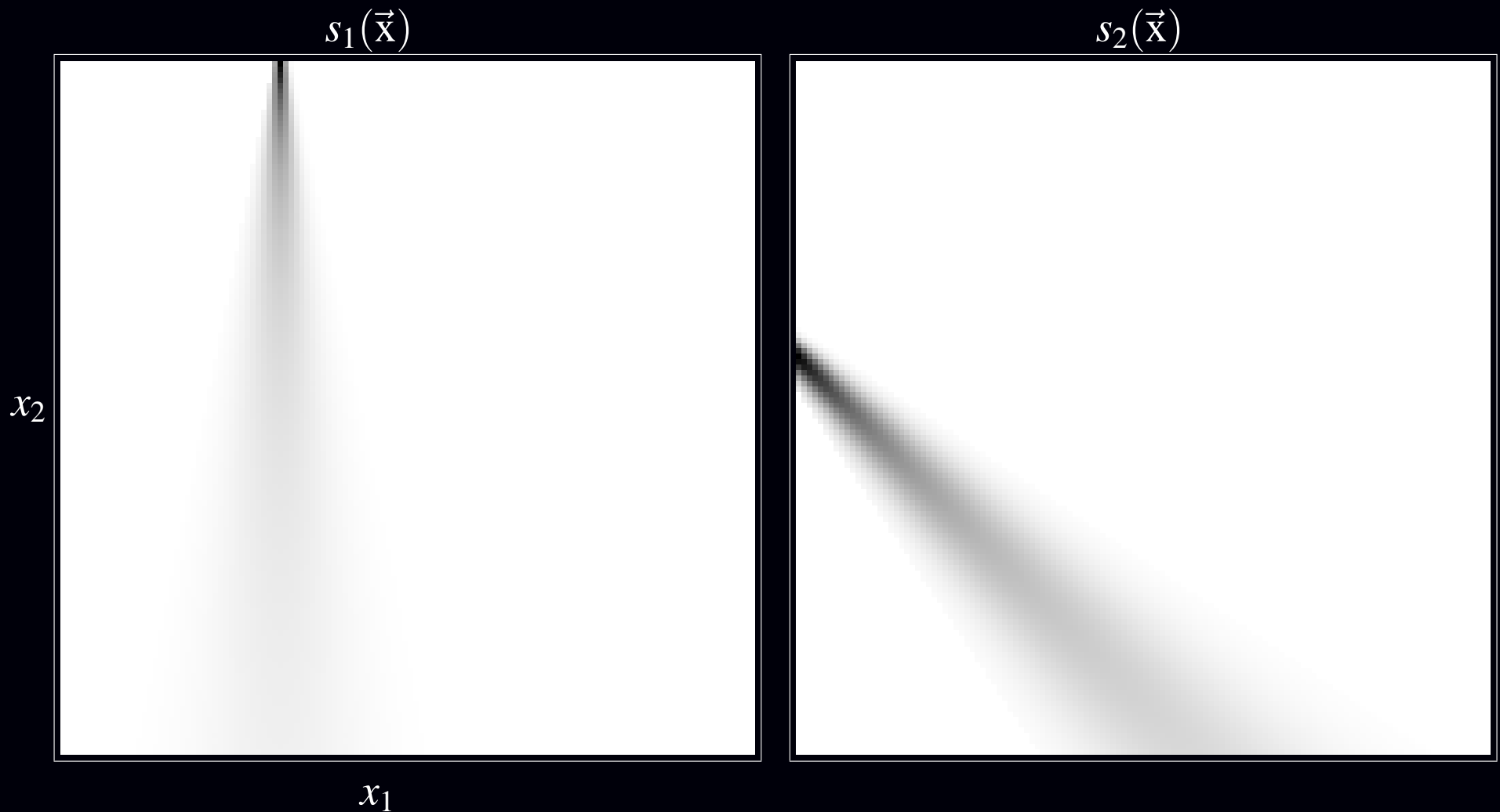
$s_i(\vec{x}) \triangleq$ probability that decay at \vec{x} is recorded by i th detector unit.

Idealized Example. Shift-invariant PSF: $s_i(\vec{x}) = h(\vec{k}_i \cdot \vec{x} - r_i)$

- r_i is the radial position of i th ray
- \vec{k}_i is the unit vector orthogonal to i th parallel ray
- $h(\cdot)$ is the shift-invariant radial PSF (e.g., Gaussian bell or rectangular function)

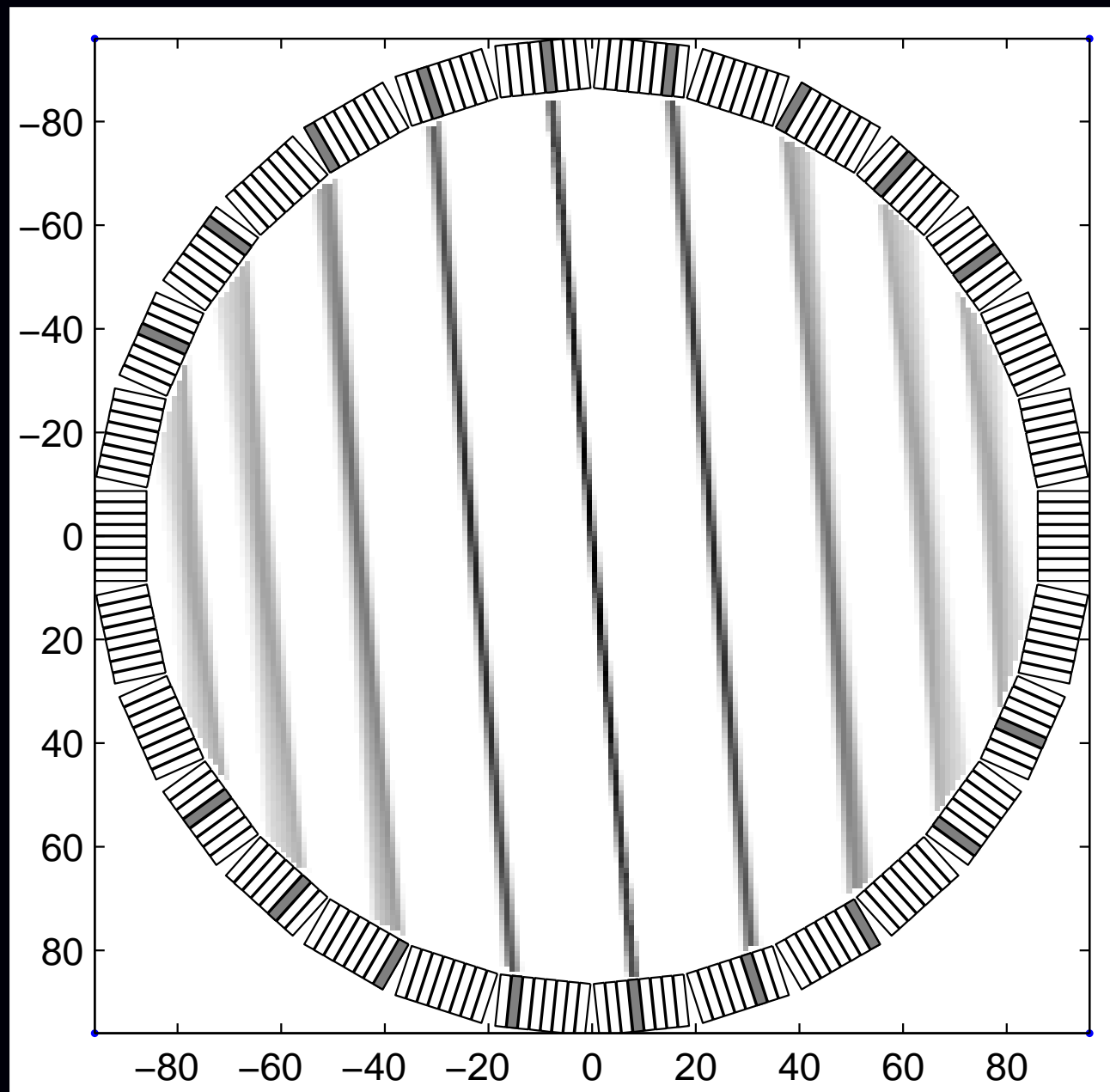


Example: SPECT Detector-Unit Sensitivity Patterns



Two representative $s_i(\vec{x})$ functions for a collimated Anger camera.

Example: PET Detector-Unit Sensitivity Patterns



Detector Unit Sensitivity Patterns

$s_i(\vec{x})$ can include the effects of

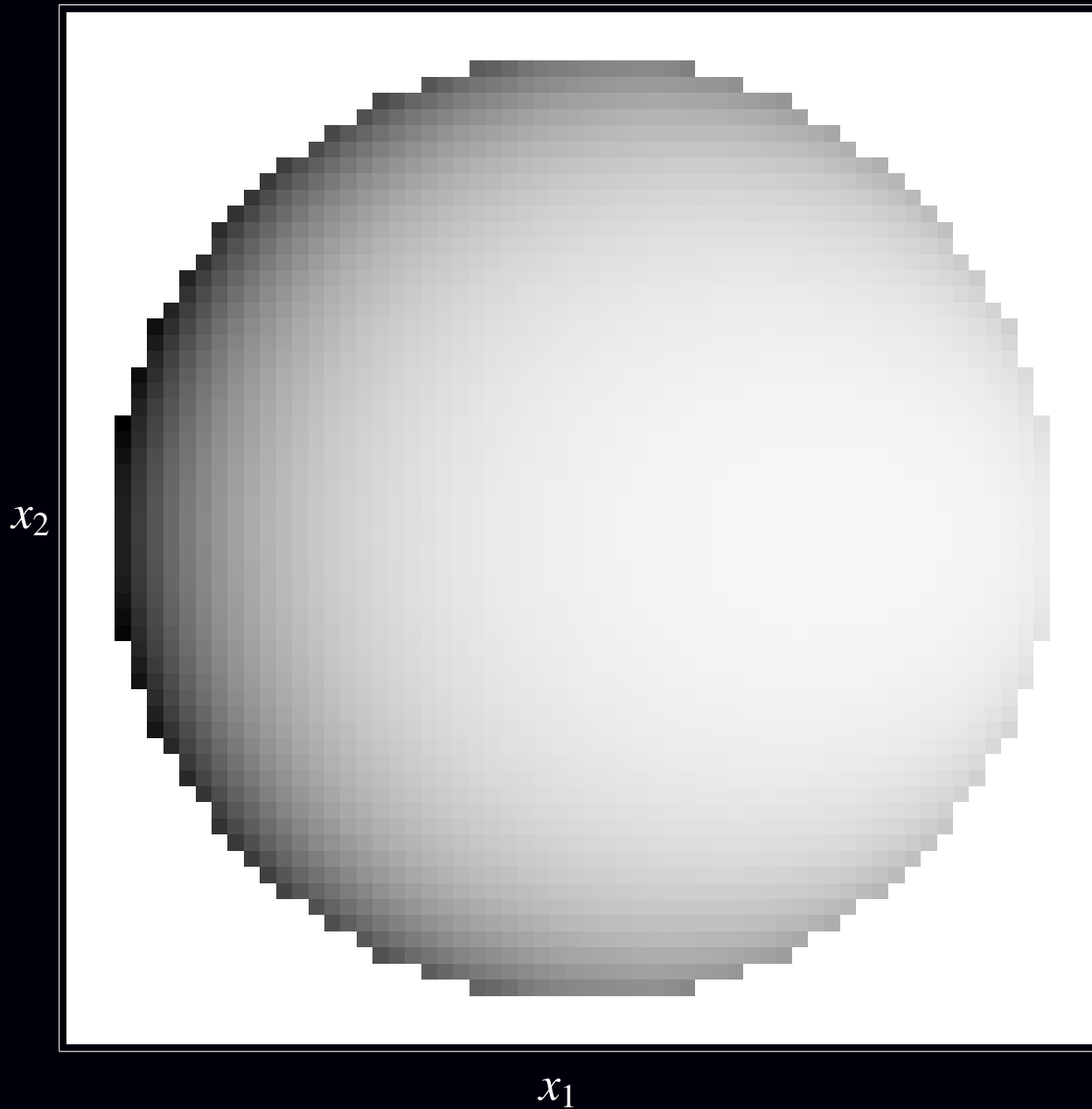
- geometry / solid angle
- collimation
- scatter
- attenuation
- detector response / scan geometry
- duty cycle (dwell time at each angle)
- detector efficiency
- positron range, noncollinearity
- ...

System sensitivity pattern:

$$s(\vec{x}) \triangleq \sum_{i=1}^{n_d} s_i(\vec{x}) = 1 - s_0(\vec{x}) \leq 1$$

(probability that decay at location \vec{x} will be detected *at all* by system)

(Overall) System Sensitivity Pattern: $s(\vec{x}) = \sum_{i=1}^{n_d} s_i(\vec{x})$



Example: collimated 180° SPECT system with uniform attenuation.

Detection Probabilities $s_i(\vec{x}_0)$ (vs det. unit index i)

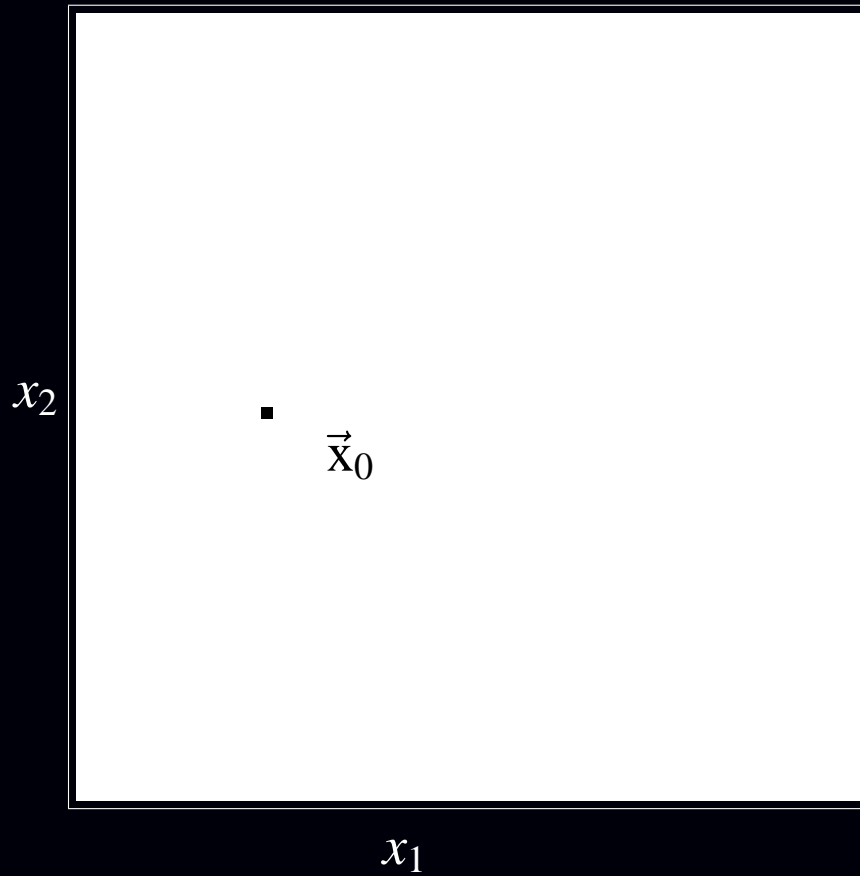
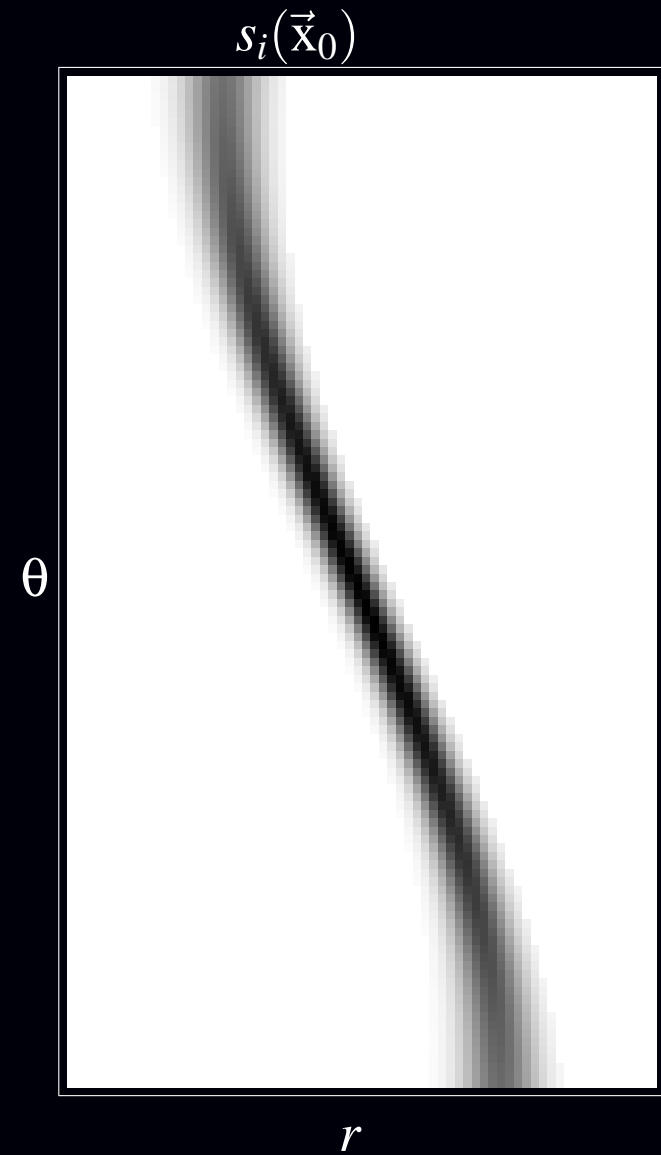


Image domain



Sinogram domain

Summary of Random Phenomena

- Number of tracer atoms injected N
- Spatial locations of tracer atoms $\left\{ \vec{X}_k(t) \right\}_{k=1}^N$
- Time of decay of tracer atoms $\left\{ T_k \right\}_{k=1}^N$
- Detection of photon $[S_k \neq 0]$
- Recording detector unit $\left\{ S_k \right\}_{i=1}^{n_d}$

Emission Scan

Record events in each detector unit for $t_1 \leq t \leq t_2$.

$Y_i \triangleq$ number of events recorded by i th detector unit during scan, for $i = 1, \dots, n_d$.

$$Y_i \triangleq \sum_{k=1}^N 1_{\{S_k=i, T_k \in [t_1, t_2]\}}.$$

The collection $\{Y_i : i = 1, \dots, n_d\}$ is our *sinogram*.

Note $0 \leq Y_i \leq N$.

Fact. Under Assumptions 1-6 above,

$$Y_i \sim \text{Poisson} \left\{ \int s_i(\vec{x}) \lambda(\vec{x}) d\vec{x} \right\} \quad (\text{cf "line integral"})$$

and Y_i 's are statistically independent random variables, where the *emission density* is given by

$$\lambda(\vec{x}) = \mu_N \int_{t_1}^{t_2} \frac{1}{\mu_T} e^{-t/\mu_T} p_t(\vec{x}) dt.$$

(Local number of decays per unit volume during scan.)

Ingredients:

- dose (injected)
- duration of scan
- decay of radionuclide
- distribution of radiotracer

Poisson Statistical Model (Emission)

Actual measured counts = “foreground” counts + “background” counts.

Sources of background counts:

- cosmic radiation / room background
- random coincidences (PET)
- scatter not accounted for in $s_i(\vec{x})$
- “crosstalk” from transmission sources in simultaneous T/E scans
- anything else not accounted for by $\int s_i(\vec{x}) \lambda(\vec{x}) d\vec{x}$

Assumption 7.

The background counts also have independent Poisson distributions.

Statistical model (continuous to discrete)

$$Y_i \sim \text{Poisson} \left\{ \int s_i(\vec{x}) \lambda(\vec{x}) d\vec{x} + r_i \right\}, \quad i = 1, \dots, n_d$$

r_i : mean number of “background” counts recorded by i th detector unit.

Emission Reconstruction Problem

Estimate the emission density $\lambda(\vec{x})$ using (something like) this model:

$$Y_i \sim \text{Poisson} \left\{ \int s_i(\vec{x}) \lambda(\vec{x}) d\vec{x} + r_i \right\}, \quad i = 1, \dots, n_d.$$

Knowns:

- $\{Y_i = y_i\}_{i=1}^{n_d}$: observed counts from each detector unit
- $s_i(\vec{x})$ sensitivity patterns (determined by system models)
- r_i 's : background contributions (determined separately)

Unknown: $\lambda(\vec{x})$

List-mode acquisitions

Recall that conventional sinogram is temporally binned:

$$Y_i \triangleq \sum_{k=1}^N 1_{\{S_k=i, T_k \in [t_1, t_2]\}}.$$

This binning discards temporal information.

List-mode measurements: record all (detector,time) pairs in a list, *i.e.*,

$$\{(S_k, T_k) : k = 1, \dots, N\}.$$

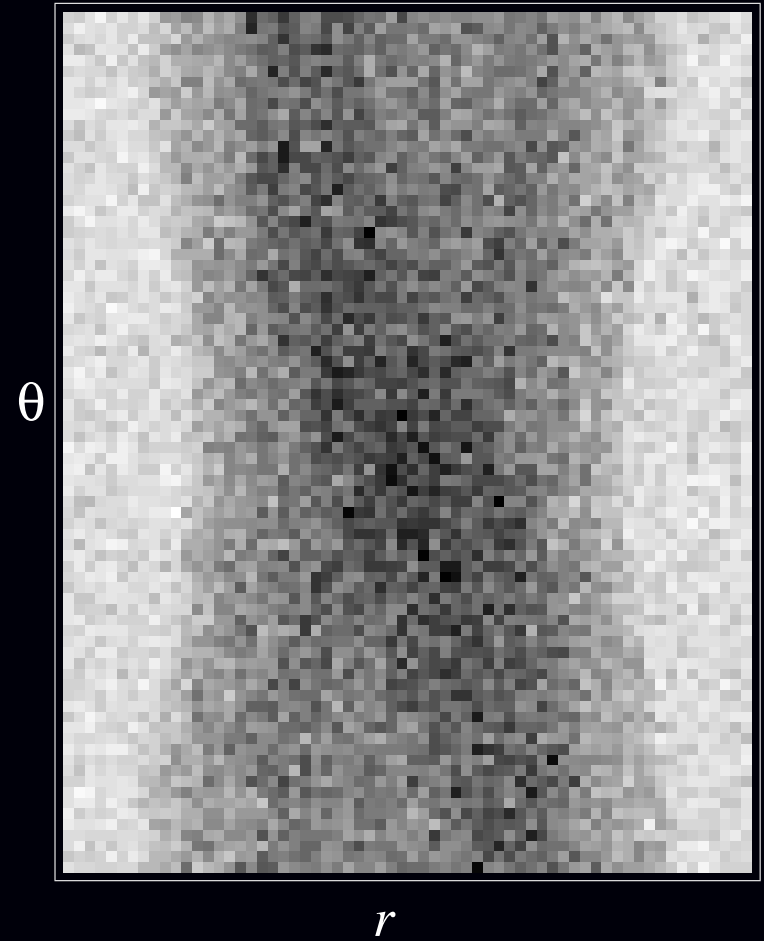
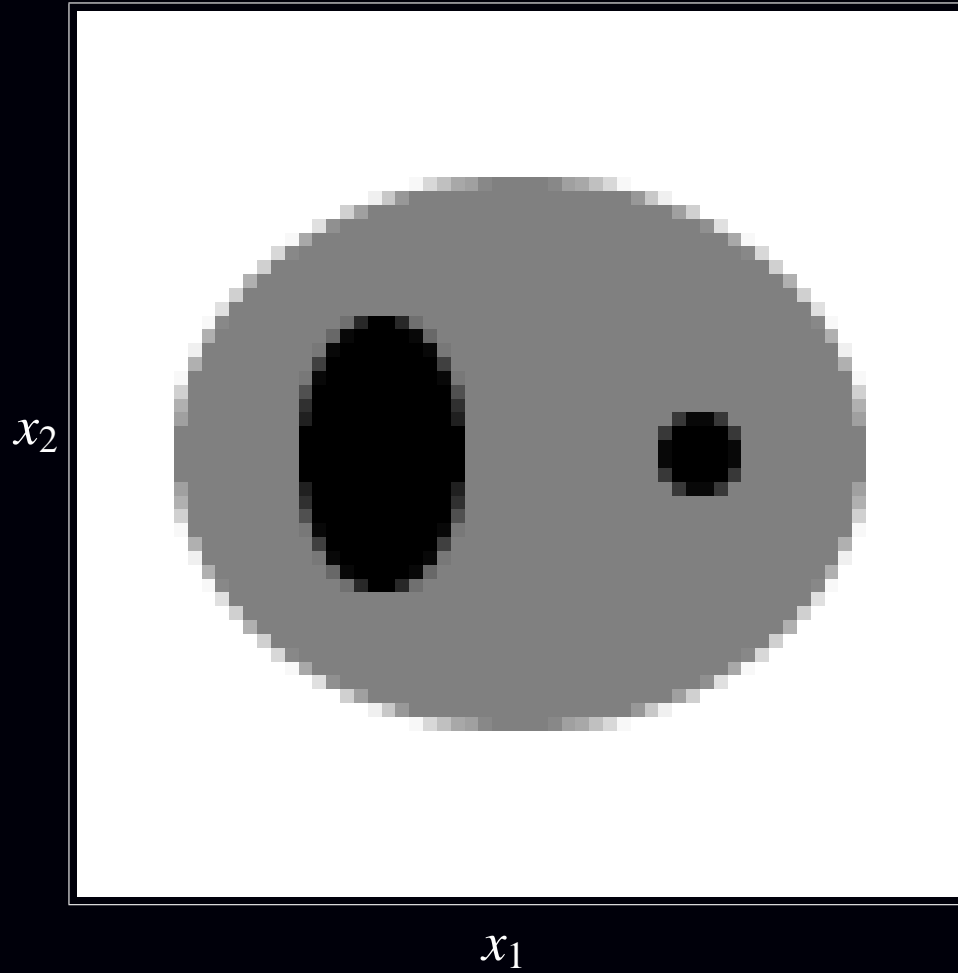
List-mode dynamic reconstruction problem:

$$\text{Estimate } \lambda(\vec{x}, t) \text{ given } \{(S_k, T_k)\}.$$

Emission Reconstruction Problem - Illustration

$\lambda(\vec{x})$

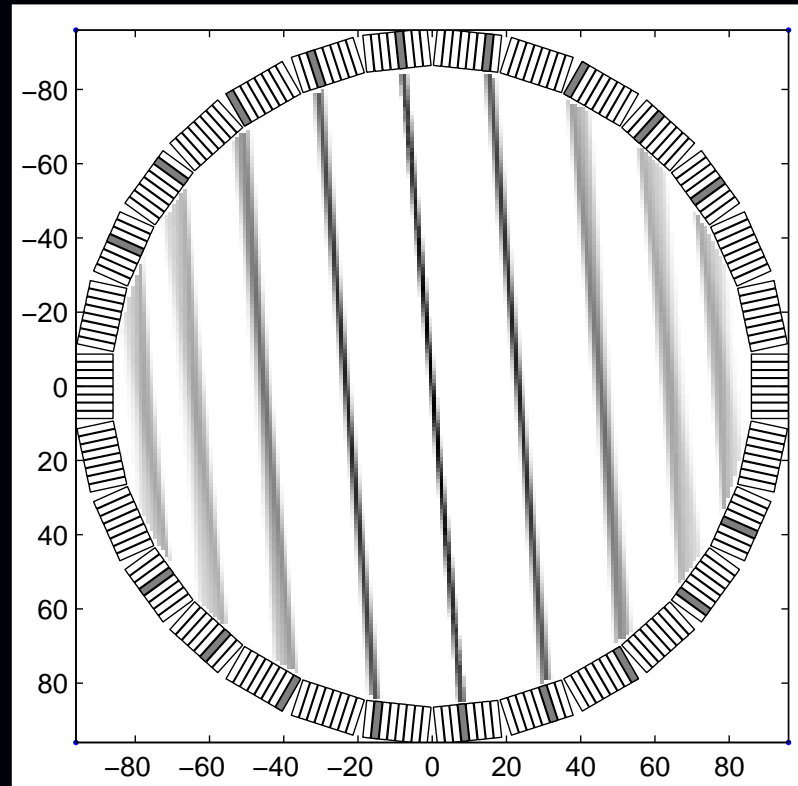
$\{Y_i\}$



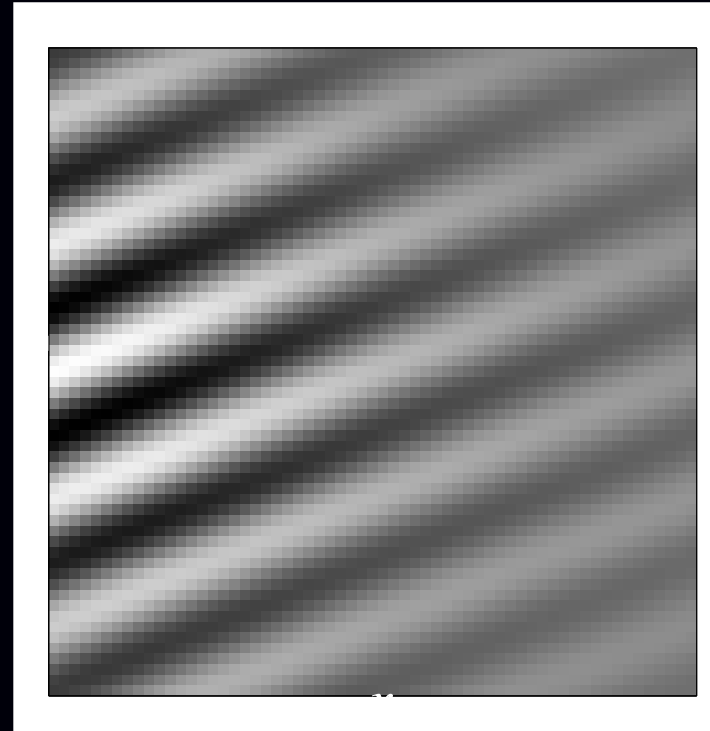
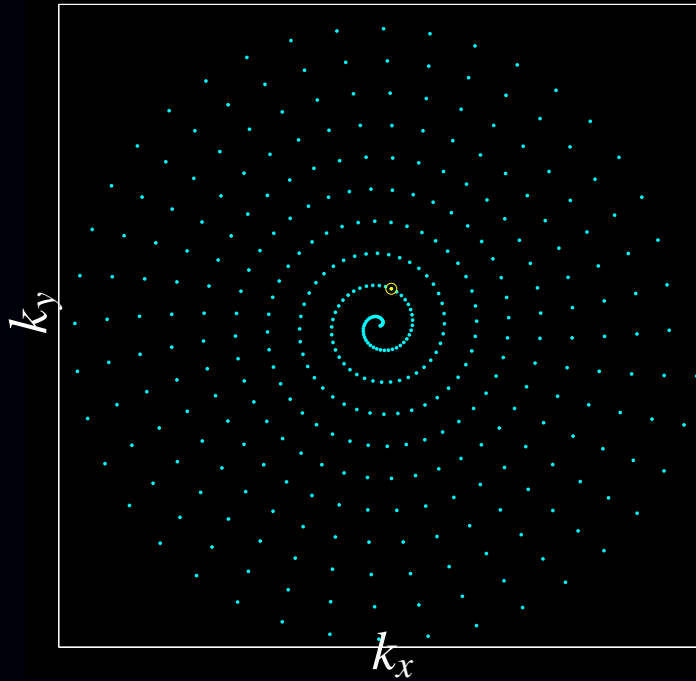
Part 1: Problem Statement(s)

Example: in PET, the goal is to reconstruct radiotracer distribution $\lambda(\vec{x})$ from photon pair coincidence measurements $\{y_i\}_{i=1}^{n_d}$, given the detector sensitivity patterns $s_i(\vec{x})$, $i = 1, \dots, n_d$, for each “line of response.”

Statistical model: $y_i \sim \text{Poisson} \left\{ \int \lambda(\vec{x}) s_i(\vec{x}) d\vec{x} + r_i \right\}$



Example: MRI “Sensitivity Pattern”



Each “k-space sample” involves the transverse magnetization $f(\vec{x})$ weighted by:

- sinusoidal (complex exponential) pattern corresponding to k-space location \vec{k}
- RF receive coil sensitivity pattern
- phase effects of field inhomogeneity
- spin relaxation effects.

$$y_i = \int f(\vec{x}) s_i(\vec{x}) d\vec{x} + \epsilon_i, \quad i = 1, \dots, n_d, \quad s_i(\vec{x}) = c_{\text{RF}}(\vec{x}) e^{-i\omega(\vec{x})t_i} e^{-t_i/T_2(\vec{x})} e^{-i2\pi\vec{k}(t_i)\cdot\vec{x}}$$

Continuous-Discrete Models

Emission tomography: $y_i \sim \text{Poisson}\left\{\int \lambda(\vec{x}) s_i(\vec{x}) d\vec{x} + r_i\right\}$

Transmission tomography (monoenergetic): $y_i \sim \text{Poisson}\left\{b_i \exp\left(-\int_{\mathcal{L}_i} \mu(\vec{x}) d\ell\right) + r_i\right\}$

Transmission (polyenergetic): $y_i \sim \text{Poisson}\left\{\int I_i(\mathcal{E}) \exp\left(-\int_{\mathcal{L}_i} \mu(\vec{x}, \mathcal{E}) d\ell\right) d\mathcal{E} + r_i\right\}$

Magnetic resonance imaging: $y_i = \int f(\vec{x}) s_i(\vec{x}) d\vec{x} + \varepsilon_i$

Discrete measurements $\mathbf{y} = (y_1, \dots, y_{n_d})$

Continuous-space unknowns: $\lambda(\vec{x}), \mu(\vec{x}), f(\vec{x})$

Goal: estimate $f(\vec{x})$ given \mathbf{y}

Solution options:

- Continuous-continuous formulations (“analytical”)
- Continuous-discrete formulations
usually $\hat{f}(\vec{x}) = \sum_{i=1}^{n_d} c_i s_i(\vec{x})$
- Discrete-discrete formulations $f(\vec{x}) \approx \sum_{j=1}^{n_p} x_j b_j(\vec{x})$

Part 2: Five Categories of Choices

- Object parameterization: function $f(\vec{r})$ vs finite coefficient vector x
- System physical model: $\{s_i(\vec{r})\}$
- Measurement statistical model $y_i \sim \boxed{?}$
- Cost function: data-mismatch and regularization
- Algorithm / initialization

No perfect choices - one can critique all approaches!

Choice 1. Object Parameterization

Finite measurements: $\{y_i\}_{i=1}^{n_d}$.

Continuous object: $f(\vec{r})$.

Hopeless?

“All models are wrong but some models are useful.”

Linear *series expansion* approach. Replace $f(\vec{r})$ by $\mathbf{x} = (x_1, \dots, x_{n_p})$ where

$$f(\vec{r}) \approx \tilde{f}(\vec{r}) = \sum_{j=1}^{n_p} x_j b_j(\vec{r}) \leftarrow \text{“basis functions”}$$

Forward projection:

$$\begin{aligned} \int s_i(\vec{r}) f(\vec{r}) d\vec{r} &= \int s_i(\vec{r}) \left[\sum_{j=1}^{n_p} x_j b_j(\vec{r}) \right] d\vec{r} = \sum_{j=1}^{n_p} \left[\int s_i(\vec{r}) b_j(\vec{r}) d\vec{r} \right] x_j \\ &= \sum_{j=1}^{n_p} a_{ij} x_j = [\mathbf{Ax}]_i, \quad \text{where } a_{ij} \triangleq \int s_i(\vec{r}) b_j(\vec{r}) d\vec{r} \end{aligned}$$

- Projection integrals become finite summations.
- a_{ij} is contribution of j th basis function (e.g., voxel) to i th measurement.
- The units of a_{ij} and x_j depend on the user-selected units of $b_j(\vec{r})$.
- The $n_d \times n_p$ matrix $\mathbf{A} = \{a_{ij}\}$ is called the *system matrix*.

(Linear) Basis Function Choices

- Fourier series (complex / not sparse)
- Circular harmonics (complex / not sparse)
- Wavelets (negative values / not sparse)
- Kaiser-Bessel window functions (blobs)
- Overlapping circles (disks) or spheres (balls)
- Polar grids, logarithmic polar grids
- “Natural pixels” $\{s_i(\vec{r})\}$
- B-splines (pyramids)
- Rectangular **pixels** / **voxels** (rect functions)
- Point masses / bed-of-nails / lattice of points / “comb” function
- Organ-based voxels (e.g., from CT in PET/CT systems)
- ...

Basis Function Considerations

Mathematical

- Represent $f(\vec{r})$ “well” with moderate n_p (approximation accuracy)
- e.g., represent a constant (uniform) function
- Orthogonality? (not essential)
- Linear independence (ensures uniqueness of expansion)
- Insensitivity to shift of basis-function grid (approximate shift invariance)
- Rotation invariance

Computational

- “Easy” to compute a_{ij} values and/or Ax
- If stored, the system matrix A should be sparse (mostly zeros).
- Easy to represent nonnegative functions e.g., if $x_j \geq 0$, then $f(\vec{r}) \geq 0$.
A sufficient condition is $b_j(\vec{r}) \geq 0$.

Nonlinear Object Parameterizations

Estimation of intensity *and* shape (e.g., location, radius, etc.)

Surface-based (homogeneous) models

- Circles / spheres
- Ellipses / ellipsoids
- Superquadrics
- Polygons
- Bi-quadratic triangular Bezier patches, ...

Other models

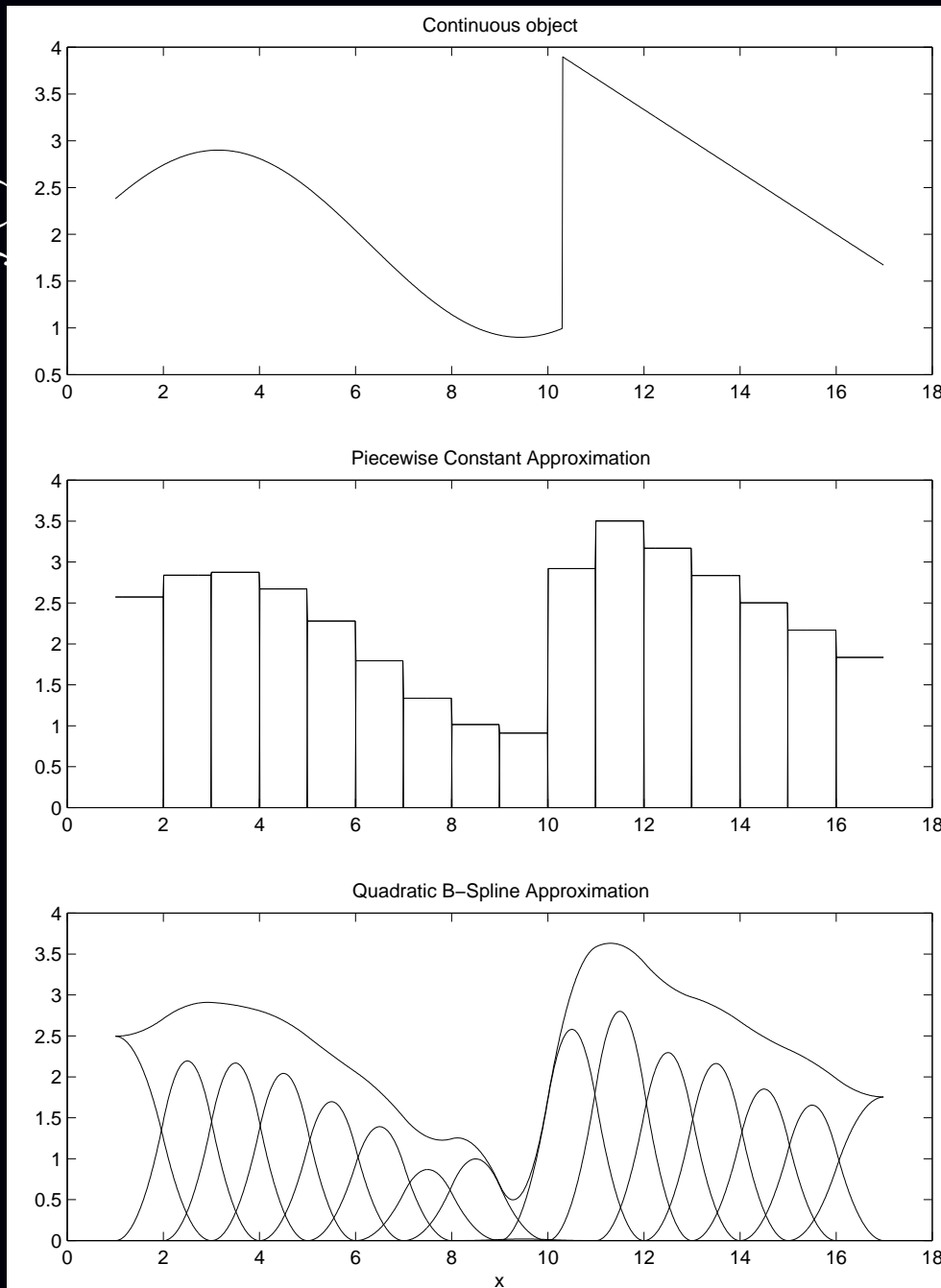
- Generalized series $f(\vec{r}) = \sum_j x_j b_j(\vec{r}, \theta)$
- Deformable templates $f(\vec{r}) = b(T_\theta(\vec{r}))$
- ...

Considerations

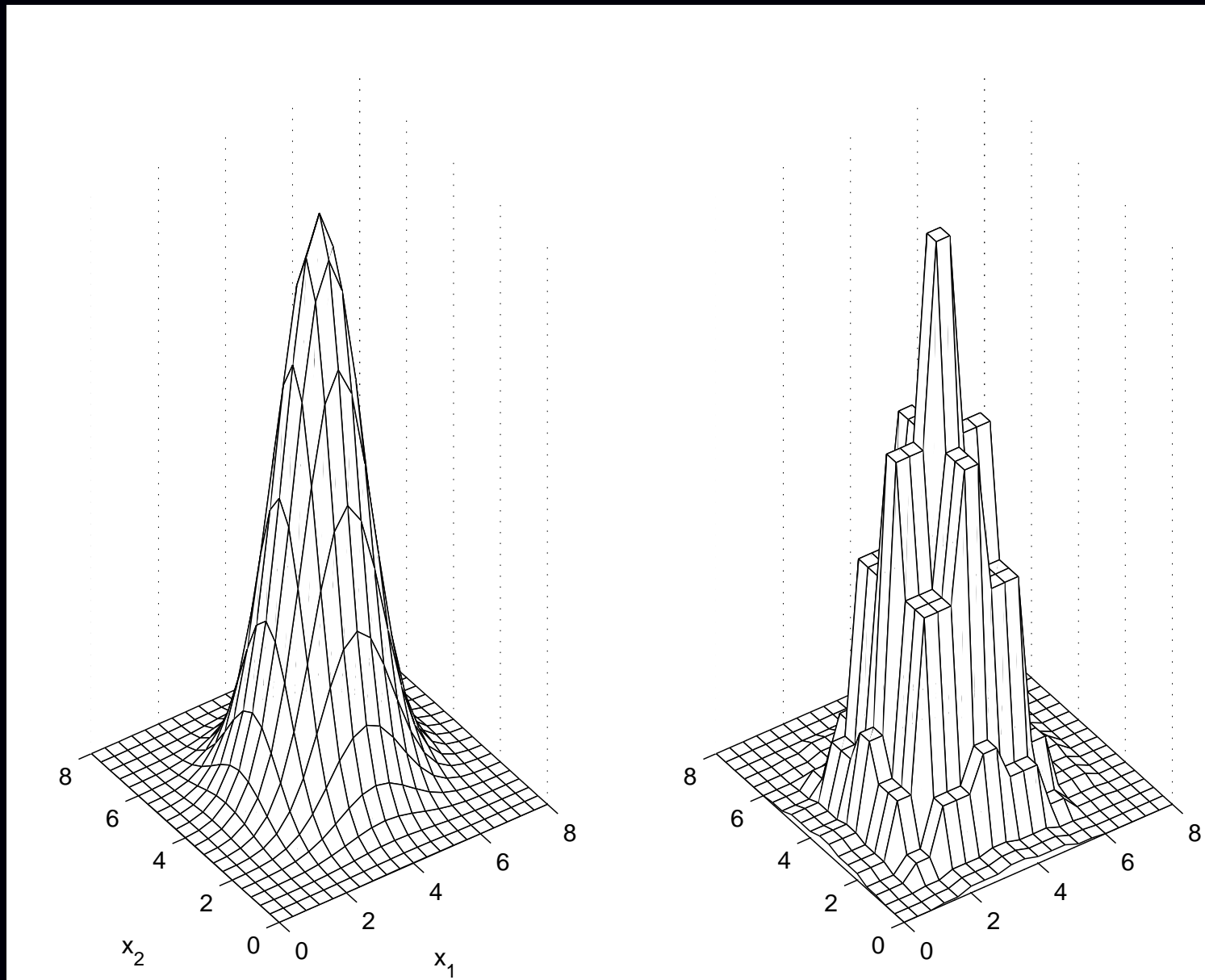
- Can be considerably more parsimonious
- If correct, yield greatly reduced estimation error
- Particularly compelling in limited-data problems
- Often oversimplified (all models are wrong but...)
- Nonlinear dependence on location induces non-convex cost functions, complicating optimization

Example Basis Functions - 1D

$f(\vec{r})$



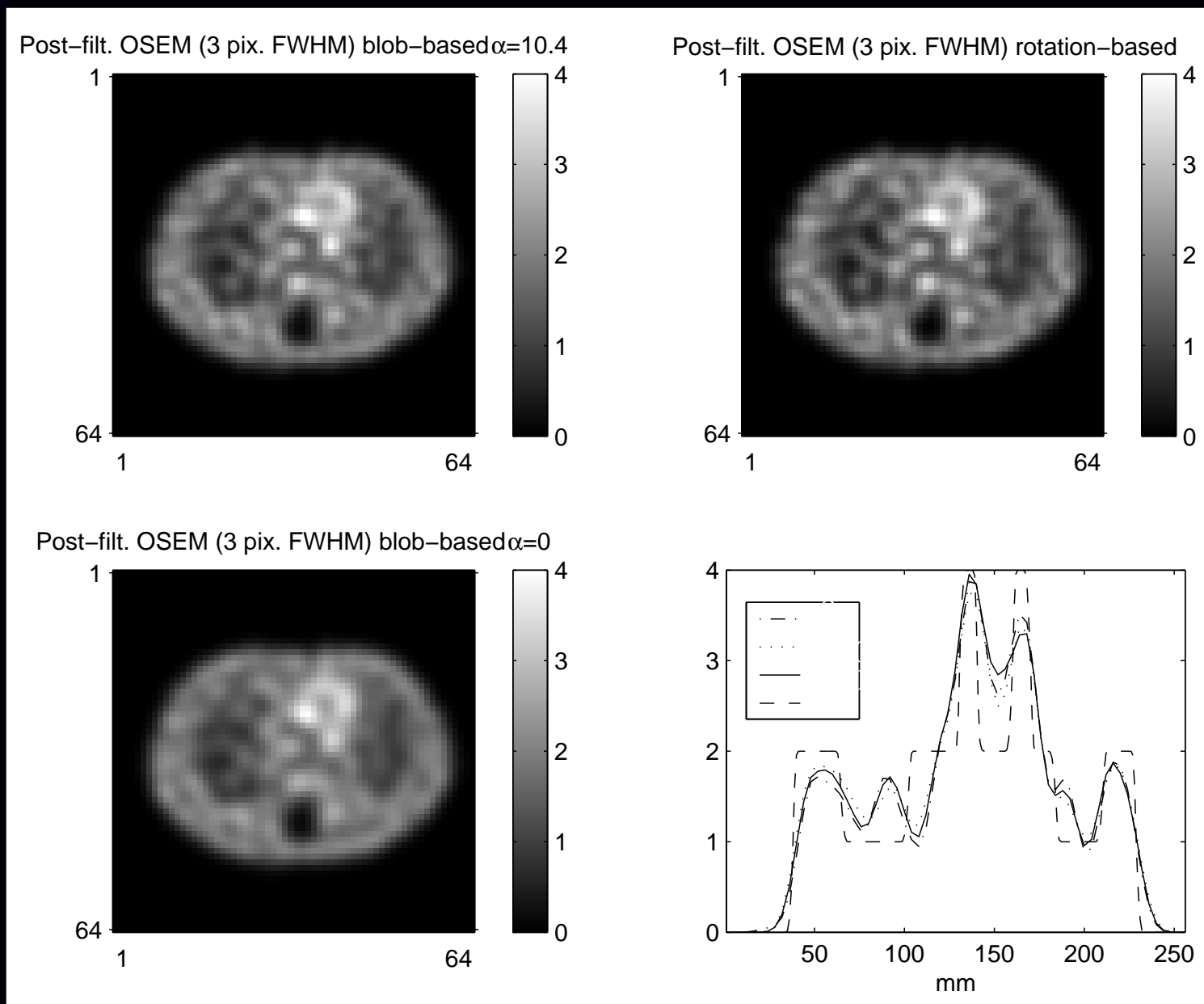
Pixel Basis Functions - 2D



Continuous image $f(\vec{r})$

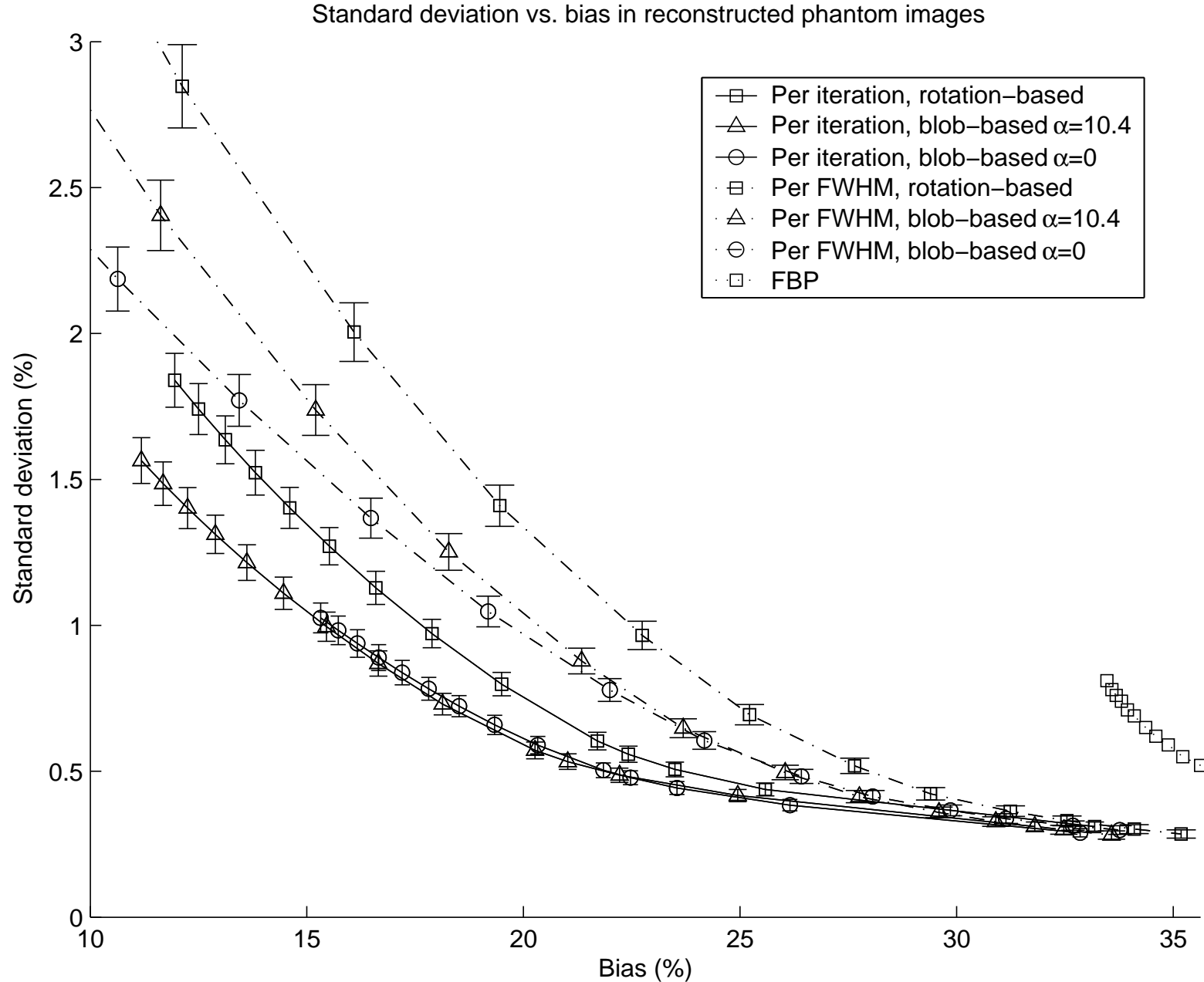
Pixel basis approximation
 $\sum_{j=1}^{n_p} x_j b_j(\vec{r})$

Blobs in SPECT: Qualitative



(2D SPECT thorax phantom simulations)

Blobs in SPECT: Quantitative



Discrete-Discrete Emission Reconstruction Problem

Having chosen a basis and *linearly* parameterized the emission density...

Estimate the emission density coefficient vector $\mathbf{x} = (x_1, \dots, x_{n_p})$ (aka “image”) using (something like) this statistical model:

$$y_i \sim \text{Poisson} \left\{ \sum_{j=1}^{n_p} a_{ij} x_j + r_i \right\}, \quad i = 1, \dots, n_d.$$

- $\{y_i\}_{i=1}^{n_d}$: observed counts from each detector unit
- $\mathbf{A} = \{a_{ij}\}$: system matrix (determined by system models)
- r_i 's : background contributions (determined separately)

Many image reconstruction problems are “find \mathbf{x} given \mathbf{y} ” where

$$y_i = g_i([\mathbf{A}\mathbf{x}]_i) + \varepsilon_i, \quad i = 1, \dots, n_d.$$

Choice 2. System Model, aka Physics

System matrix elements:
$$a_{ij} = \int s_i(\vec{r}) b_j(\vec{r}) d\vec{r}$$

- scan geometry
- collimator/detector response
- attenuation
- scatter (object, collimator, scintillator)
- duty cycle (dwell time at each angle)
- detector efficiency / dead-time losses
- positron range, noncollinearity, crystal penetration, ...
- ...

Considerations

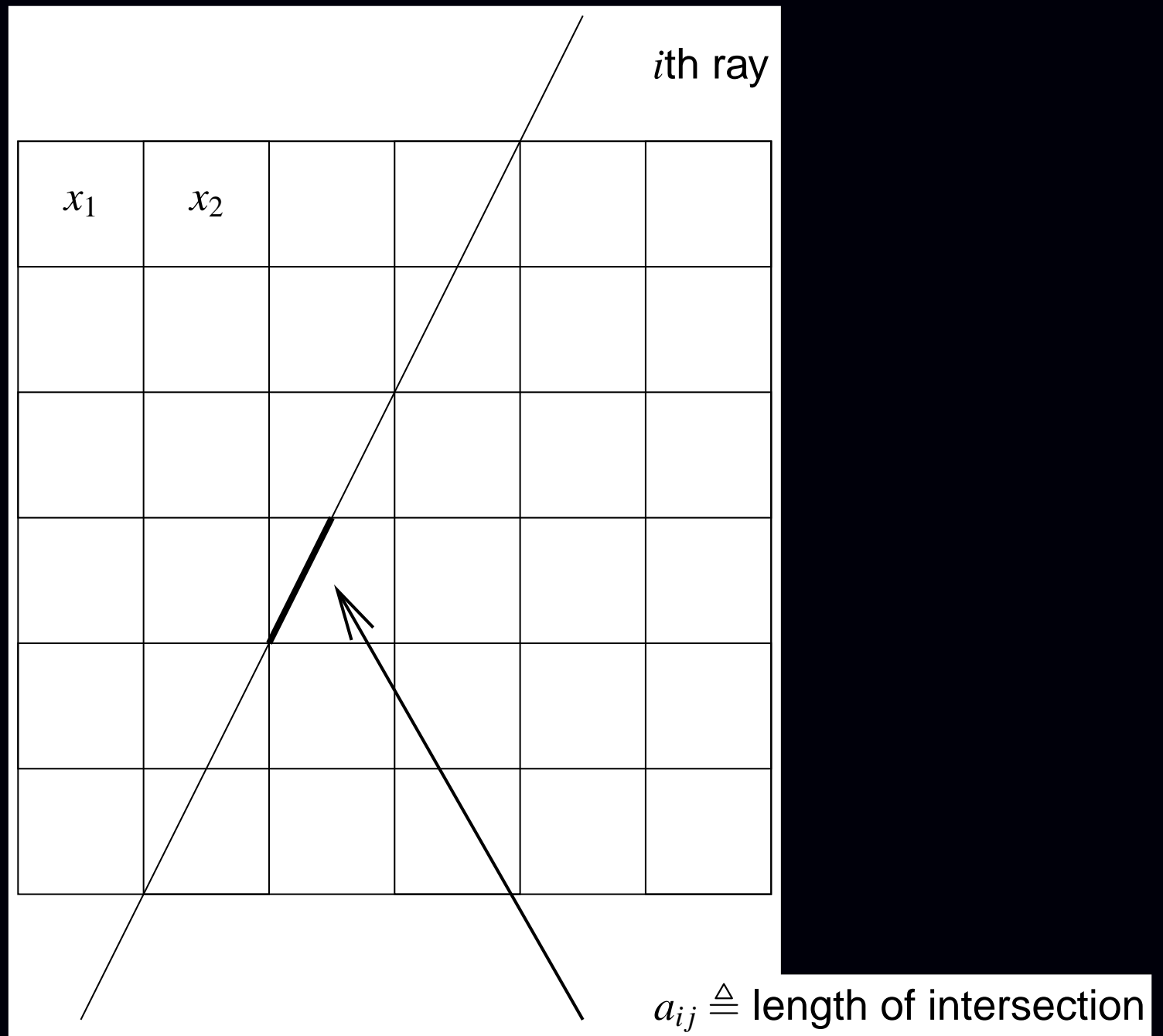
- Improving system model can improve
 - Quantitative accuracy
 - Spatial resolution
 - Contrast, SNR, detectability
- Computation time (and storage vs compute-on-fly)
- Model uncertainties
(e.g., calculated scatter probabilities based on noisy attenuation map)
- Artifacts due to over-simplifications

Measured System Model?

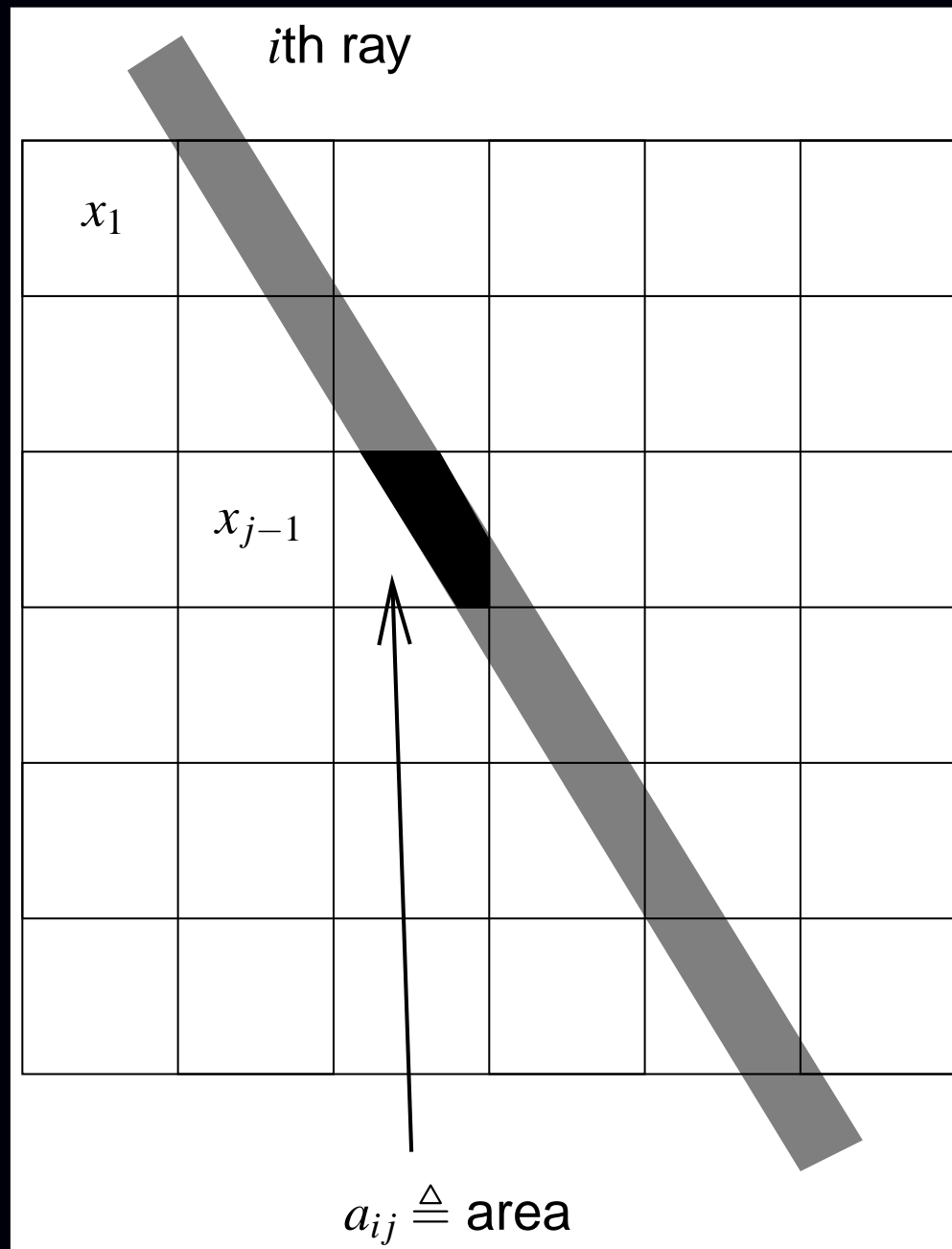
Determine a_{ij} 's by scanning a voxel-sized cube source over the imaging volume and recording counts in all detector units (separately for each voxel).

- Avoids mathematical model approximations
- Scatter / attenuation added later (object dependent), approximately
- Small probabilities \implies long scan times
- Storage
- Repeat for every voxel size of interest
- Repeat if detectors change

“Line Length” System Model for Tomography

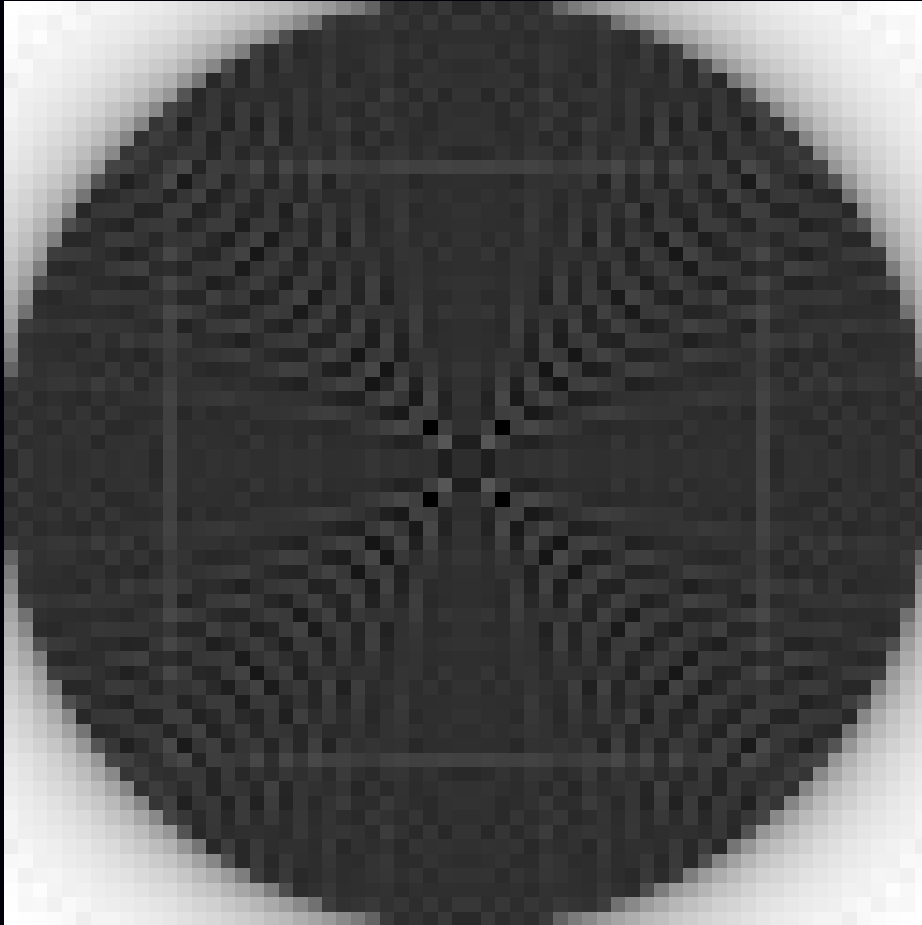


“Strip Area” System Model for Tomography

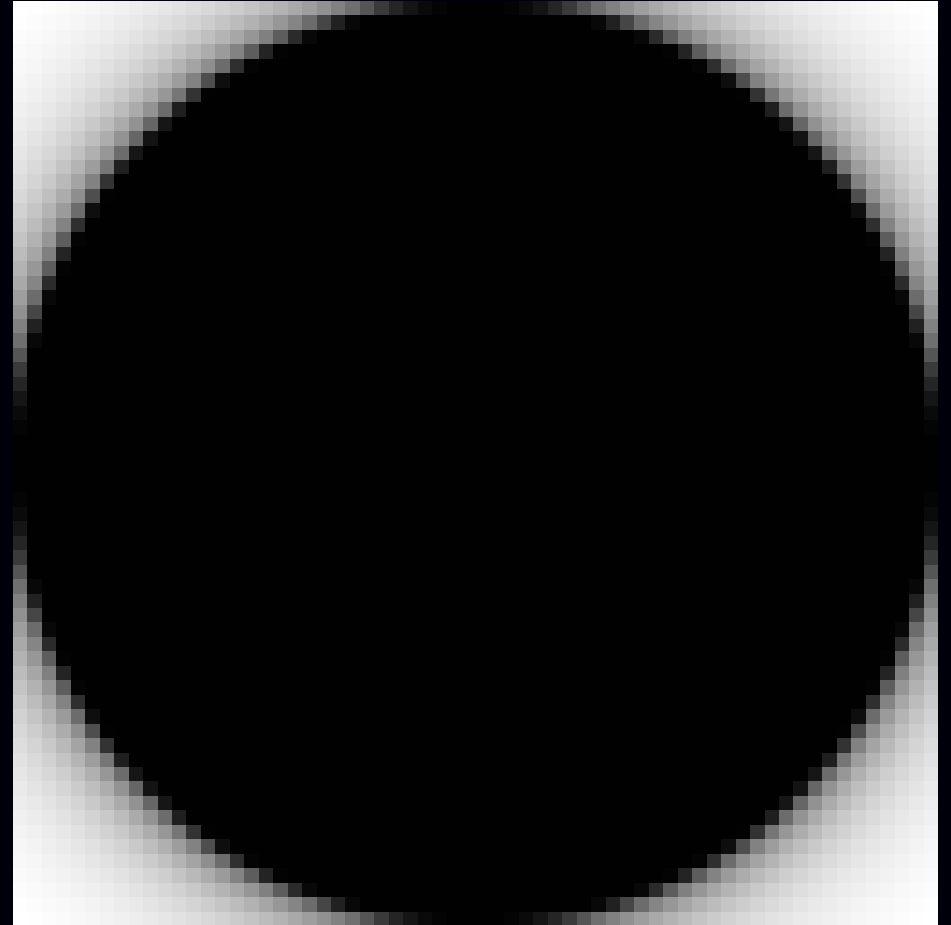


(Implicit) System Sensitivity Patterns

$$\sum_{i=1}^{n_d} a_{ij} \approx s(\vec{r}_j) = \sum_{i=1}^{n_d} s_i(\vec{r}_j)$$

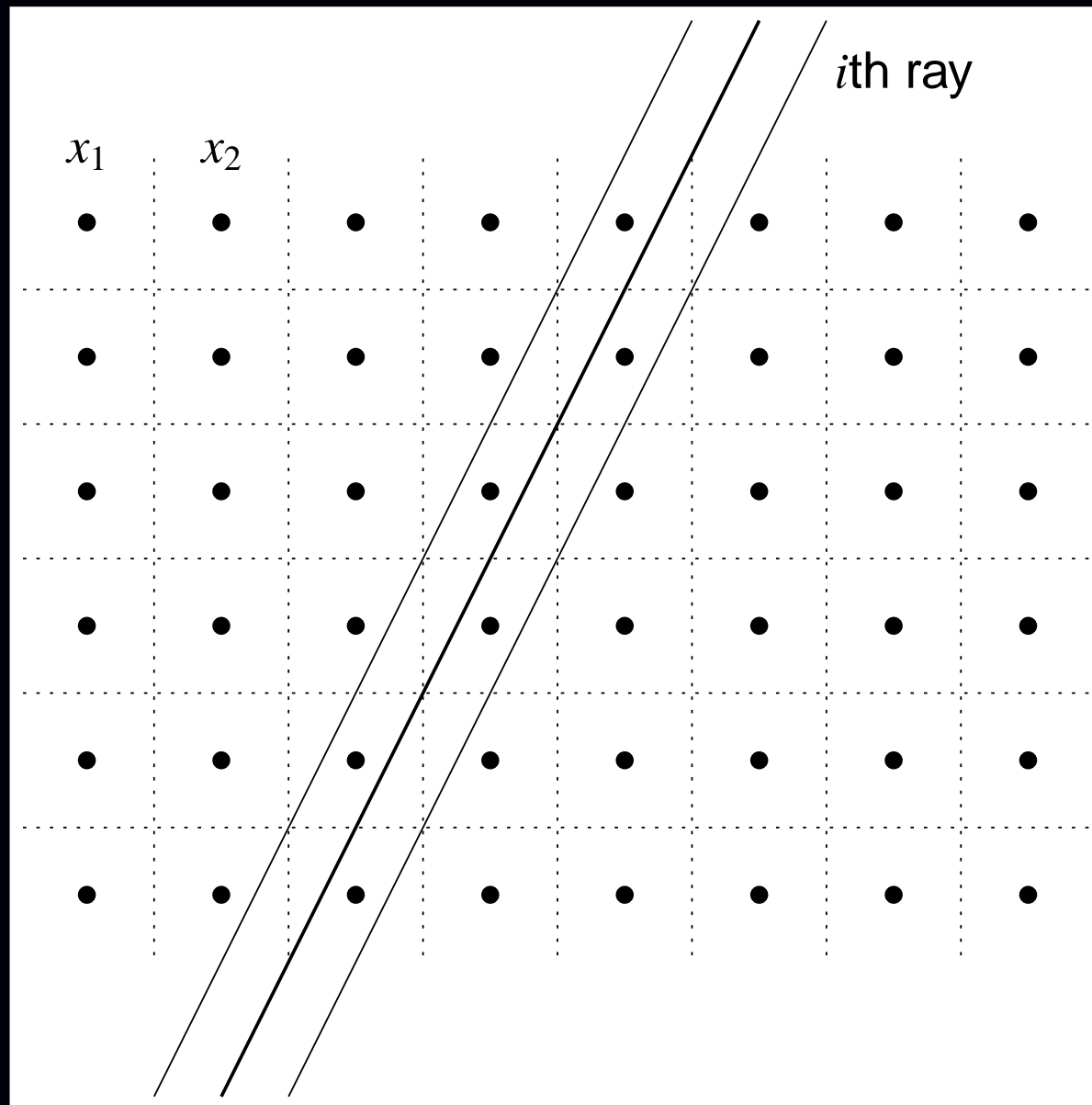


Line Length



Strip Area

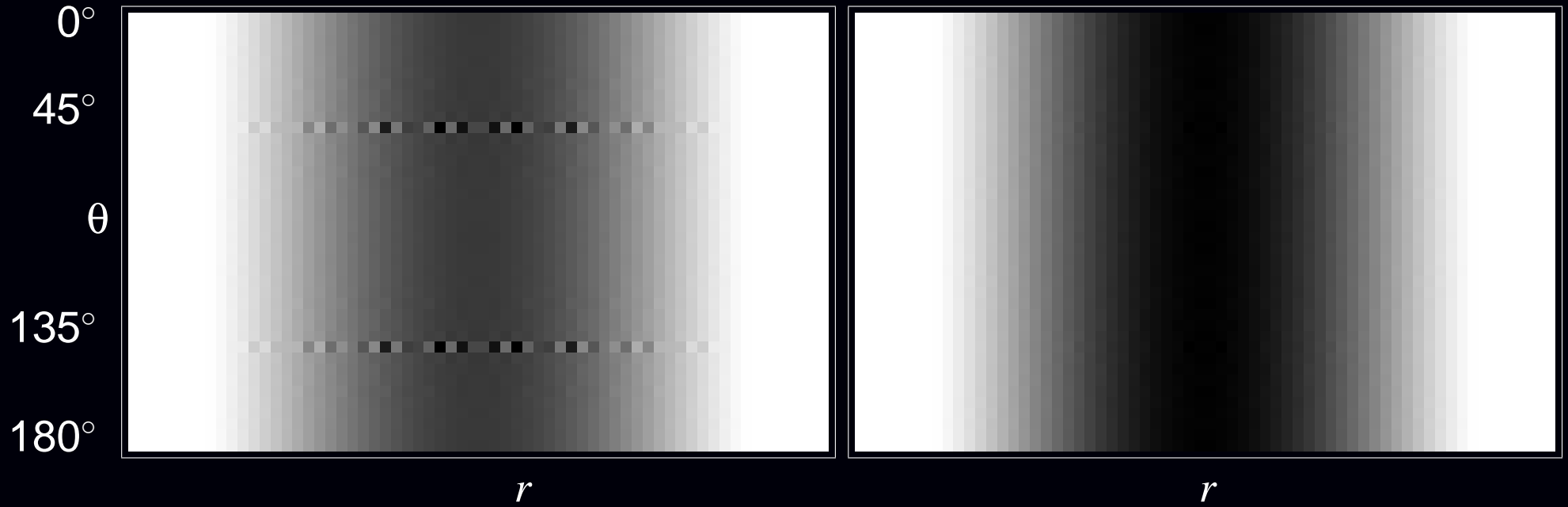
Point-Lattice Projector/Backprojector



a_{ij} 's determined by linear interpolation

Point-Lattice Artifacts

Projections (sinograms) of uniform disk object:



Point Lattice

Strip Area

Forward- / Back-projector “Pairs”

Forward projection (image domain to projection domain):

$$\bar{y}_i = \int s_i(\vec{r}) f(\vec{r}) d\vec{r} = \sum_{j=1}^{n_p} a_{ij} x_j = [\mathbf{Ax}]_i, \quad \text{or} \quad \bar{\mathbf{y}} = \mathbf{Ax}$$

Backprojection (projection domain to image domain):

$$\mathbf{A}'\mathbf{y} = \left\{ \sum_{i=1}^{n_d} a_{ij} y_i \right\}_{j=1}^{n_p}$$

The term “forward/backprojection pair” often corresponds to an implicit choice for the object basis and the system model.

Sometimes $\mathbf{A}'\mathbf{y}$ is implemented as \mathbf{By} for some “backprojector” $\mathbf{B} \neq \mathbf{A}'$

Least-squares solutions (for example):

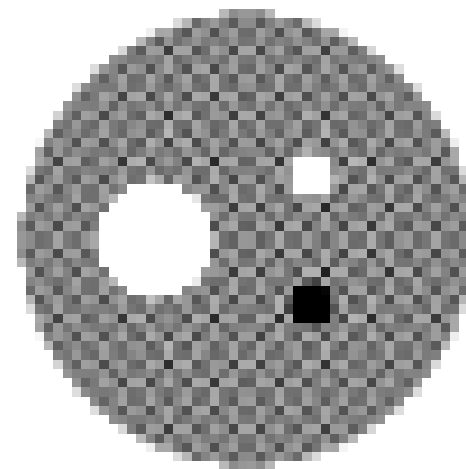
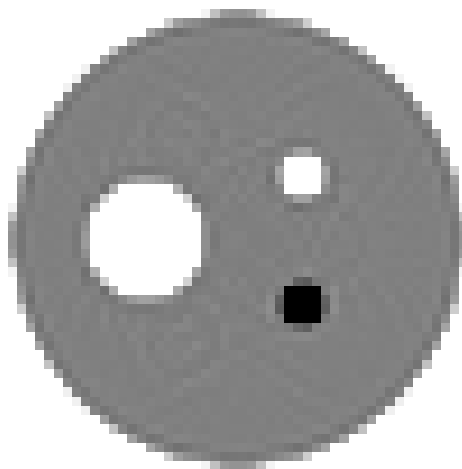
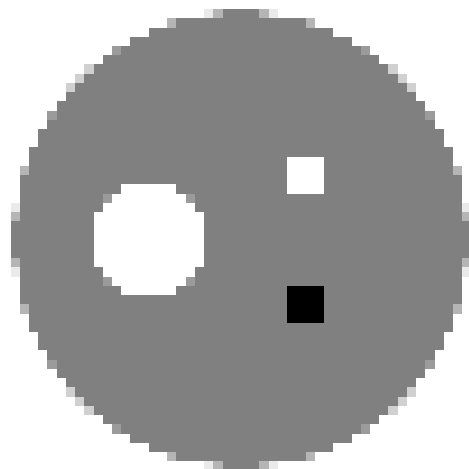
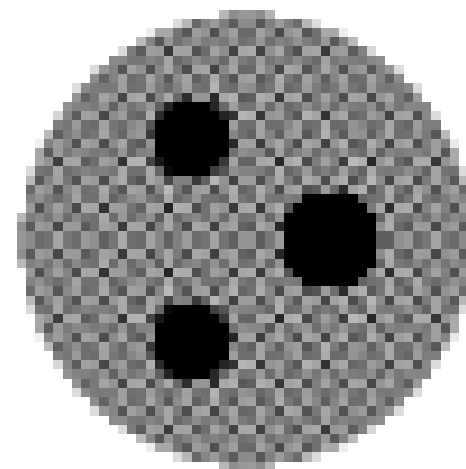
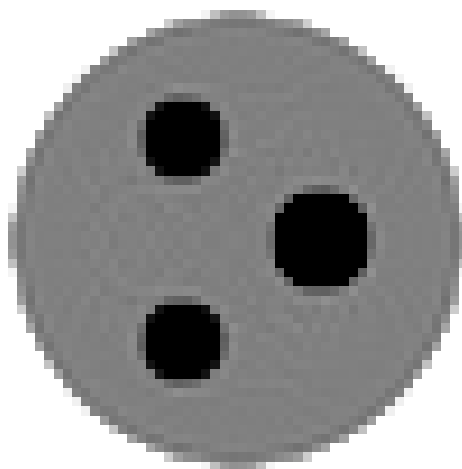
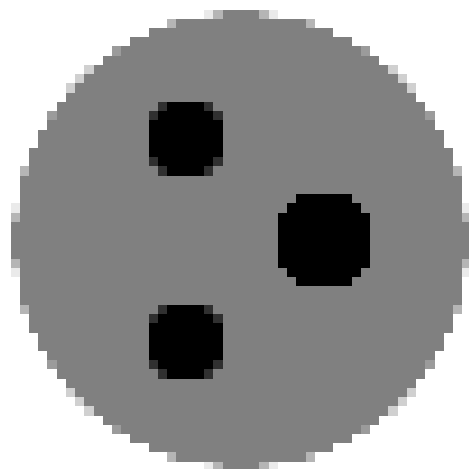
$$\hat{\mathbf{x}} = [\mathbf{A}'\mathbf{A}]^{-1} \mathbf{A}'\mathbf{y} \neq [\mathbf{BA}]^{-1} \mathbf{By}$$

Mismatched Backprojector $B \neq A'$

x

$\hat{x}(PWLS - CG)$

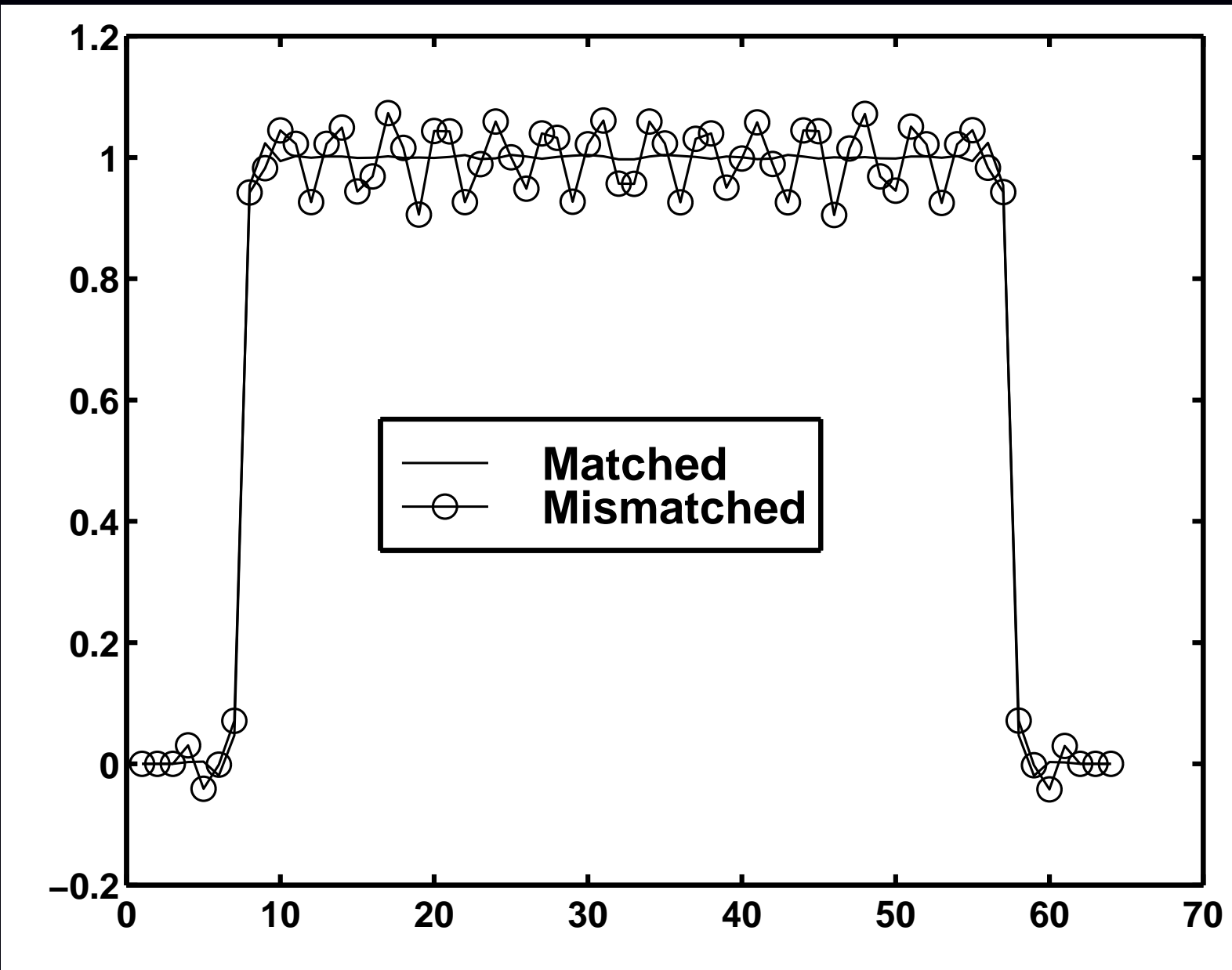
$\hat{x}(PWLS - CG)$



Matched

Mismatched

Horizontal Profiles



System Model Tricks

- **Factorize** (e.g., PET Gaussian detector response)

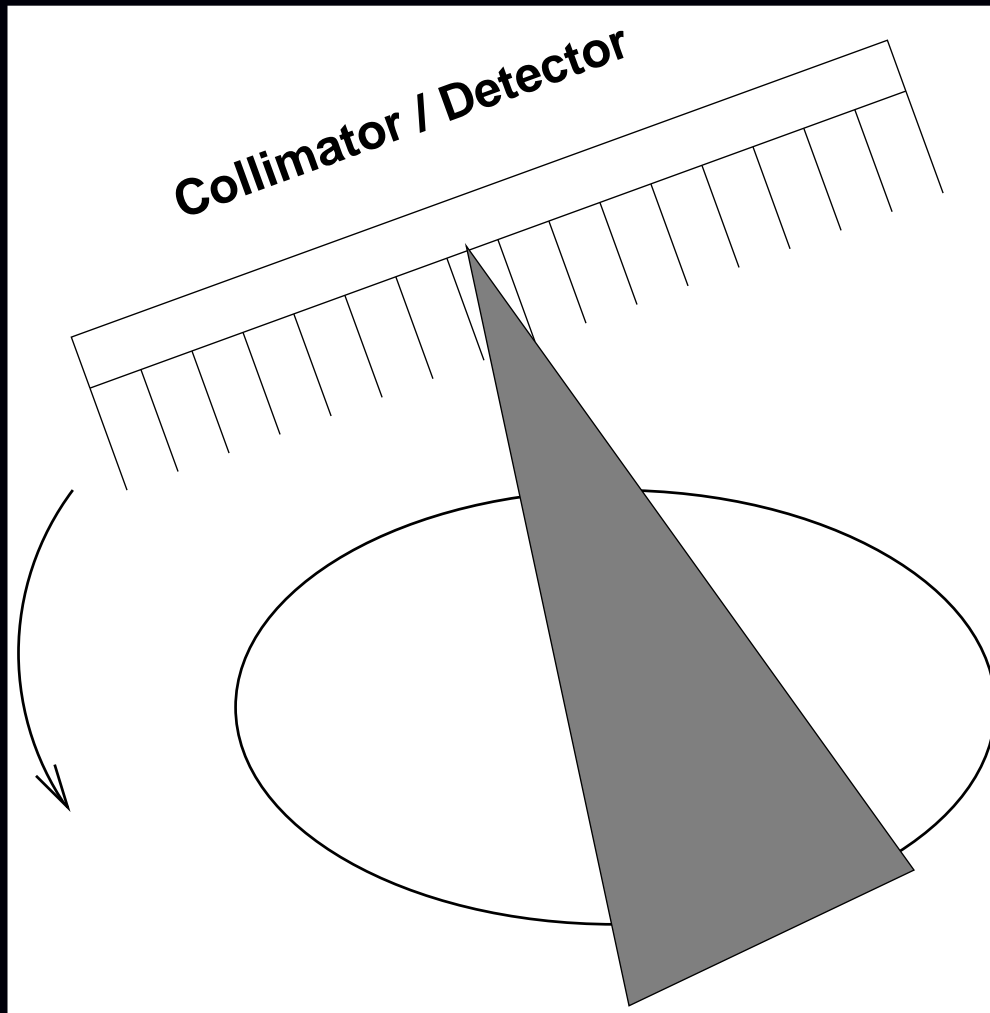
$$A \approx SG$$

(geometric projection followed by Gaussian smoothing)

- **Symmetry**
- **Rotate and Sum**
- **Gaussian diffusion**
for SPECT Gaussian detector response
- **Correlated Monte Carlo** (Beekman *et al.*)

In all cases, consistency of backprojector with A' requires care.

SPECT System Modeling



Complications: nonuniform attenuation, depth-dependent PSF, Compton scatter
(MR system models discussed in Part II)

Choice 3. Statistical Models

After modeling the system physics, we have a deterministic “model:”

$$y_i \approx g_i([\mathbf{Ax}]_i)$$

for some functions g_i , e.g., $g_i(l) = l + r_i$ for emission tomography.

Statistical modeling is concerned with the “ \approx ” aspect.

Considerations

- More accurate models:
 - can lead to lower variance images,
 - may incur additional computation,
 - may involve additional algorithm complexity
(e.g., proper transmission Poisson model has nonconcave log-likelihood)
- Statistical model errors (e.g., deadtime)
- Incorrect models (e.g., log-processed transmission data)

Statistical Model Choices for Emission Tomography

- “None.” Assume $\mathbf{y} - \mathbf{r} = \mathbf{Ax}$. “Solve algebraically” to find \mathbf{x} .
- White Gaussian noise. Ordinary least squares: minimize $\|\mathbf{y} - \mathbf{Ax}\|^2$
(This is the appropriate statistical model for MR.)
- Non-white Gaussian noise. Weighted least squares: minimize

$$\|\mathbf{y} - \mathbf{Ax}\|_{\mathbf{w}}^2 = \sum_{i=1}^{n_d} w_i (y_i - [\mathbf{Ax}]_i)^2, \quad \text{where} \quad [\mathbf{Ax}]_i \triangleq \sum_{j=1}^{n_p} a_{ij} x_j$$

(e.g., for Fourier rebinned (FORE) PET data)

- Ordinary Poisson model (ignoring or precorrecting for background)

$$y_i \sim \text{Poisson}\{[\mathbf{Ax}]_i\}$$

- Poisson model

$$y_i \sim \text{Poisson}\{[\mathbf{Ax}]_i + r_i\}$$

- Shifted Poisson model (for randoms precorrected PET)

$$y_i = y_i^{\text{prompt}} - y_i^{\text{delay}} \sim \text{Poisson}\{[\mathbf{Ax}]_i + 2r_i\} - 2r_i$$

Shifted Poisson model for PET

Precorrected random coincidences: $y_i = y_i^{\text{prompt}} - y_i^{\text{delay}}$

$$y_i^{\text{prompt}} \sim \text{Poisson}\{[\mathbf{A}\mathbf{x}]_i + r_i\}$$

$$y_i^{\text{delay}} \sim \text{Poisson}\{r_i\}$$

$$E[y_i] = [\mathbf{A}\mathbf{x}]_i$$

$$\text{Var}\{y_i\} = [\mathbf{A}\mathbf{x}]_i + 2r_i \quad \text{Mean} \neq \text{Variance} \implies \text{not Poisson!}$$

Statistical model choices

- Ordinary Poisson model: ignore randoms

$$[y_i]_+ \sim \text{Poisson}\{[\mathbf{A}\mathbf{x}]_i\}$$

Causes bias due to truncated negatives

- Data-weighted least-squares (Gaussian model):

$$y_i \sim \mathcal{N}([\mathbf{A}\mathbf{x}]_i, \hat{\sigma}_i^2), \quad \hat{\sigma}_i^2 = \max(y_i + 2\hat{r}_i, \sigma_{\min}^2)$$

Causes bias due to data-weighting

- Shifted Poisson model (matches 2 moments):

$$[y_i + 2\hat{r}_i]_+ \sim \text{Poisson}\{[\mathbf{A}\mathbf{x}]_i + 2\hat{r}_i\}$$

Insensitive to inaccuracies in \hat{r}_i .

One can further reduce bias by retaining negative values of $y_i + 2\hat{r}_i$.

Shifted-Poisson Model for X-ray CT

A model that includes both photon variability and electronic readout noise:

$$y_i \sim \text{Poisson}\{\bar{y}_i(\boldsymbol{\mu})\} + N(0, \sigma^2)$$

Shifted Poisson approximation

$$[y_i + \sigma^2]_+ \sim \text{Poisson}\{\bar{y}_i(\boldsymbol{\mu}) + \sigma^2\}$$

or just use WLS...

Complications:

- Intractability of likelihood for Poisson+Gaussian
- Compound Poisson distribution due to photon-energy-dependent detector signal.

X-ray statistical modeling is a current research area in several groups!

Choice 4. Cost Functions

Components:

- *Data-mismatch* term
- *Regularization* term (and regularization parameter β)
- Constraints (e.g., nonnegativity)

Cost function:

$$\Psi(\mathbf{x}) = \text{DataMismatch}(\mathbf{y}, \mathbf{Ax}) + \beta \text{Roughness}(\mathbf{x})$$

Reconstruct image $\hat{\mathbf{x}}$ by minimization:

$$\hat{\mathbf{x}} \triangleq \arg \min_{\mathbf{x} \geq 0} \Psi(\mathbf{x})$$

Actually *several* sub-choices to make for Choice 4 ...

Distinguishes “statistical methods” from “algebraic methods” for “ $\mathbf{y} = \mathbf{Ax}$.”

Why Cost Functions?

(vs “procedure” e.g., adaptive neural net with wavelet denoising)

Theoretical reasons

ML is based on minimizing a cost function: the negative log-likelihood

- ML is asymptotically consistent
- ML is asymptotically unbiased
- ML is asymptotically efficient (under true statistical model...)
- **Estimation**: Penalized-likelihood achieves uniform CR bound asymptotically
- **Detection**: Qi and Huesman showed analytically that MAP reconstruction outperforms FBP for SKE/BKE lesion detection (T-MI, Aug. 2001)

Practical reasons

- Stability of estimates (if Ψ and algorithm chosen properly)
- Predictability of properties (despite nonlinearities)
- Empirical evidence (?)

Bayesian Framework

Given a prior distribution $p(\mathbf{x})$ for image vectors \mathbf{x} , by Bayes' rule:

$$\text{posterior: } p(\mathbf{x}|\mathbf{y}) = p(\mathbf{y}|\mathbf{x}) p(\mathbf{x}) / p(\mathbf{y})$$

so

$$\log p(\mathbf{x}|\mathbf{y}) = \log p(\mathbf{y}|\mathbf{x}) + \log p(\mathbf{x}) - \log p(\mathbf{y})$$

- $-\log p(\mathbf{y}|\mathbf{x})$ corresponds to data mismatch term (negative log-likelihood)
- $-\log p(\mathbf{x})$ corresponds to regularizing penalty function

Maximum a posteriori (MAP) estimator:

$$\hat{\mathbf{x}} = \arg \max_{\mathbf{x}} \log p(\mathbf{x}|\mathbf{y}) = \arg \max_{\mathbf{x}} \log p(\mathbf{y}|\mathbf{x}) + \log p(\mathbf{x})$$

- Has certain optimality properties (provided $p(\mathbf{y}|\mathbf{x})$ and $p(\mathbf{x})$ are correct).
- Same form as Ψ

Choice 4.1: Data-Mismatch Term

Options (for emission tomography):

- Negative log-likelihood of statistical model. Poisson *emission* case:

$$-L(\mathbf{x}; \mathbf{y}) = -\log p(\mathbf{y}|\mathbf{x}) = \sum_{i=1}^{n_d} ([\mathbf{Ax}]_i + r_i) - y_i \log([\mathbf{Ax}]_i + r_i) + \log y_i!$$

- Ordinary (unweighted) least squares: $\sum_{i=1}^{n_d} \frac{1}{2} (y_i - \hat{r}_i - [\mathbf{Ax}]_i)^2$
- Data-weighted least squares: $\sum_{i=1}^{n_d} \frac{1}{2} (y_i - \hat{r}_i - [\mathbf{Ax}]_i)^2 / \hat{\sigma}_i^2$, $\hat{\sigma}_i^2 = \max(y_i + \hat{r}_i, \sigma_{\min}^2)$, (causes bias due to data-weighting).
- Reweighted least-squares: $\hat{\sigma}_i^2 = [\mathbf{Ax}]_i + \hat{r}_i$
- Model-weighted least-squares (nonquadratic, but convex!)

$$\sum_{i=1}^{n_d} \frac{1}{2} (y_i - \hat{r}_i - [\mathbf{Ax}]_i)^2 / ([\mathbf{Ax}]_i + \hat{r}_i)$$

- Nonquadratic cost-functions that are robust to outliers
- ...

Considerations

- Faithfulness to statistical model vs computation
- Ease of optimization (convex?, quadratic?)
- Effect of statistical modeling errors

Choice 4.2: Regularization

Forcing too much “data fit” gives noisy images

Ill-conditioned problems: small data noise causes large image noise

Solutions:

- Noise-reduction methods
- True regularization methods

Noise-reduction methods

- Modify the *data*
 - Prefilter or “denoise” the sinogram measurements
 - Extrapolate missing (e.g., truncated) data
- Modify an *algorithm* derived for an ill-conditioned problem
 - Stop algorithm before convergence
 - Run to convergence, post-filter
 - Toss in a filtering step every iteration or couple iterations
 - Modify update to “dampen” high-spatial frequencies

Noise-Reduction vs True Regularization

Advantages of **noise-reduction** methods

- Simplicity (?)
- Familiarity
- Appear less subjective than using penalty functions or priors
- Only fiddle factors are # of iterations, or amount of smoothing
- Resolution/noise tradeoff usually varies with iteration (stop when image looks good - in principle)
- Changing post-smoothing does not require re-iterating

Advantages of **true regularization** methods

- Stability (unique minimizer & convergence \implies initialization independence)
- Faster convergence
- Predictability
- Resolution can be made object independent
- Controlled resolution (e.g., spatially uniform, edge preserving)
- Start with reasonable image (e.g., FBP) \implies reach solution faster.

True Regularization Methods

Redefine the *problem* to eliminate ill-conditioning, rather than patching the data or algorithm!

Options

- Use bigger pixels (fewer basis functions)
 - Visually unappealing
 - Can only preserve edges coincident with pixel edges
 - Results become even less invariant to translations
- Method of sieves (constrain image roughness)
 - Condition number for “pre-emission space” can be even worse
 - Lots of iterations
 - Commutability condition rarely holds exactly in practice
 - Degenerates to post-filtering in some cases
- Change cost function by adding a roughness penalty / prior

$$\hat{\mathbf{x}} = \arg \min_x \Psi(\mathbf{x}), \quad \Psi(\mathbf{x}) = \mathcal{L}(\mathbf{x}) + \beta R(\mathbf{x})$$

- Disadvantage: apparently subjective choice of penalty
- Apparent difficulty in choosing penalty parameter(s), e.g., β (cf. apodizing filter / cutoff frequency in FBP)

Penalty Function Considerations

- Computation
- Algorithm complexity
- Uniqueness of minimizer of $\Psi(\mathbf{x})$
- Resolution properties (edge preserving?)
- # of adjustable parameters
- Predictability of properties (resolution and noise)

Choices

- separable vs nonseparable
- quadratic vs nonquadratic
- convex vs nonconvex

Penalty Functions: Separable vs Nonseparable

Separable

- Identity norm: $R(\mathbf{x}) = \frac{1}{2}\mathbf{x}'\mathbf{I}\mathbf{x} = \sum_{j=1}^{n_p} x_j^2/2$
penalizes large values of \mathbf{x} , but causes “squashing bias”
- Entropy: $R(\mathbf{x}) = \sum_{j=1}^{n_p} x_j \log x_j$
- Gaussian prior with mean μ_j , variance σ_j^2 : $R(\mathbf{x}) = \sum_{j=1}^{n_p} \frac{(x_j - \mu_j)^2}{2\sigma_j^2}$
- Gamma prior $R(\mathbf{x}) = \sum_{j=1}^{n_p} p(x_j, \mu_j, \sigma_j)$ where $p(x, \mu, \sigma)$ is Gamma pdf

The first two basically keep pixel values from “blowing up.”

The last two encourage pixels values to be close to prior means μ_j .

$$\text{General separable form: } R(\mathbf{x}) = \sum_{j=1}^{n_p} f_j(x_j)$$

Slightly simpler for minimization, but these do not explicitly enforce smoothness. The simplicity advantage has been overcome in newer algorithms.

Penalty Functions: Separable vs Nonseparable

Nonseparable (partially couple pixel values) to penalize *roughness*

x_1	x_2	x_3
x_4	x_5	

Example

$$R(\mathbf{x}) = (x_2 - x_1)^2 + (x_3 - x_2)^2 + (x_5 - x_4)^2 + (x_4 - x_1)^2 + (x_5 - x_2)^2$$

2	2	2
2	1	

$$R(\mathbf{x}) = 1$$

3	3	1
2	2	

$$R(\mathbf{x}) = 6$$

1	3	1
2	2	

$$R(\mathbf{x}) = 10$$

Rougher images \implies larger $R(\mathbf{x})$ values

Roughness Penalty Functions

First-order neighborhood and pairwise pixel differences:

$$R(\mathbf{x}) = \sum_{j=1}^{n_p} \frac{1}{2} \sum_{k \in \mathcal{N}_j} \psi(x_j - x_k)$$

$\mathcal{N}_j \triangleq$ *neighborhood* of j th pixel (e.g., left, right, up, down)
 ψ called the *potential function*

Finite-difference approximation to continuous roughness measure:

$$R(f(\cdot)) = \int \|\nabla f(\vec{r})\|^2 d\vec{r} = \int \left| \frac{\partial}{\partial x} f(\vec{r}) \right|^2 + \left| \frac{\partial}{\partial y} f(\vec{r}) \right|^2 + \left| \frac{\partial}{\partial z} f(\vec{r}) \right|^2 d\vec{r}.$$

Second derivatives also useful:
(More choices!)

$$\left. \frac{\partial^2}{\partial x^2} f(\vec{r}) \right|_{\vec{r}=\vec{r}_j} \approx f(\vec{r}_{j+1}) - 2f(\vec{r}_j) + f(\vec{r}_{j-1})$$

$$R(\mathbf{x}) = \sum_{j=1}^{n_p} \psi(x_{j+1} - 2x_j + x_{j-1}) + \dots$$

Penalty Functions: General Form

$$R(\mathbf{x}) = \sum_k \psi_k([\mathbf{C}\mathbf{x}]_k) \quad \text{where} \quad [\mathbf{C}\mathbf{x}]_k = \sum_{j=1}^{n_p} c_{kj}x_j$$

Example:

x_1	x_2	x_3
x_4	x_5	

$$\mathbf{C}\mathbf{x} = \begin{bmatrix} -1 & 1 & 0 & 0 & 0 \\ 0 & -1 & 1 & 0 & 0 \\ 0 & 0 & 0 & -1 & 1 \\ -1 & 0 & 0 & 1 & 0 \\ 0 & -1 & 0 & 0 & 1 \end{bmatrix} \begin{bmatrix} x_1 \\ x_2 \\ x_3 \\ x_4 \\ x_5 \end{bmatrix} = \begin{bmatrix} x_2 - x_1 \\ x_3 - x_2 \\ x_5 - x_4 \\ x_4 - x_1 \\ x_5 - x_2 \end{bmatrix}$$

$$\begin{aligned} R(\mathbf{x}) &= \sum_{k=1}^5 \psi_k([\mathbf{C}\mathbf{x}]_k) \\ &= \psi_1(x_2 - x_1) + \psi_2(x_3 - x_2) + \psi_3(x_5 - x_4) + \psi_4(x_4 - x_1) + \psi_5(x_5 - x_2) \end{aligned}$$

Penalty Functions: Quadratic vs Nonquadratic

$$R(\mathbf{x}) = \sum_k \psi_k([\mathbf{C}\mathbf{x}]_k)$$

Quadratic ψ_k

If $\psi_k(t) = t^2/2$, then $R(\mathbf{x}) = \frac{1}{2}\mathbf{x}'\mathbf{C}'\mathbf{C}\mathbf{x}$, a quadratic form.

- Simpler optimization
- Global smoothing

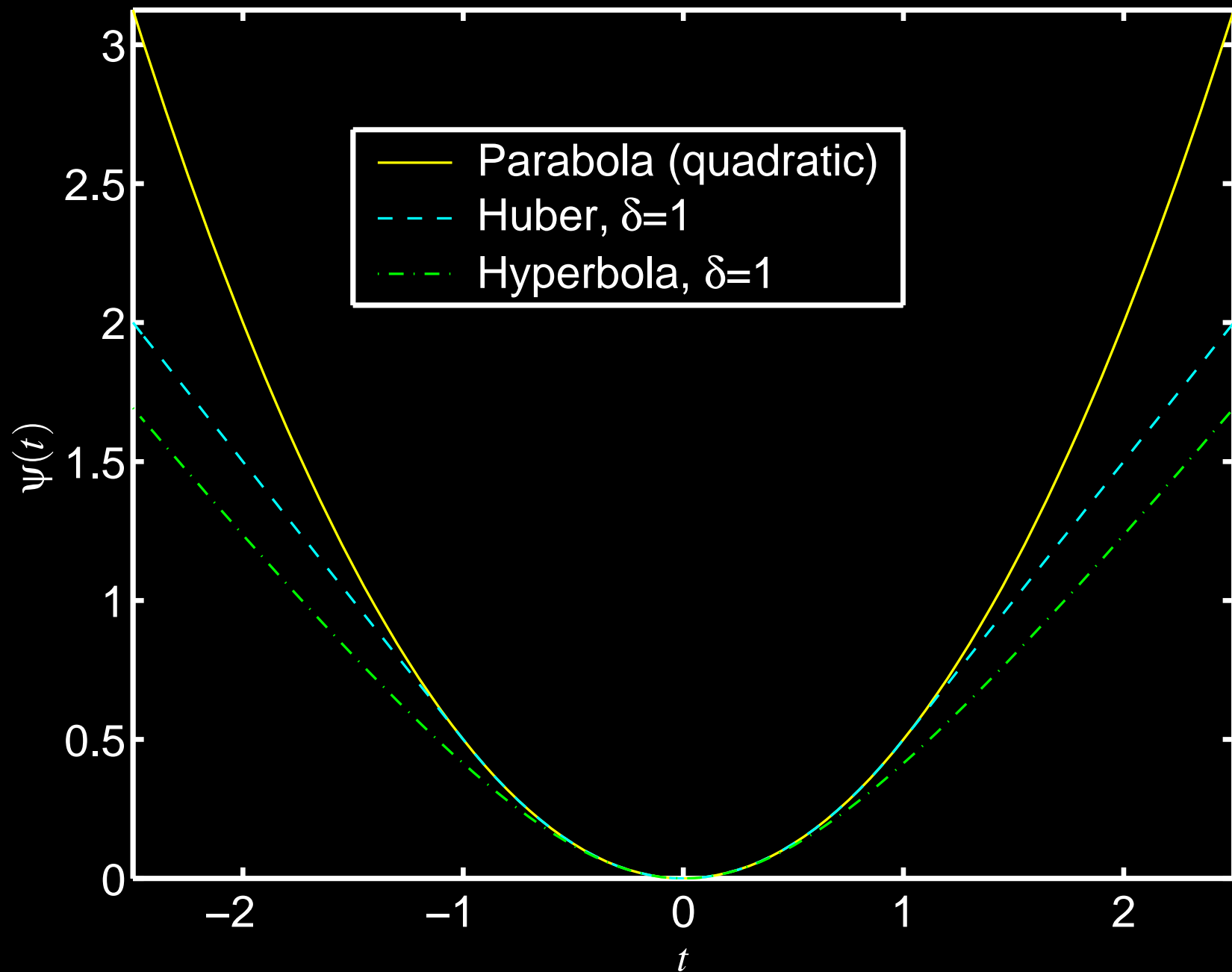
Nonquadratic ψ_k

- Edge preserving
- More complicated optimization. (This is essentially solved in convex case.)
- Unusual noise properties
- Analysis/prediction of resolution and noise properties is difficult
- More adjustable parameters (e.g., δ)

Example: Huber function. $\psi(t) \triangleq \begin{cases} t^2/2, & |t| \leq \delta \\ \delta|t| - \delta^2/2, & |t| > \delta \end{cases}$

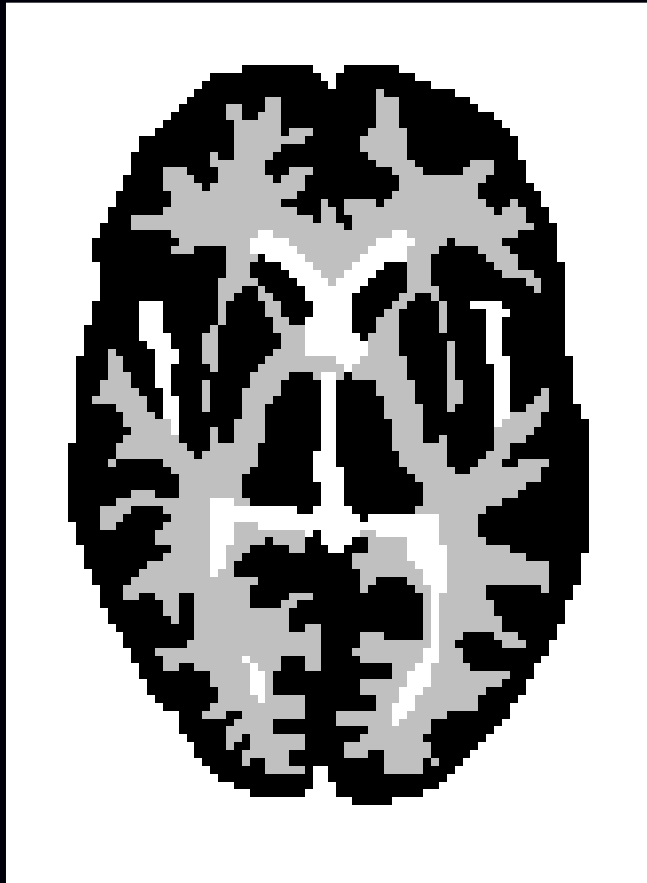
Example: Hyperbola function. $\psi(t) \triangleq \delta^2 \left(\sqrt{1 + (t/\delta)^2} - 1 \right)$

Quadratic vs Non-quadratic Potential Functions

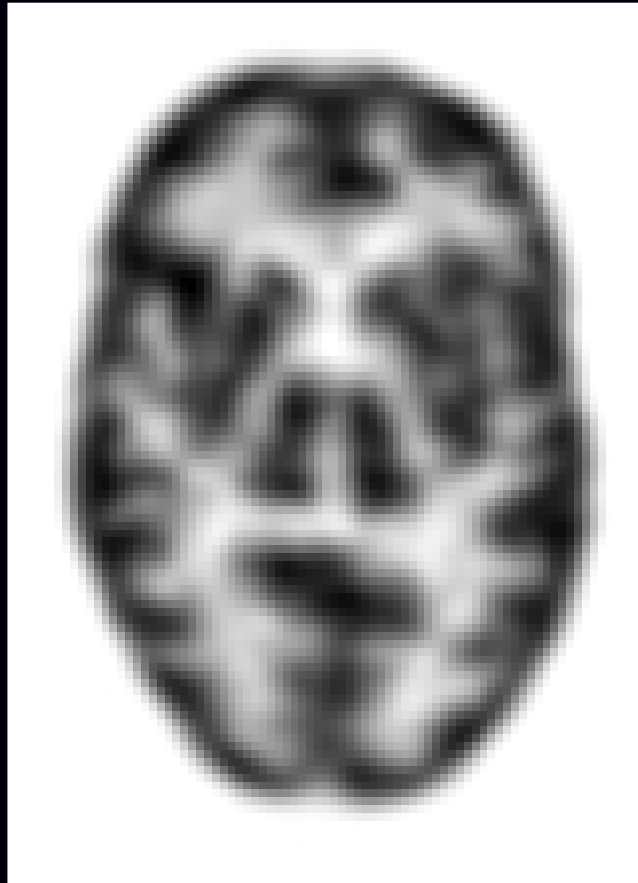


Lower cost for large differences \implies edge preservation

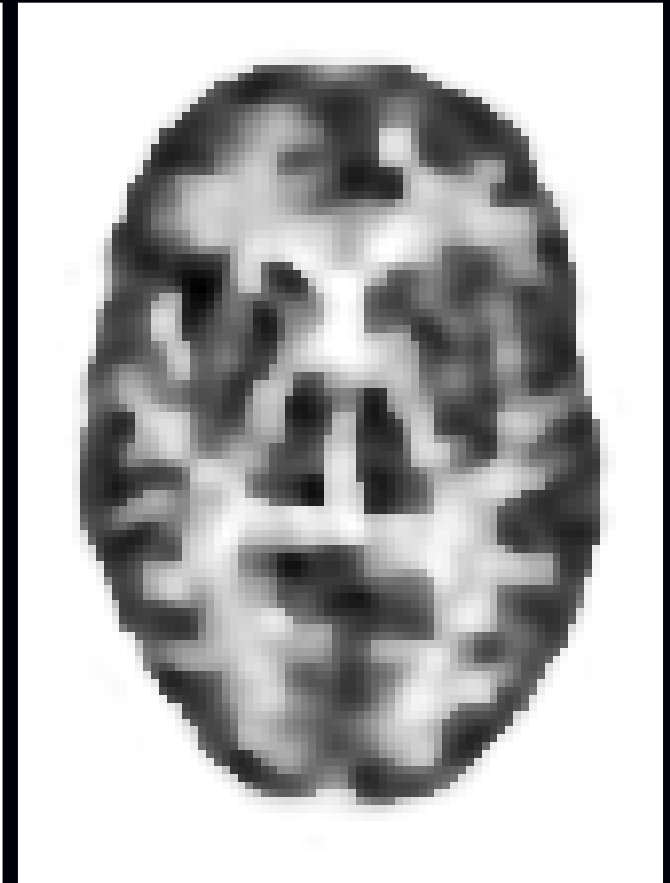
Edge-Preserving Reconstruction Example



Phantom

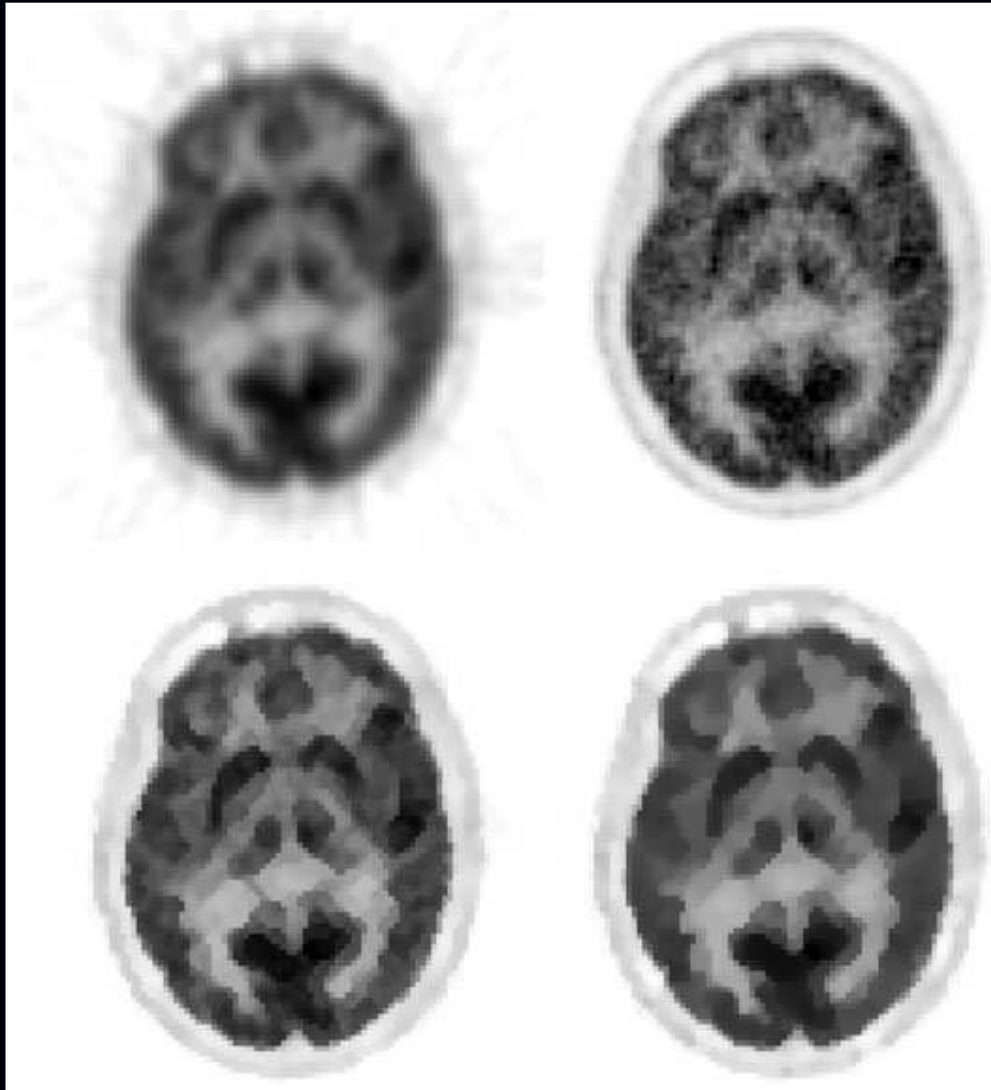


Quadratic Penalty



Huber Penalty

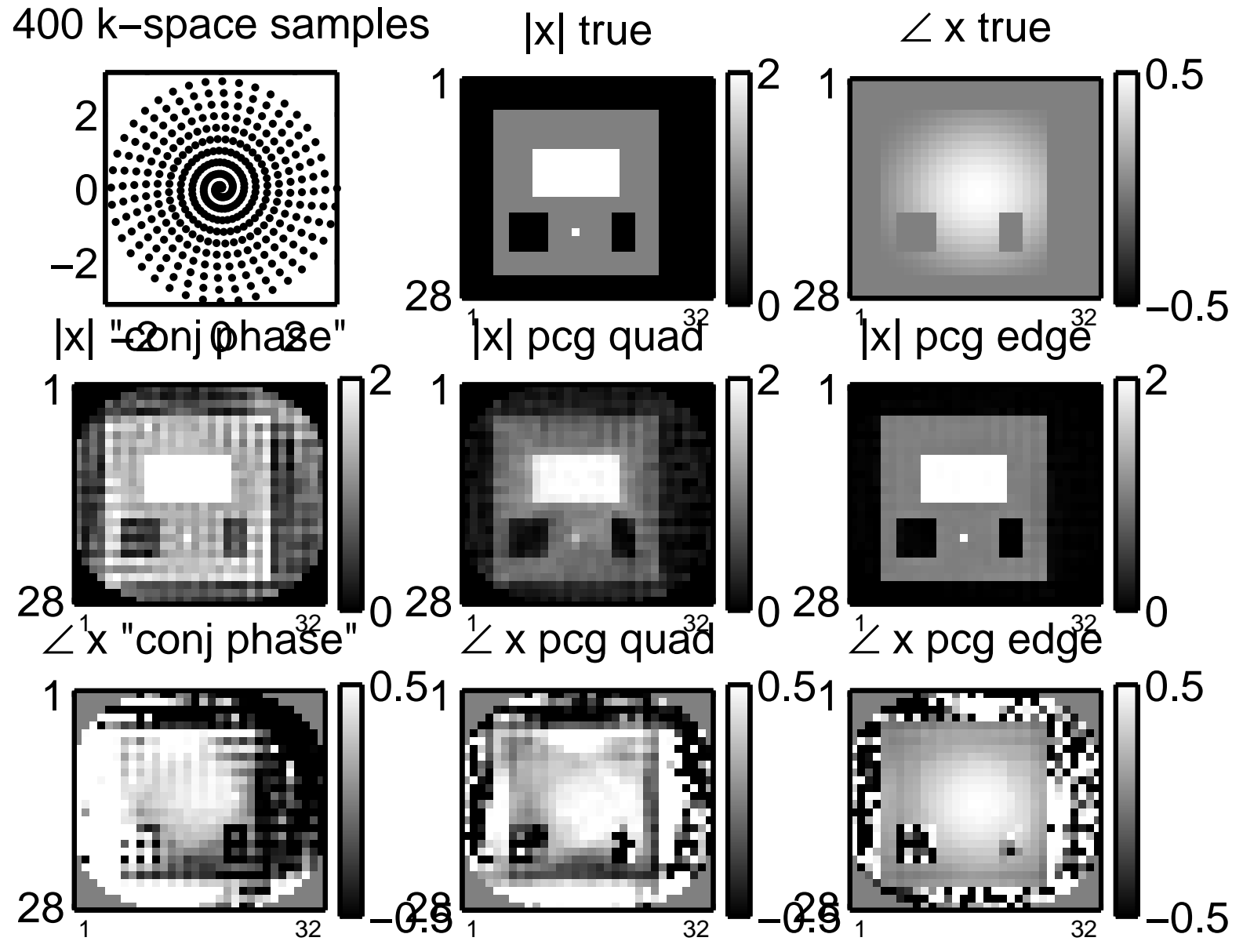
More “Edge Preserving” Regularization



Chlewicki *et al.*, PMB, Oct. 2004: “Noise reduction and convergence of Bayesian algorithms with blobs based on the Huber function and median root prior”

Piecewise Constant "Cartoon" Objects

400 k-space samples



Total Variation Regularization

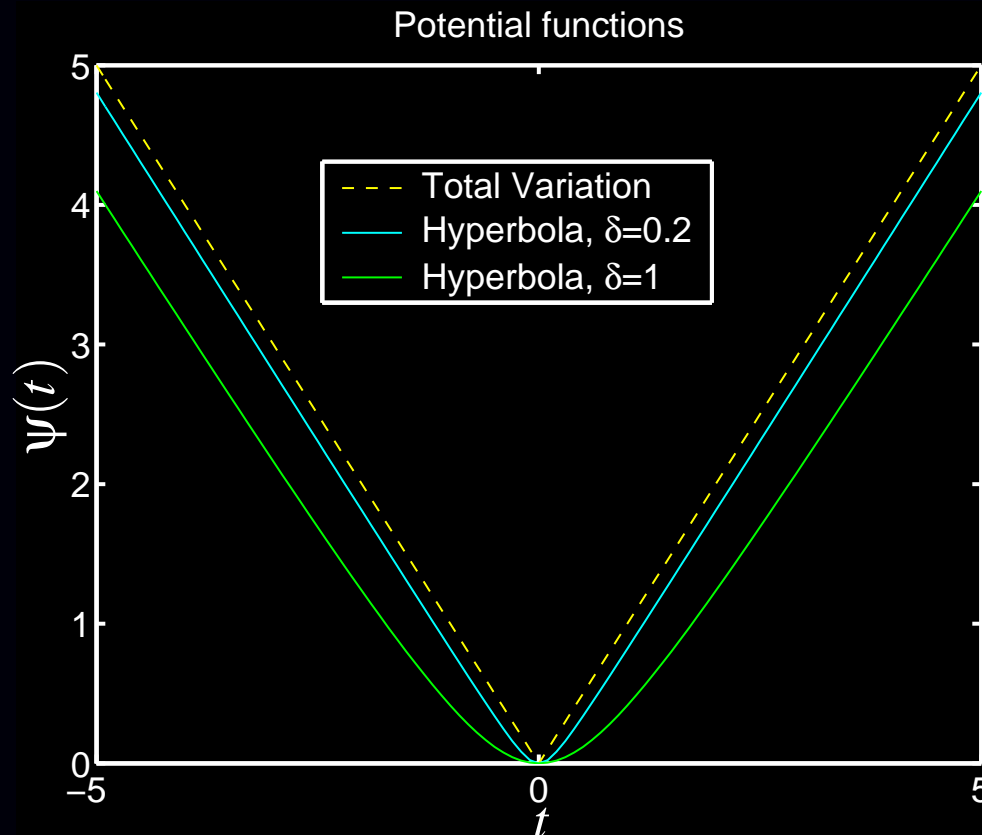
Non-quadratic roughness penalty:

$$\int \|\nabla f(\vec{r})\| d\vec{r} \approx \sum_k |[\mathbf{C}\mathbf{x}]_k|$$

Uses *magnitude* instead of *squared magnitude* of gradient.

Problem: $|\cdot|$ is not differentiable.

Practical solution: $|t| \approx \delta \left(\sqrt{1 + (t/\delta)^2} - 1 \right)$ (hyperbola!)



Penalty Functions: Convex vs Nonconvex

Convex

- Easier to optimize
- Guaranteed unique minimizer of Ψ (for convex negative log-likelihood)

Nonconvex

- Greater degree of edge preservation
- Nice images for piecewise-constant phantoms!
- Even more unusual noise properties
- Multiple extrema
- More complicated optimization (simulated / deterministic annealing)
- Estimator \hat{x} becomes a discontinuous function of data Y

Nonconvex examples

- “broken parabola”

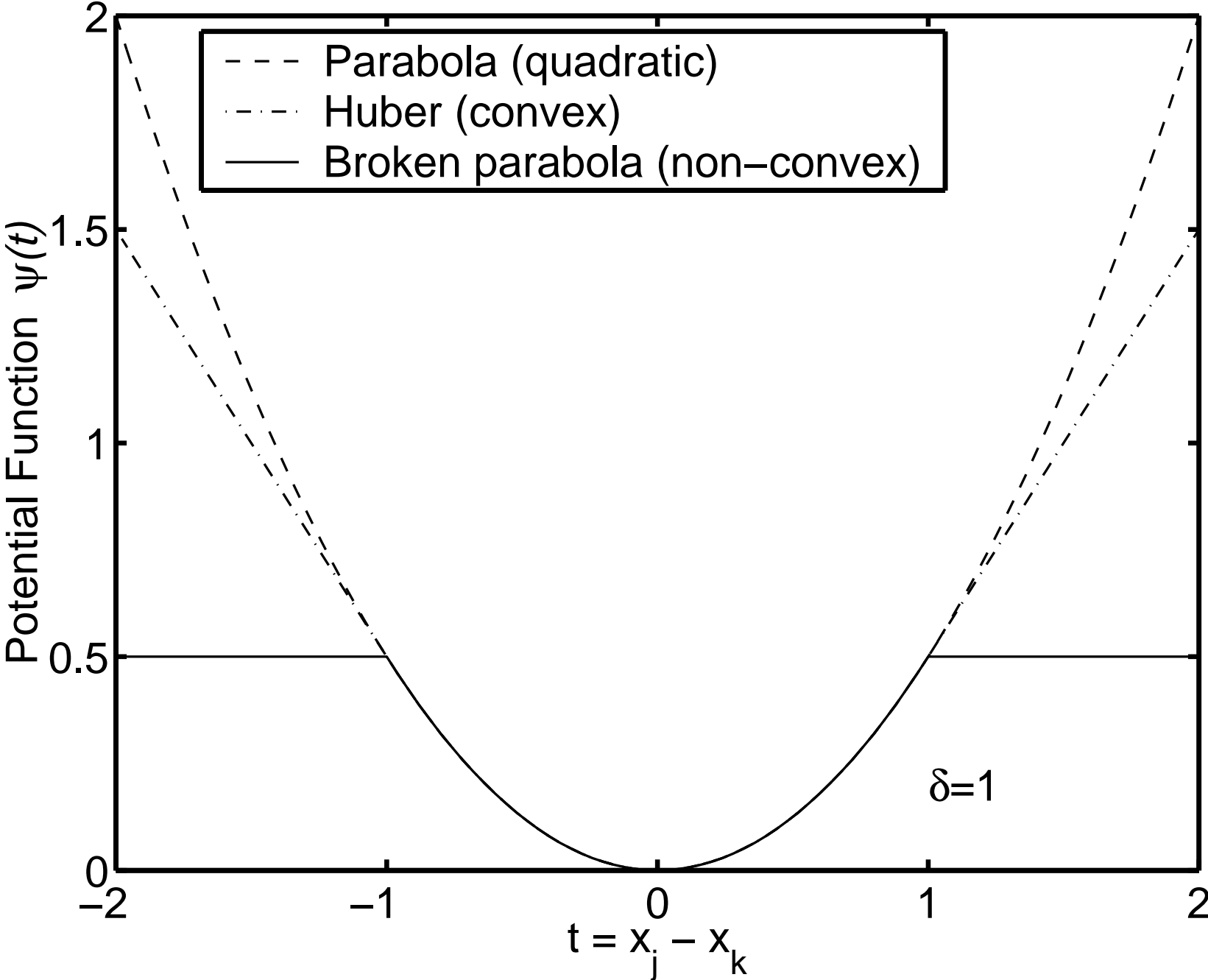
$$\psi(t) = \min(t^2, t_{\max}^2)$$

- true median root prior:

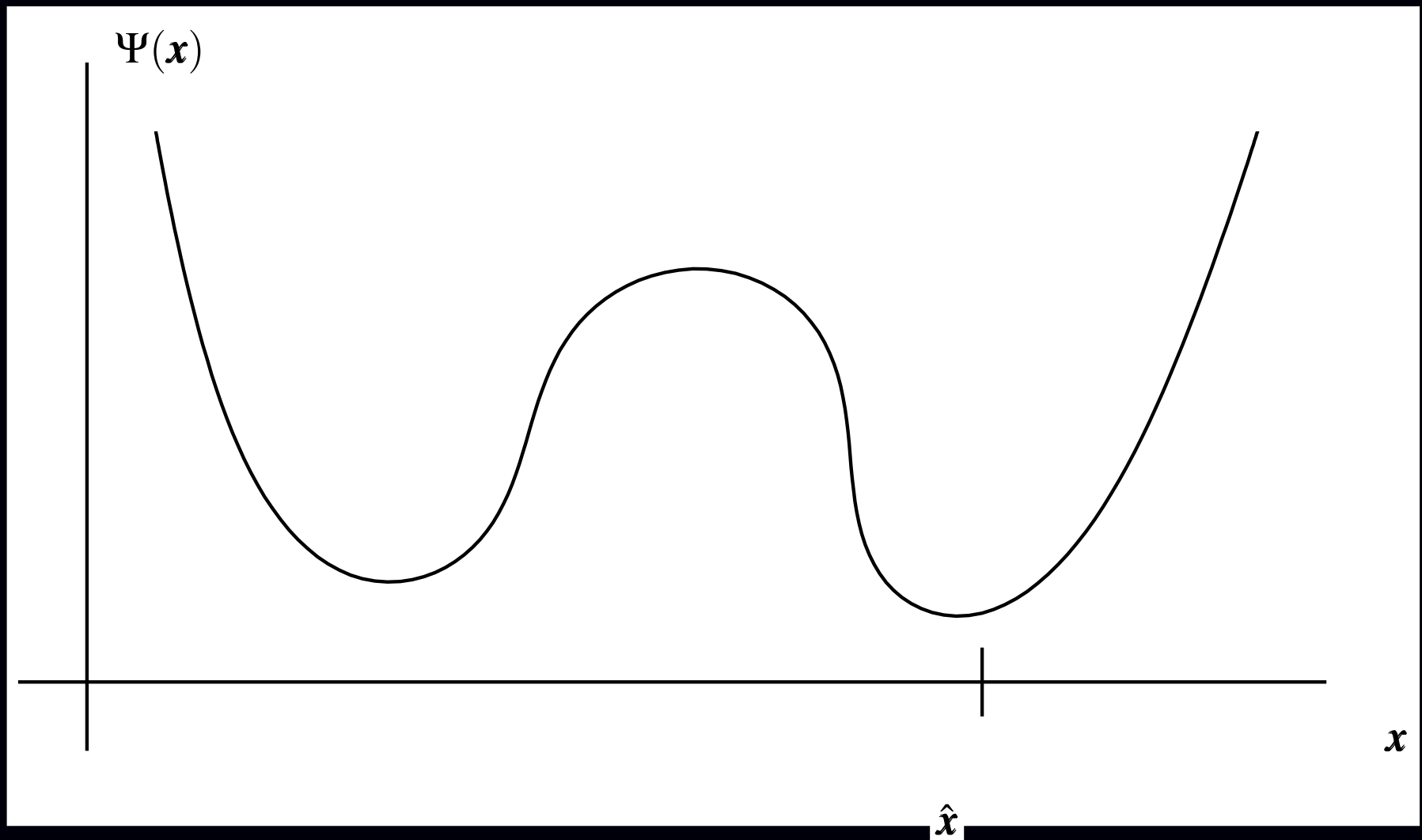
$$R(\mathbf{x}) = \sum_{j=1}^{n_p} \frac{(x_j - \text{median}_j(\mathbf{x}))^2}{\text{median}_j(\mathbf{x})} \quad \text{where } \text{median}_j(\mathbf{x}) \text{ is local median}$$

Exception: orthonormal wavelet threshold *denoising* via nonconvex potentials!

Potential Functions



Local Extrema and Discontinuous Estimators



Small change in data \implies large change in minimizer \hat{x} .
Using convex penalty functions obviates this problem.

Augmented Regularization Functions

Replace roughness penalty $R(\mathbf{x})$ with $R(\mathbf{x}|\mathbf{b}) + \alpha R(\mathbf{b})$, where the elements of \mathbf{b} (often binary) indicate boundary locations.

- Line-site methods
- Level-set methods

Joint estimation problem:

$$(\hat{\mathbf{x}}, \hat{\mathbf{b}}) = \arg \min_{\mathbf{x}, \mathbf{b}} \Psi(\mathbf{x}, \mathbf{b}), \quad \Psi(\mathbf{x}, \mathbf{b}) = \ell(\mathbf{x})[\mathbf{x}; \mathbf{y}] + \beta R(\mathbf{x}|\mathbf{b}) + \alpha R(\mathbf{b}).$$

Example: b_{jk} indicates the presence of edge between pixels j and k :

$$R(\mathbf{x}|\mathbf{b}) = \sum_{j=1}^{n_p} \sum_{k \in \mathcal{N}_j} (1 - b_{jk}) \frac{1}{2} (x_j - x_k)^2$$

Penalty to discourage too many edges (e.g.):

$$R(\mathbf{b}) = \sum_{jk} b_{jk}.$$

- Can encourage local edge continuity
- May require annealing methods for minimization

Modified Penalty Functions

$$R(\mathbf{x}) = \sum_{j=1}^{n_p} \frac{1}{2} \sum_{k \in \mathcal{N}_j} w_{jk} \Psi(x_j - x_k)$$

Adjust weights $\{w_{jk}\}$ to

- Control resolution properties
- Incorporate anatomical side information (MR/CT)
(avoid smoothing across anatomical boundaries)

Recommendations

- Emission tomography:
 - Begin with quadratic (nonseparable) penalty functions
 - Consider modified penalty for resolution control and choice of β
 - Use modest regularization and post-filter more if desired
- Transmission tomography (attenuation maps), X-ray CT
 - consider convex nonquadratic (e.g., Huber) penalty functions
 - choose δ based on attenuation map **units** (water, bone, etc.)
 - choice of regularization parameter β remains nontrivial,
learn appropriate values by experience for given study type

Choice 4.3: Constraints

- Nonnegativity
- Known support
- Count preserving
- Upper bounds on values
e.g., maximum μ of attenuation map in transmission case

Considerations

- Algorithm complexity
- Computation
- Convergence rate
- Bias (in low-count regions)
- ...

Open Problems

Modeling

- Noise in a_{ij} values (system model errors)
- Noise in \hat{r}_i values (estimates of scatter / randoms)
- Statistics of corrected measurements
- Statistics of measurements with deadtime losses

For PL or MAP reconstruction, Qi (MIC 2004) has derived a bound on system model errors relative to data noise.

Cost functions

- Performance prediction for nonquadratic penalties
- Effect of nonquadratic penalties on detection tasks
- Choice of regularization parameters for nonquadratic regularization

Summary

- 1. Object parameterization: function $f(\vec{r})$ vs vector x
- 2. System physical model: $s_i(\vec{r})$
- 3. Measurement statistical model $Y_i \sim \boxed{?}$
- 4. Cost function: data-mismatch / regularization / constraints

Reconstruction Method \triangleq Cost Function + Algorithm

Naming convention: “criterion”-“algorithm”:

- ML-EM, MAP-OSL, PL-SAGE, PWLS+SOR, PWLS-CG, ...

Part 3. Algorithms

Method = Cost Function + Algorithm

Outline

- Ideal algorithm
- Classical general-purpose algorithms
- Considerations:
 - nonnegativity
 - parallelization
 - convergence rate
 - monotonicity
- Algorithms tailored to cost functions for imaging
 - Optimization transfer
 - EM-type methods
 - Poisson emission problem
 - Poisson transmission problem
- Ordered-subsets / block-iterative algorithms
 - Recent convergent versions (relaxation, incrementalism)

Why iterative algorithms?

- For nonquadratic Ψ , no closed-form solution for minimizer.
- For quadratic Ψ with nonnegativity constraints, no closed-form solution.
- For quadratic Ψ without constraints, closed-form solutions:

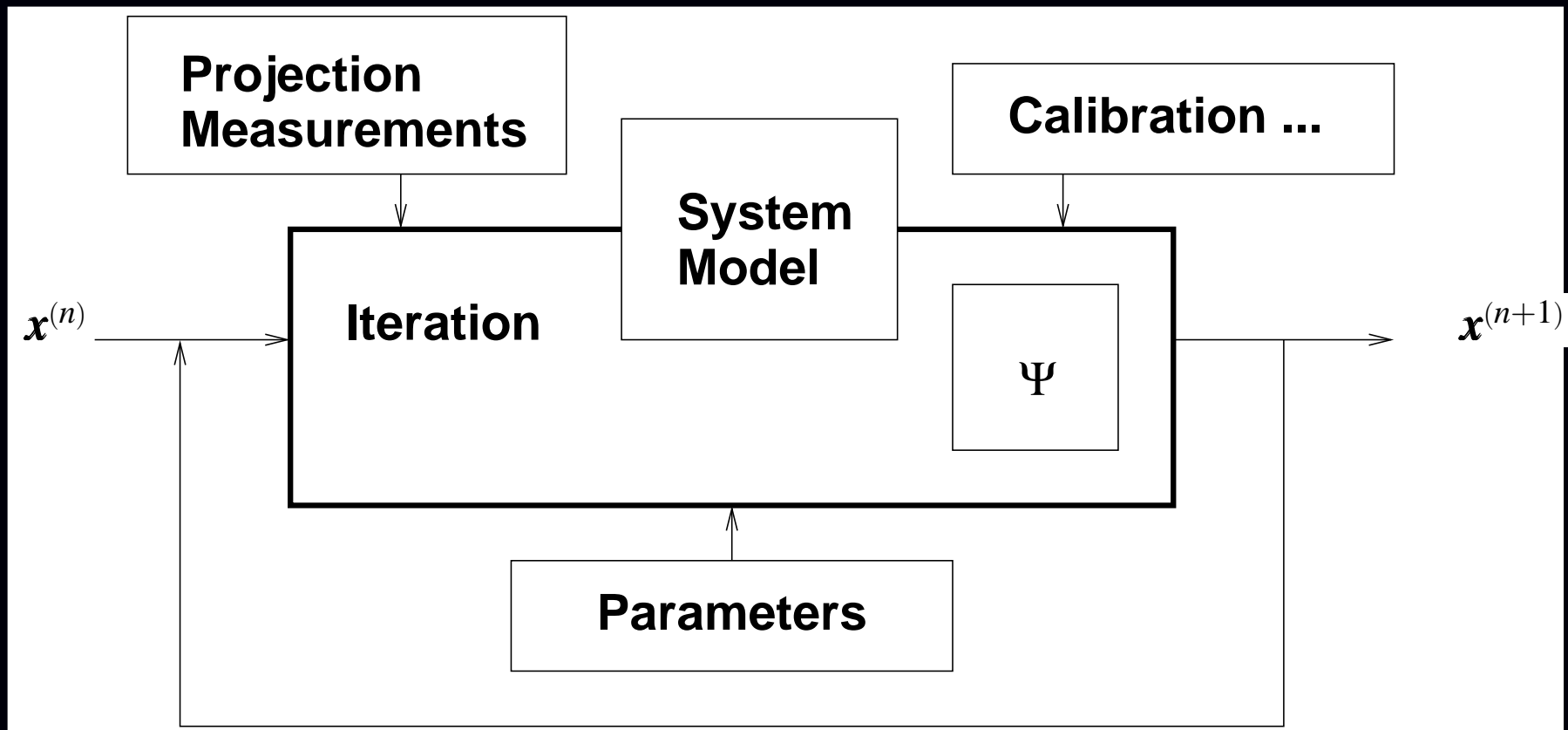
$$\text{PWLS: } \hat{\mathbf{x}} = \arg \min_x \|\mathbf{y} - \mathbf{Ax}\|_{\mathbf{W}^{1/2}}^2 + \mathbf{x}'\mathbf{Rx} = [\mathbf{A}'\mathbf{WA} + \mathbf{R}]^{-1}\mathbf{A}'\mathbf{W}\mathbf{y}$$

$$\text{OLS: } \hat{\mathbf{x}} = \arg \min_x \|\mathbf{y} - \mathbf{Ax}\|^2 = [\mathbf{A}'\mathbf{A}]^{-1}\mathbf{A}'\mathbf{y}$$

Impractical (memory and computation) for realistic problem sizes.
 \mathbf{A} is sparse, but $\mathbf{A}'\mathbf{A}$ is not.

All algorithms are imperfect. No single best solution.

General Iteration



Deterministic iterative mapping: $\mathbf{x}^{(n+1)} = \mathcal{M}(\mathbf{x}^{(n)})$

Ideal Algorithm

$$\mathbf{x}^* \triangleq \arg \min_{\mathbf{x} \geq 0} \Psi(\mathbf{x}) \quad (\text{global minimizer})$$

Properties

stable and convergent

converges quickly

globally convergent

fast

robust

user friendly

parallelizable

simple

flexible

(matrix stored by row or column, or factored, or projector/backprojector)

$\{\mathbf{x}^{(n)}\}$ converges to \mathbf{x}^* if run indefinitely

$\{\mathbf{x}^{(n)}\}$ gets “close” to \mathbf{x}^* in just a few iterations

$\lim_n \mathbf{x}^{(n)}$ independent of starting image $\mathbf{x}^{(0)}$

requires minimal computation per iteration

insensitive to finite numerical precision

nothing to adjust (e.g., acceleration factors)

(when necessary)

easy to program and debug

accommodates any type of system model

Choices: forgo one or more of the above

Classic Algorithms

Non-gradient based

- Exhaustive search
- Nelder-Mead simplex (amoeba)

Converge very slowly, but work with nondifferentiable cost functions.

Gradient based

- Gradient descent

$$\mathbf{x}^{(n+1)} \triangleq \mathbf{x}^{(n)} - \alpha \nabla \Psi(\mathbf{x}^{(n)})$$

Choosing α to ensure convergence is nontrivial.

- Steepest descent

$$\mathbf{x}^{(n+1)} \triangleq \mathbf{x}^{(n)} - \alpha_n \nabla \Psi(\mathbf{x}^{(n)}) \quad \text{where} \quad \alpha_n \triangleq \arg \min_{\alpha} \Psi(\mathbf{x}^{(n)} - \alpha \nabla \Psi(\mathbf{x}^{(n)}))$$

Computing stepsize α_n can be expensive or inconvenient.

Limitations

- Converge slowly.
- Do not easily accommodate nonnegativity constraint.

Gradients & Nonnegativity - A Mixed Blessing

Unconstrained optimization of differentiable cost functions:

$$\nabla \Psi(\mathbf{x}) = \mathbf{0} \quad \text{when } \mathbf{x} = \mathbf{x}^*$$

- A necessary condition always.
- A sufficient condition for strictly convex cost functions.
- Iterations search for zero of gradient.

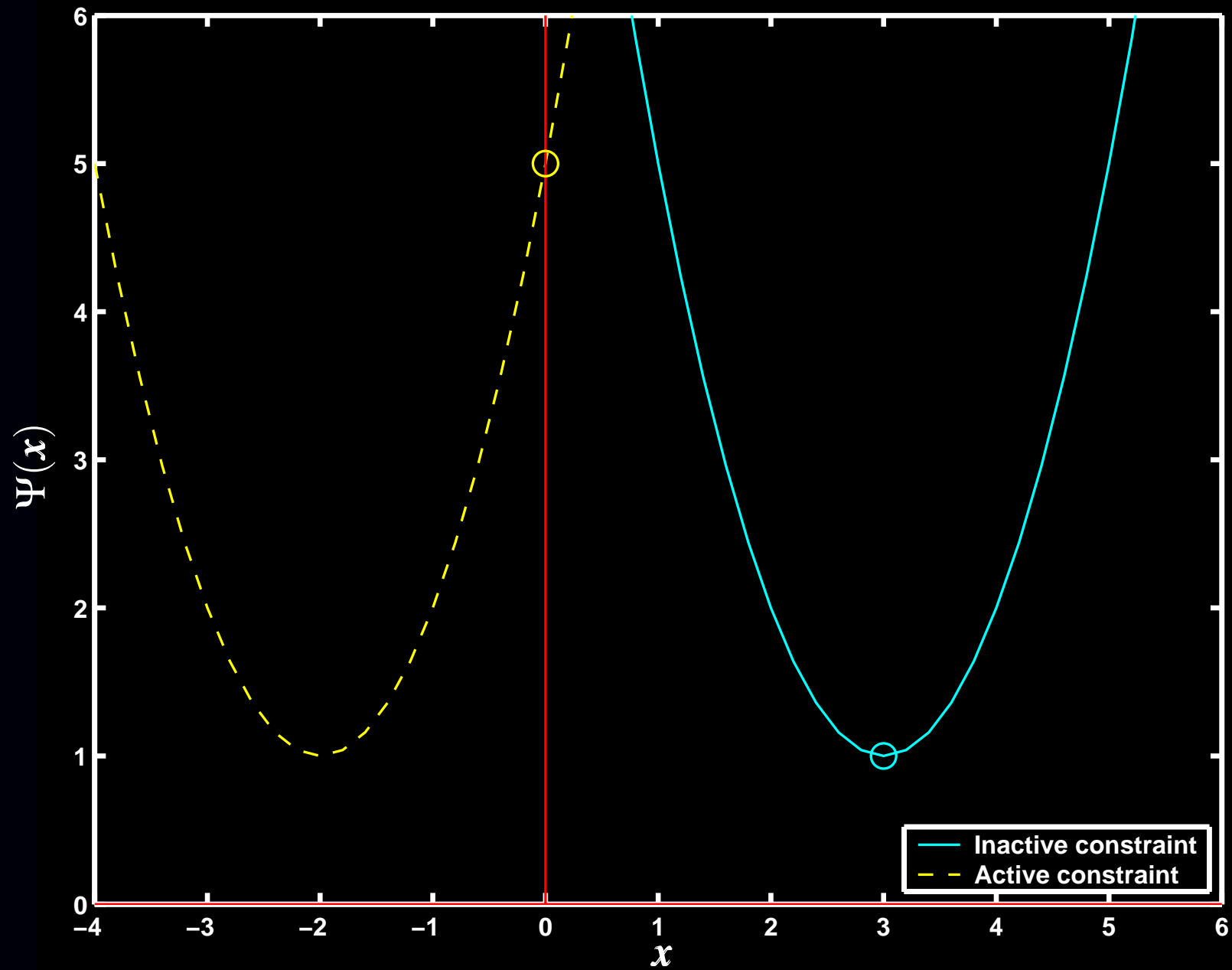
Nonnegativity-constrained minimization:

Karush-Kuhn-Tucker conditions

$$\left. \frac{\partial}{\partial x_j} \Psi(\mathbf{x}) \right|_{\mathbf{x}=\mathbf{x}^*} \quad \text{is} \quad \begin{cases} = 0, & x_j^* > 0 \\ \geq 0, & x_j^* = 0 \end{cases}$$

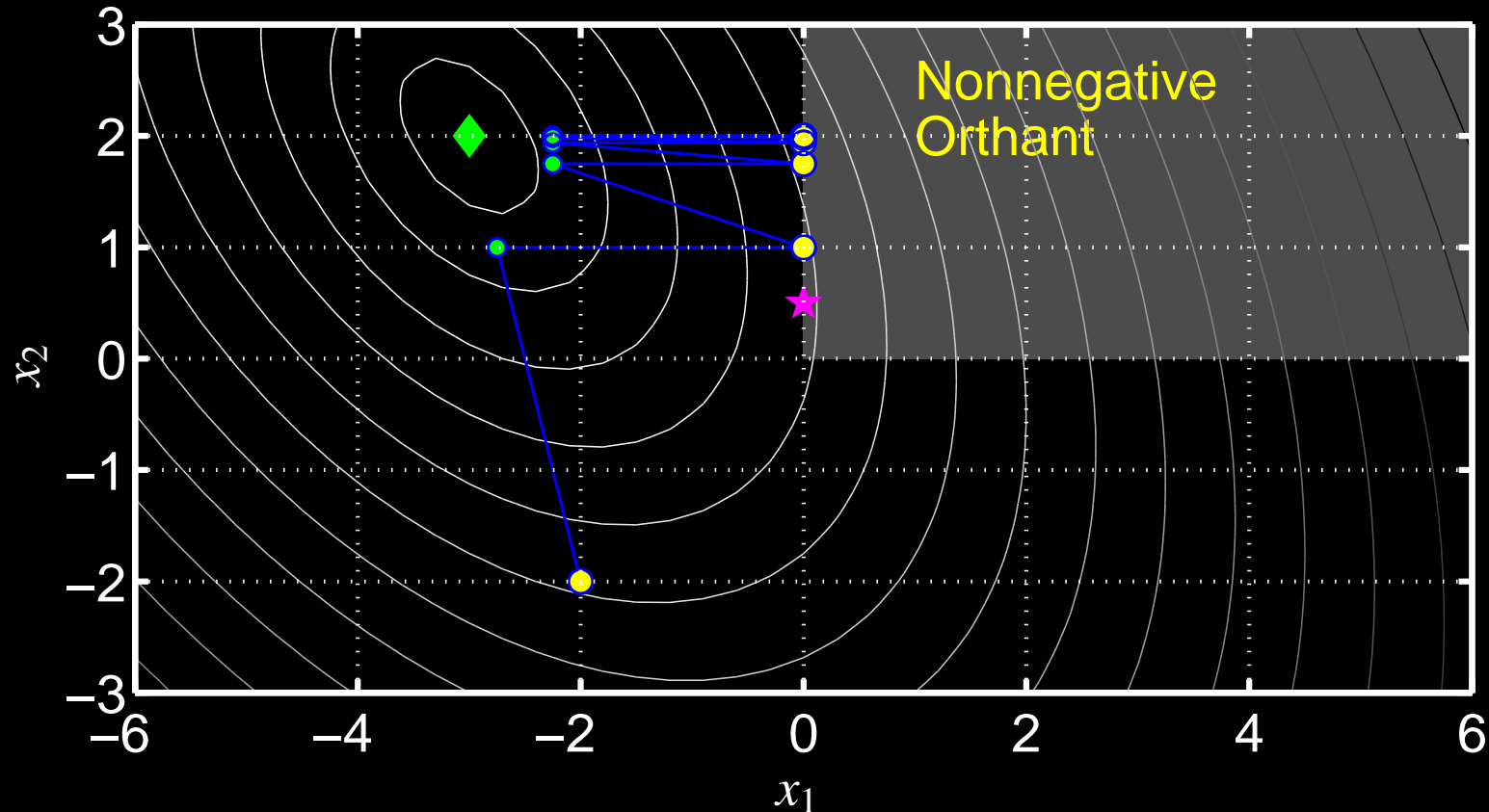
- A necessary condition always.
- A sufficient condition for strictly convex cost functions.
- Iterations search for ???
- $0 = x_j^* \frac{\partial}{\partial x_j} \Psi(\mathbf{x}^*)$ is a necessary condition, but never sufficient condition.

Karush-Kuhn-Tucker Illustrated



Why Not Clip Negatives?

WLS with Clipped Newton–Raphson



Newton-Raphson with negatives set to zero each iteration.
Fixed-point of iteration is not the constrained minimizer!

Newton-Raphson Algorithm

$$\mathbf{x}^{(n+1)} = \mathbf{x}^{(n)} - [\nabla^2 \Psi(\mathbf{x}^{(n)})]^{-1} \nabla \Psi(\mathbf{x}^{(n)})$$

Advantage:

- Super-linear convergence rate (if convergent)

Disadvantages:

- Requires twice-differentiable Ψ
- Not guaranteed to converge
- Not guaranteed to monotonically decrease Ψ
- Does not enforce nonnegativity constraint
- Computing Hessian $\nabla^2 \Psi$ often expensive
- Impractical for image recovery due to matrix inverse

General purpose remedy: bound-constrained Quasi-Newton algorithms

Newton's Quadratic Approximation

2nd-order Taylor series:

$$\Psi(\mathbf{x}) \approx \phi(\mathbf{x}; \mathbf{x}^{(n)}) \triangleq \Psi(\mathbf{x}^{(n)}) + \nabla \Psi(\mathbf{x}^{(n)}) (\mathbf{x} - \mathbf{x}^{(n)}) + \frac{1}{2} (\mathbf{x} - \mathbf{x}^{(n)})^T \nabla^2 \Psi(\mathbf{x}^{(n)}) (\mathbf{x} - \mathbf{x}^{(n)})$$

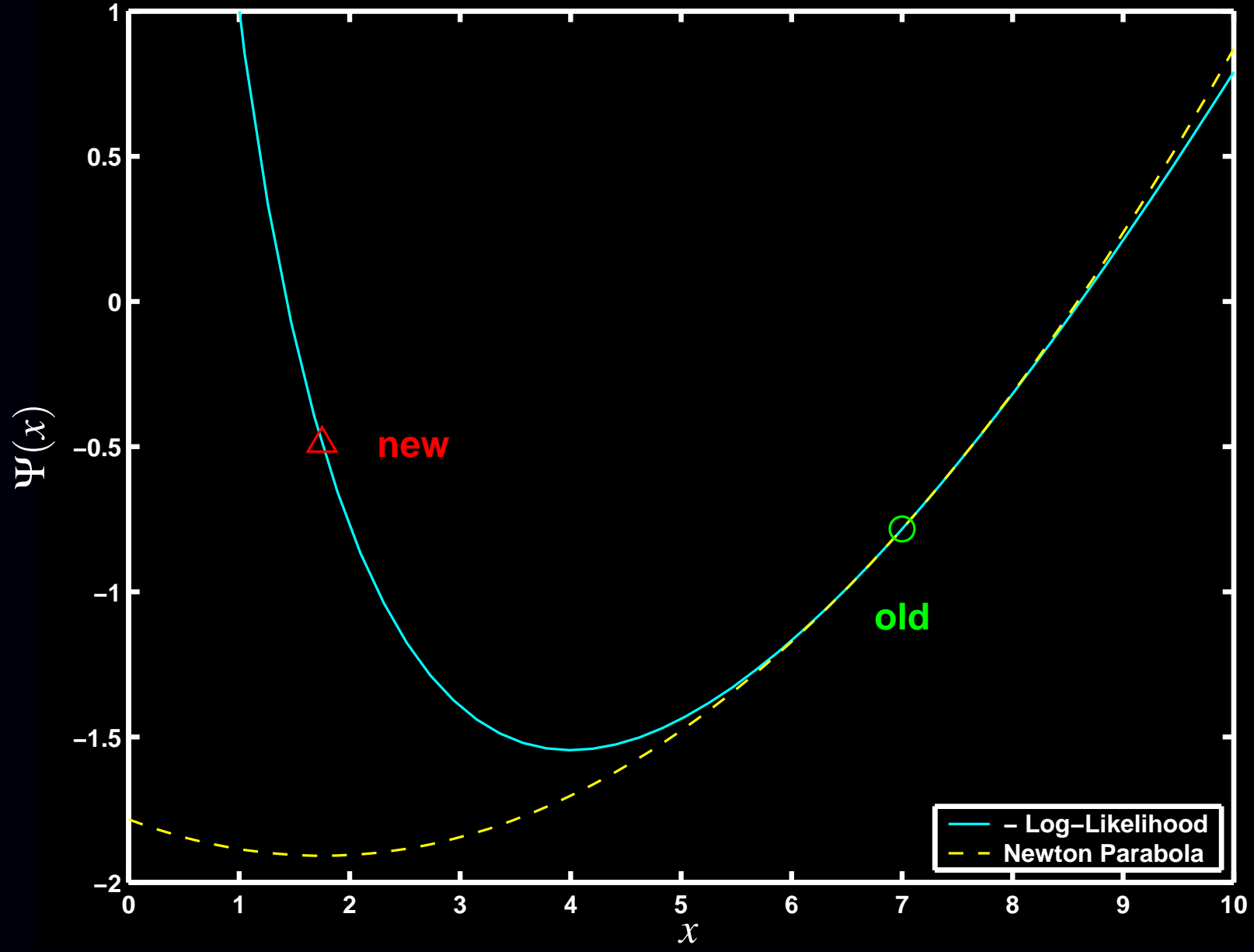
Set $\mathbf{x}^{(n+1)}$ to the (“easily” found) minimizer of this quadratic approximation:

$$\begin{aligned} \mathbf{x}^{(n+1)} &\triangleq \arg \min_{\mathbf{x}} \phi(\mathbf{x}; \mathbf{x}^{(n)}) \\ &= \mathbf{x}^{(n)} - [\nabla^2 \Psi(\mathbf{x}^{(n)})]^{-1} \nabla \Psi(\mathbf{x}^{(n)}) \end{aligned}$$

Can be nonmonotone for Poisson emission tomography log-likelihood, even for a single pixel and single ray:

$$\Psi(x) = (x + r) - y \log(x + r).$$

Nonmonotonicity of Newton-Raphson



Consideration: Monotonicity

An algorithm is monotonic if

$$\Psi(\mathbf{x}^{(n+1)}) \leq \Psi(\mathbf{x}^{(n)}), \quad \forall \mathbf{x}^{(n)}.$$

Three categories of algorithms:

- Nonmonotonic (or unknown)
- Forced monotonic (e.g., by line search)
- **Intrinsically monotonic** (by design, simplest to implement)

Forced monotonicity

Most nonmonotonic algorithms can be converted to forced monotonic algorithms by adding a line-search step:

$$\mathbf{x}^{\text{temp}} \triangleq \mathcal{M}(\mathbf{x}^{(n)}), \quad \mathbf{d} = \mathbf{x}^{\text{temp}} - \mathbf{x}^{(n)}$$
$$\mathbf{x}^{(n+1)} \triangleq \mathbf{x}^{(n)} - \alpha_n \mathbf{d}^{(n)} \quad \text{where} \quad \alpha_n \triangleq \arg \min_{\alpha} \Psi(\mathbf{x}^{(n)} - \alpha \mathbf{d}^{(n)})$$

Inconvenient, sometimes expensive, nonnegativity problematic.

Conjugate Gradient (CG) Algorithm

Advantages:

- Fast converging (if suitably preconditioned) (in unconstrained case)
- Monotonic (forced by line search in nonquadratic case)
- Global convergence (unconstrained case)
- Flexible use of system matrix A and tricks
- Easy to implement in unconstrained quadratic case
- Highly parallelizable

Disadvantages:

- Nonnegativity constraint awkward (slows convergence?)
- Line-search somewhat awkward in nonquadratic cases
- Possible need to “restart” after many iterations

Highly recommended for unconstrained quadratic problems (e.g., PWLS without nonnegativity). Useful (but perhaps not ideal) for Poisson case too.

Consideration: Parallelization

Simultaneous (fully parallelizable)

update all pixels simultaneously using all data

EM, Conjugate gradient, ISRA, OSL, SIRT, MART, ...

Block iterative (ordered subsets)

update (nearly) all pixels using one subset of the data at a time

OSEM, RBBI, ...

Row action

update many pixels using a single ray at a time

ART, RAMLA

Pixel grouped (multiple column action)

update some (but not all) pixels simultaneously a time, using all data

Grouped coordinate descent, multi-pixel SAGE

(Perhaps the most nontrivial to implement)

Sequential (column action)

update one pixel at a time, using all (relevant) data

Coordinate descent, SAGE

Coordinate Descent Algorithm

aka Gauss-Siedel, successive over-relaxation (SOR), iterated conditional modes (ICM)

Update one pixel at a time, holding others fixed to their most recent values:

$$x_j^{\text{new}} = \arg \min_{x_j \geq 0} \Psi \left(x_1^{\text{new}}, \dots, x_{j-1}^{\text{new}}, x_j, x_{j+1}^{\text{old}}, \dots, x_{n_p}^{\text{old}} \right), \quad j = 1, \dots, n_p$$

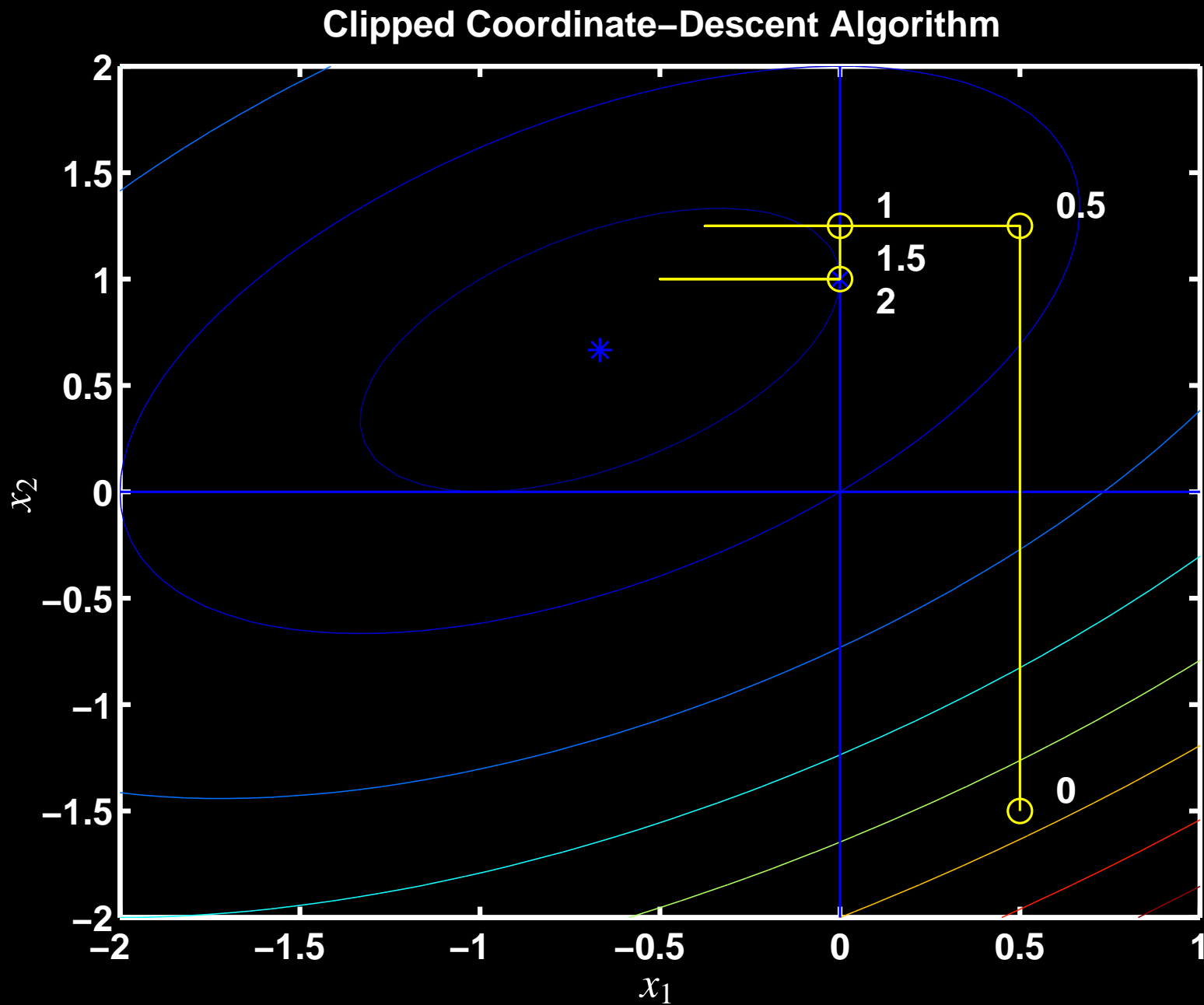
Advantages:

- Intrinsically monotonic
- Fast converging (from good initial image)
- Global convergence
- Nonnegativity constraint trivial

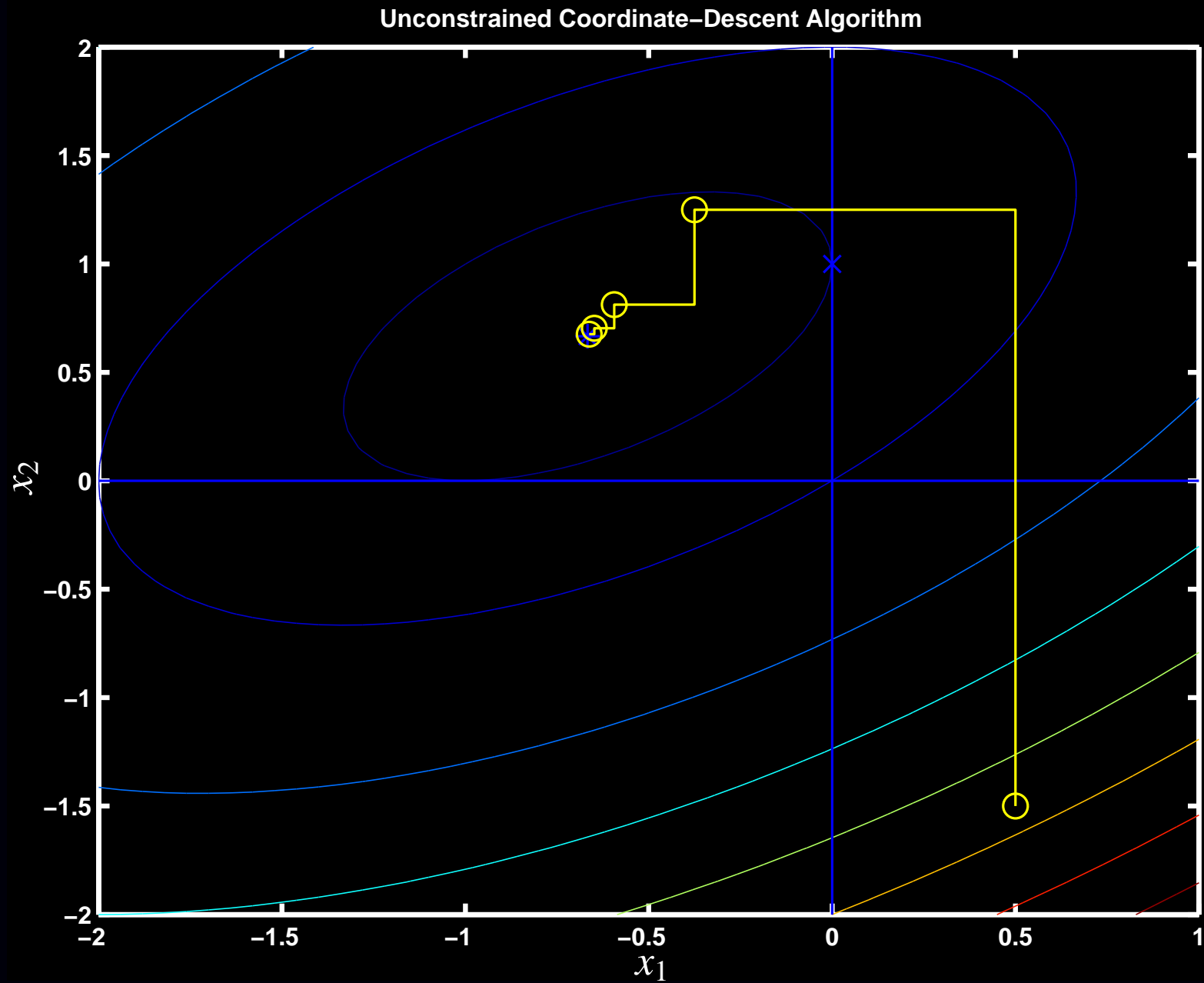
Disadvantages:

- Requires column access of system matrix A
- Cannot exploit some “tricks” for A , e.g., factorizations
- Expensive “arg min” for nonquadratic problems
- Poorly parallelizable

Constrained Coordinate Descent Illustrated



Coordinate Descent - Unconstrained



Coordinate-Descent Algorithm Summary

Recommended when all of the following apply:

- quadratic or nearly-quadratic convex cost function
- nonnegativity constraint desired
- precomputed and stored system matrix A with column access
- parallelization not needed (standard workstation)

Cautions:

- Good initialization (e.g., properly scaled FBP) essential.
(Uniform image or zero image cause slow initial convergence.)
- Must be programmed carefully to be efficient.
(Standard Gauss-Seidel implementation is suboptimal.)
- Updates high-frequencies fastest \implies poorly suited to unregularized case

Used daily in UM clinic for 2D SPECT / PWLS / nonuniform attenuation

Summary of General-Purpose Algorithms

Gradient-based

- Fully parallelizable
- Inconvenient line-searches for nonquadratic cost functions
- Fast converging in unconstrained case
- Nonnegativity constraint inconvenient

Coordinate-descent

- Very fast converging
- Nonnegativity constraint trivial
- Poorly parallelizable
- Requires precomputed/stored system matrix

CD is well-suited to moderate-sized 2D problem (e.g., 2D PET), but poorly suited to large 2D problems (X-ray CT) and fully 3D problems

Neither is ideal.

∴ need *special-purpose algorithms* for image reconstruction!

Data-Mismatch Functions Revisited

For fast converging, intrinsically monotone algorithms, consider the form of Ψ .

WLS:

$$\ell(\mathbf{x}) = \sum_{i=1}^{n_d} \frac{1}{2} w_i (y_i - [\mathbf{Ax}]_i)^2 = \sum_{i=1}^{n_d} h_i([\mathbf{Ax}]_i), \quad \text{where } h_i(l) \triangleq \frac{1}{2} w_i (y_i - l)^2.$$

Emission Poisson (negative) log-likelihood:

$$\ell(\mathbf{x}) = \sum_{i=1}^{n_d} ([\mathbf{Ax}]_i + r_i) - y_i \log([\mathbf{Ax}]_i + r_i) = \sum_{i=1}^{n_d} h_i([\mathbf{Ax}]_i)$$

where $h_i(l) \triangleq (l + r_i) - y_i \log(l + r_i)$.

Transmission Poisson log-likelihood:

$$\ell(\mathbf{x}) = \sum_{i=1}^{n_d} \left(b_i e^{-[\mathbf{Ax}]_i} + r_i \right) - y_i \log \left(b_i e^{-[\mathbf{Ax}]_i} + r_i \right) = \sum_{i=1}^{n_d} h_i([\mathbf{Ax}]_i)$$

where $h_i(l) \triangleq (b_i e^{-l} + r_i) - y_i \log(b_i e^{-l} + r_i)$.

MRI, polyenergetic X-ray CT, confocal microscopy, image restoration, ...
All have same *partially separable* form.

General Imaging Cost Function

General form for data-mismatch function:

$$\ell(\mathbf{x}) = \sum_{i=1}^{n_d} h_i([\mathbf{A}\mathbf{x}]_i)$$

General form for regularizing penalty function:

$$R(\mathbf{x}) = \sum_k \psi_k([\mathbf{C}\mathbf{x}]_k)$$

General form for cost function:

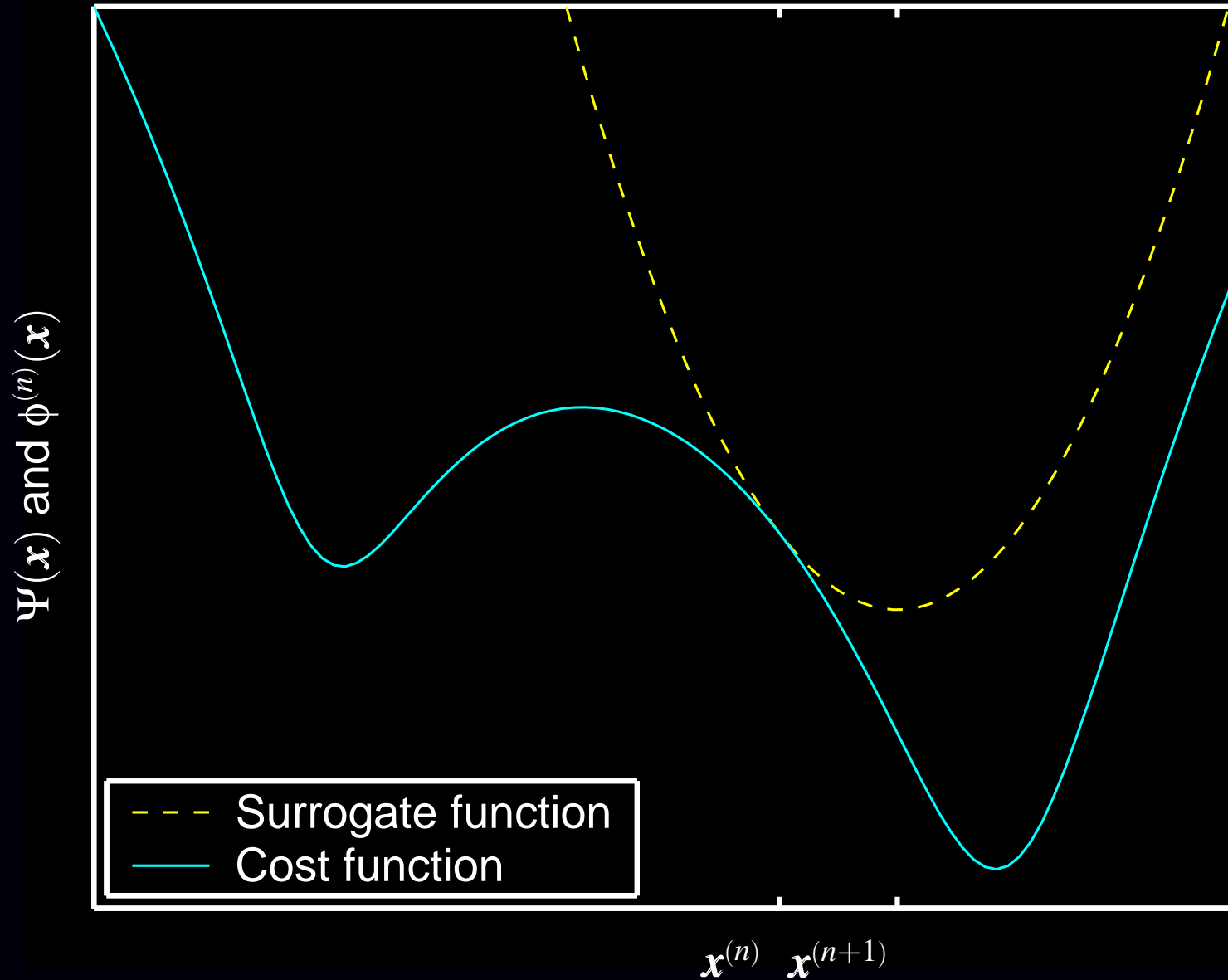
$$\Psi(\mathbf{x}) = \ell(\mathbf{x}) + \beta R(\mathbf{x}) = \sum_{i=1}^{n_d} h_i([\mathbf{A}\mathbf{x}]_i) + \beta \sum_k \psi_k([\mathbf{C}\mathbf{x}]_k)$$

Properties of Ψ we can exploit:

- summation form (due to independence of measurements)
- convexity of h_i functions (usually)
- summation argument (inner product of \mathbf{x} with i th row of \mathbf{A})

Most methods that use these properties are forms of *optimization transfer*.

Optimization Transfer Illustrated



Optimization Transfer

General iteration:

$$\mathbf{x}^{(n+1)} = \arg \min_{\mathbf{x} \geq \mathbf{0}} \phi(\mathbf{x}; \mathbf{x}^{(n)})$$

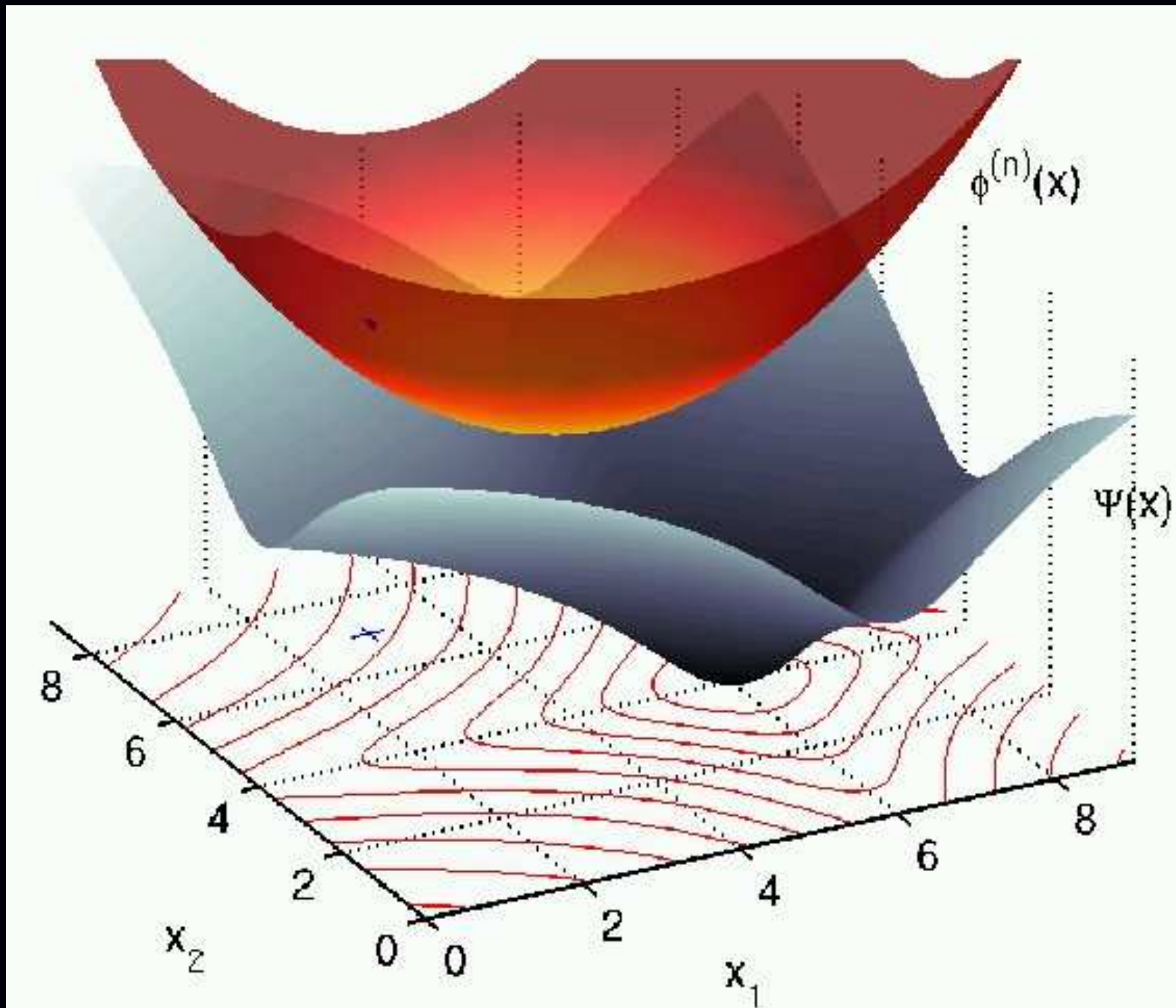
Monotonicity conditions (cost function Ψ decreases provided these hold):

- $\phi(\mathbf{x}^{(n)}; \mathbf{x}^{(n)}) = \Psi(\mathbf{x}^{(n)})$ (matched current value)
- $\nabla_{\mathbf{x}} \phi(\mathbf{x}; \mathbf{x}^{(n)}) \Big|_{\mathbf{x}=\mathbf{x}^{(n)}} = \nabla \Psi(\mathbf{x}) \Big|_{\mathbf{x}=\mathbf{x}^{(n)}}$ (matched gradient)
- $\phi(\mathbf{x}; \mathbf{x}^{(n)}) \geq \Psi(\mathbf{x}) \quad \forall \mathbf{x} \geq \mathbf{0}$ (lies above)

These 3 (sufficient) conditions are satisfied by the Q function of the EM algorithm (and its relatives like SAGE).

The 3rd condition is *not* satisfied by the Newton-Raphson quadratic approximation, which leads to its nonmonotonicity.

Optimization Transfer in 2d



Optimization Transfer of EM Algorithm

E-step: choose surrogate function $\phi(\mathbf{x}; \mathbf{x}^{(n)})$

M-step: minimize surrogate function

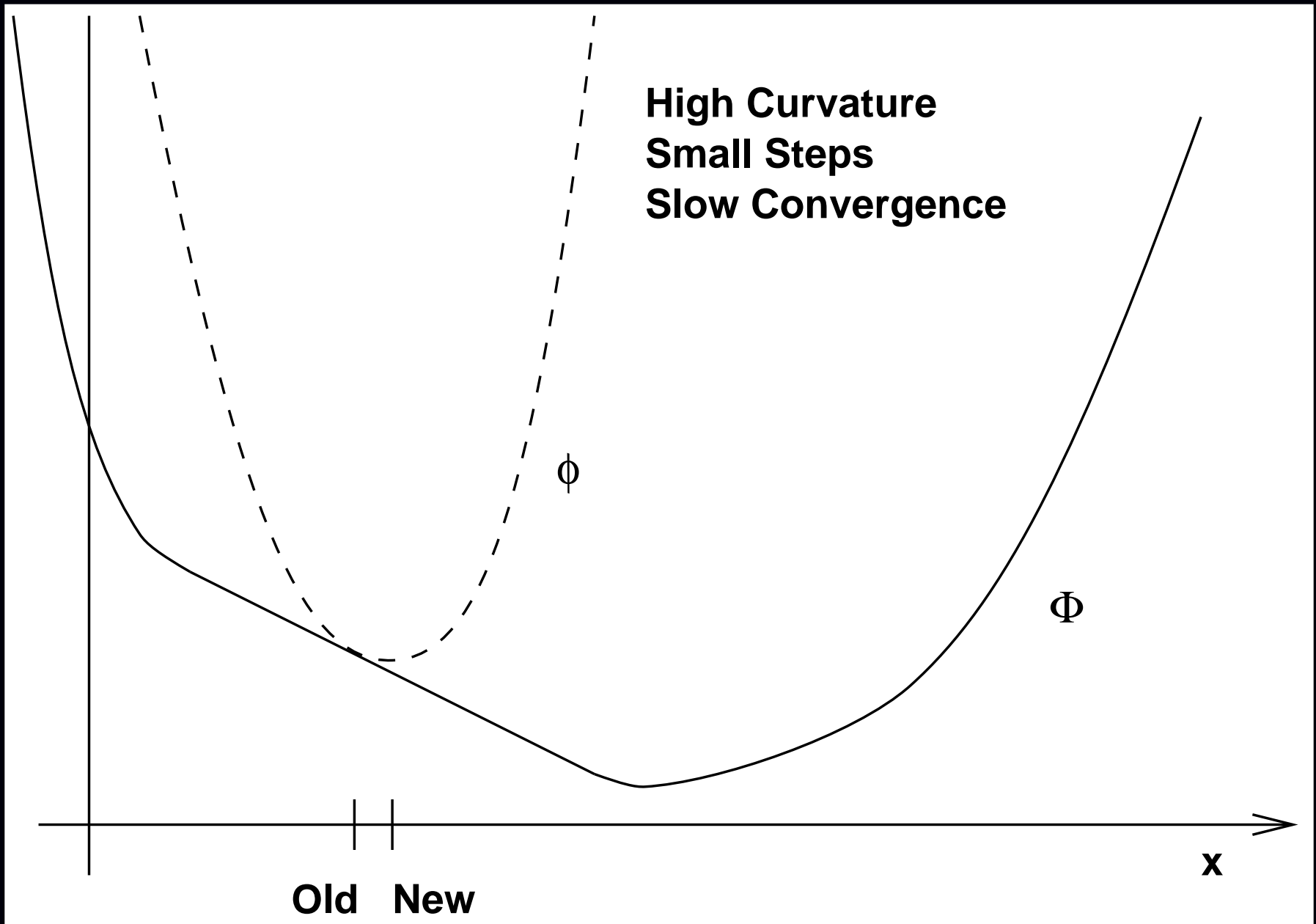
$$\mathbf{x}^{(n+1)} = \arg \min_{\mathbf{x} \geq \mathbf{0}} \phi(\mathbf{x}; \mathbf{x}^{(n)})$$

Designing surrogate functions

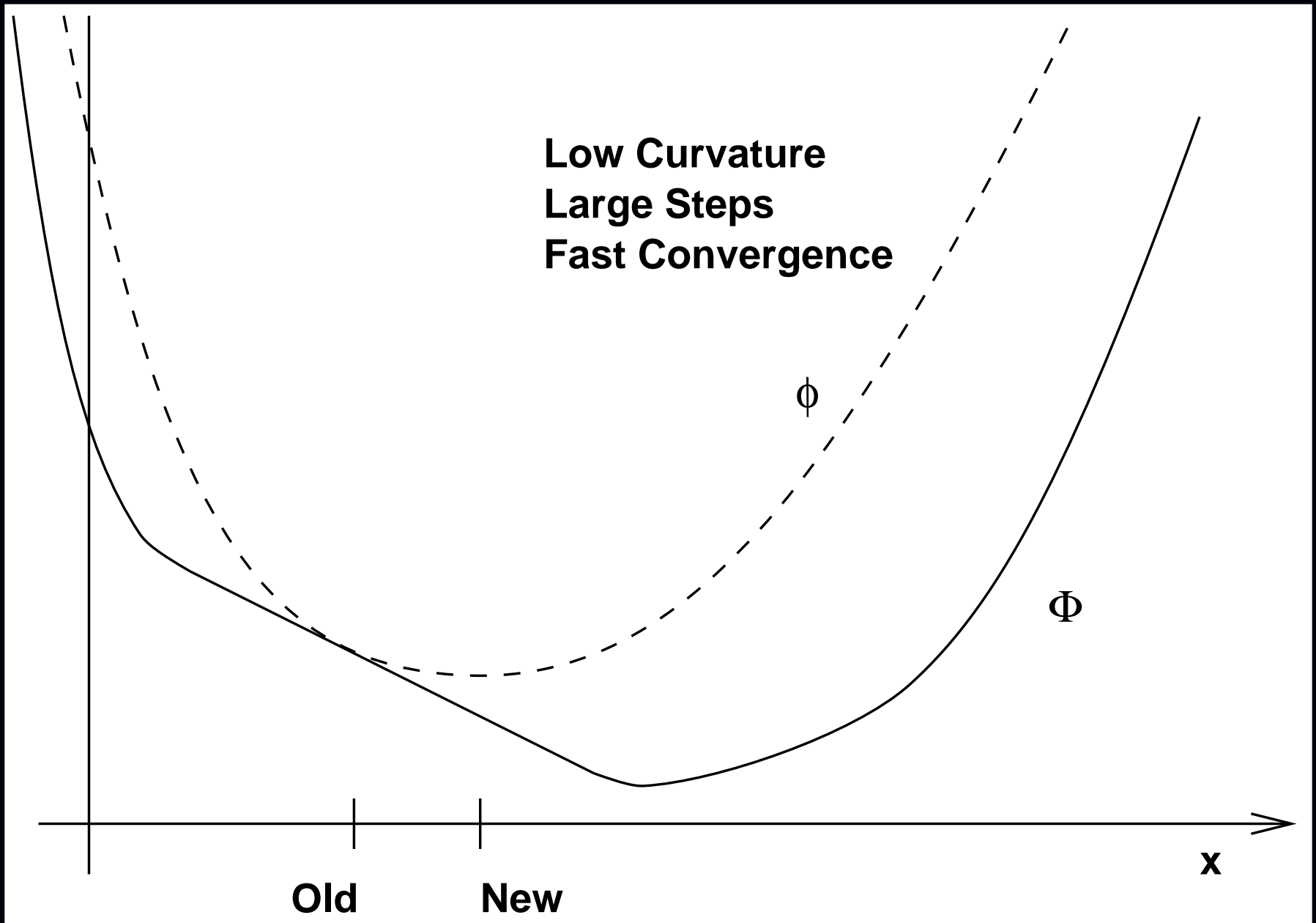
- Easy to “compute”
- Easy to minimize
- Fast convergence rate

Often mutually incompatible goals \therefore compromises

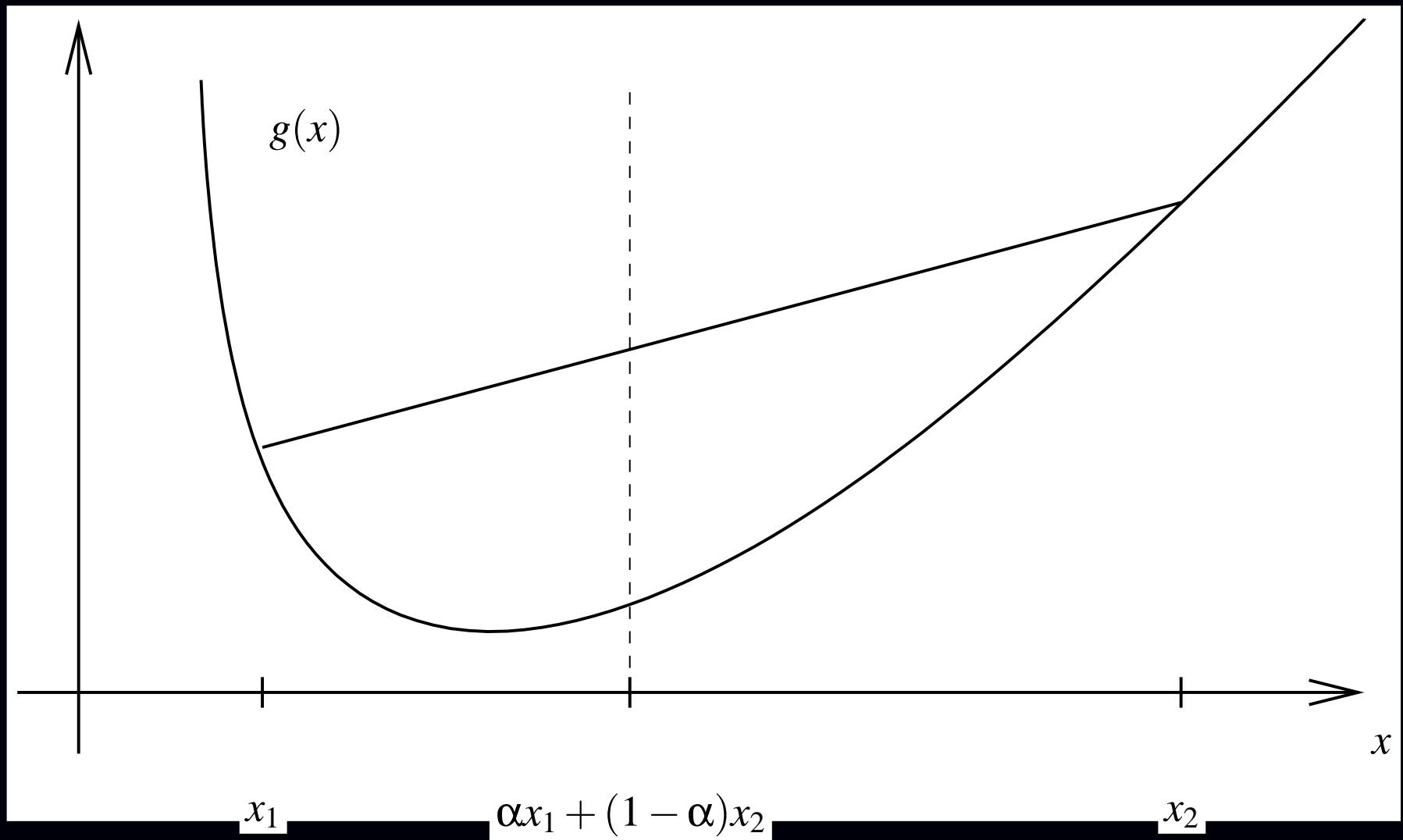
Convergence Rate: Slow



Convergence Rate: Fast



Tool: Convexity Inequality



g convex $\implies g(\alpha x_1 + (1 - \alpha)x_2) \leq \alpha g(x_1) + (1 - \alpha)g(x_2)$ for $\alpha \in [0, 1]$

More generally: $\alpha_k \geq 0$ and $\sum_k \alpha_k = 1 \implies g(\sum_k \alpha_k x_k) \leq \sum_k \alpha_k g(x_k)$. Sum outside!

Example 1: Classical ML-EM Algorithm

Negative Poisson log-likelihood cost function (unregularized):

$$\Psi(\mathbf{x}) = \sum_{i=1}^{n_d} h_i([\mathbf{Ax}]_i), \quad h_i(l) = (l + r_i) - y_i \log(l + r_i).$$

Intractable to minimize directly due to summation within logarithm.

Clever trick due to De Pierro (let $\bar{y}_i^{(n)} = [\mathbf{Ax}^{(n)}]_i + r_i$):

$$[\mathbf{Ax}]_i = \sum_{j=1}^{n_p} a_{ij}x_j = \sum_{j=1}^{n_p} \left[\frac{a_{ij}x_j^{(n)}}{\bar{y}_i^{(n)}} \right] \left(\frac{x_j^{(n)}\bar{y}_i^{(n)}}{x_j^{(n)}\bar{y}_i^{(n)}} \right).$$

Since the h_i 's are *convex* in Poisson emission model:

$$h_i([\mathbf{Ax}]_i) = h_i\left(\sum_{j=1}^{n_p} \left[\frac{a_{ij}x_j^{(n)}}{\bar{y}_i^{(n)}} \right] \left(\frac{x_j^{(n)}\bar{y}_i^{(n)}}{x_j^{(n)}\bar{y}_i^{(n)}} \right)\right) \leq \sum_{j=1}^{n_p} \left[\frac{a_{ij}x_j^{(n)}}{\bar{y}_i^{(n)}} \right] h_i\left(\frac{x_j^{(n)}\bar{y}_i^{(n)}}{x_j^{(n)}\bar{y}_i^{(n)}}\right)$$

$$\Psi(\mathbf{x}) = \sum_{i=1}^{n_d} h_i([\mathbf{Ax}]_i) \leq \phi(\mathbf{x}; \mathbf{x}^{(n)}) \triangleq \sum_{i=1}^{n_d} \sum_{j=1}^{n_p} \left[\frac{a_{ij}x_j^{(n)}}{\bar{y}_i^{(n)}} \right] h_i\left(\frac{x_j^{(n)}\bar{y}_i^{(n)}}{x_j^{(n)}\bar{y}_i^{(n)}}\right)$$

Replace convex cost function $\Psi(\mathbf{x})$ with *separable* surrogate function $\phi(\mathbf{x}; \mathbf{x}^{(n)})$.

“ML-EM Algorithm” M-step

E-step gave separable surrogate function:

$$\phi(\mathbf{x}; \mathbf{x}^{(n)}) = \sum_{j=1}^{n_p} \phi_j(x_j; \mathbf{x}^{(n)}), \quad \text{where} \quad \phi_j(x_j; \mathbf{x}^{(n)}) \triangleq \sum_{i=1}^{n_d} \left[\frac{a_{ij} x_j^{(n)}}{\bar{y}_i^{(n)}} \right] h_i \left(\frac{x_j}{x_j^{(n)}} \bar{y}_i^{(n)} \right).$$

M-step separates:

$$\mathbf{x}^{(n+1)} = \arg \min_{\mathbf{x} \geq 0} \phi(\mathbf{x}; \mathbf{x}^{(n)}) \implies x_j^{(n+1)} = \arg \min_{x_j \geq 0} \phi_j(x_j; \mathbf{x}^{(n)}), \quad j = 1, \dots, n_p$$

Minimizing:

$$\frac{\partial}{\partial x_j} \phi_j(x_j; \mathbf{x}^{(n)}) = \sum_{i=1}^{n_d} a_{ij} h_i \left(\bar{y}_i^{(n)} x_j / x_j^{(n)} \right) = \sum_{i=1}^{n_d} a_{ij} \left[1 - \frac{y_i}{\bar{y}_i^{(n)} x_j / x_j^{(n)}} \right] \Big|_{x_j = x_j^{(n+1)}} = 0.$$

Solving (in case $r_i = 0$):

$$x_j^{(n+1)} = x_j^{(n)} \left[\sum_{i=1}^{n_d} a_{ij} \frac{y_i}{[\mathbf{A} \mathbf{x}^{(n)}]_i} \right] / \left(\sum_{i=1}^{n_d} a_{ij} \right), \quad j = 1, \dots, n_p$$

- Derived without any statistical considerations, unlike classical EM formulation.
- Uses only convexity and algebra.
- Guaranteed monotonic: surrogate function ϕ satisfies the 3 required properties.
- M-step trivial due to *separable surrogate*.

ML-EM is Scaled Gradient Descent

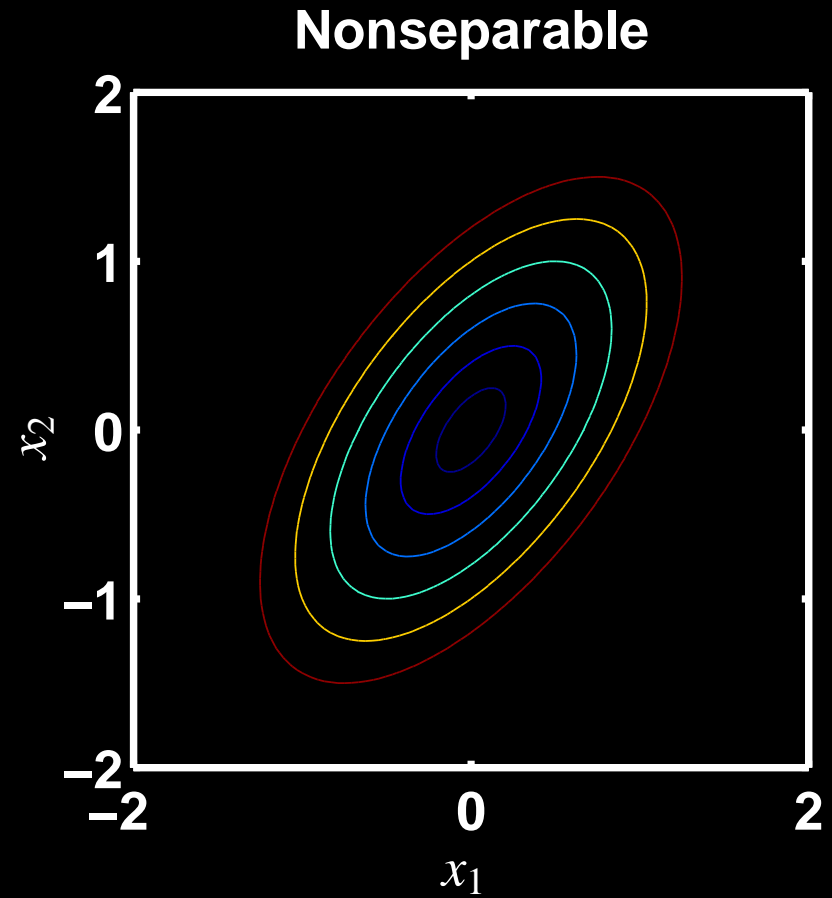
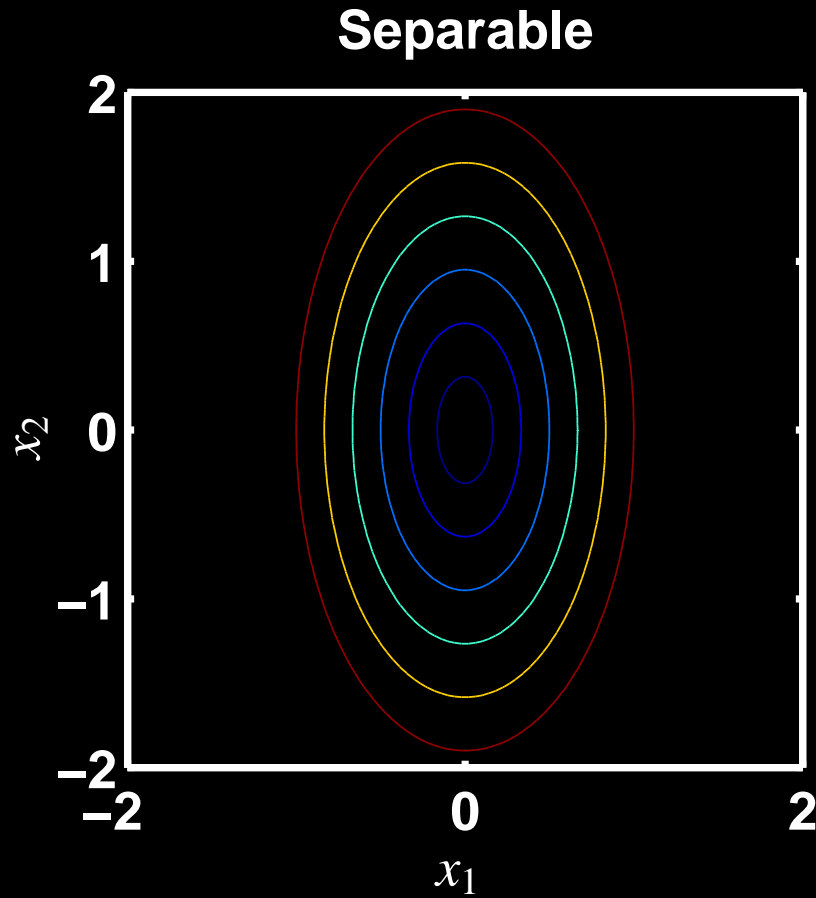
$$\begin{aligned}x_j^{(n+1)} &= x_j^{(n)} \left[\sum_{i=1}^{n_d} a_{ij} \frac{y_i}{\bar{y}_i^{(n)}} \right] / \left(\sum_{i=1}^{n_d} a_{ij} \right) \\&= x_j^{(n)} + x_j^{(n)} \left[\sum_{i=1}^{n_d} a_{ij} \left(\frac{y_i}{\bar{y}_i^{(n)}} - 1 \right) \right] / \left(\sum_{i=1}^{n_d} a_{ij} \right) \\&= \boxed{x_j^{(n)} - \left(\frac{x_j^{(n)}}{\sum_{i=1}^{n_d} a_{ij}} \right) \frac{\partial}{\partial x_j} \Psi(\mathbf{x}^{(n)})}, \quad j = 1, \dots, n_p\end{aligned}$$

$$\mathbf{x}^{(n+1)} = \mathbf{x}^{(n)} + \mathbf{D}(\mathbf{x}^{(n)}) \nabla \Psi(\mathbf{x}^{(n)})$$

This particular diagonal scaling matrix remarkably

- ensures monotonicity,
- ensures nonnegativity.

Consideration: Separable vs Nonseparable



Contour plots: loci of equal function values.

Uncoupled vs coupled minimization.

Separable Surrogate Functions (Easy M-step)

The preceding EM derivation structure applies to *any* cost function of the form

$$\Psi(\mathbf{x}) = \sum_{i=1}^{n_d} h_i([\mathbf{A}\mathbf{x}]_i).$$

cf ISRA (for nonnegative LS), “convex algorithm” for transmission reconstruction

Derivation yields a separable surrogate function

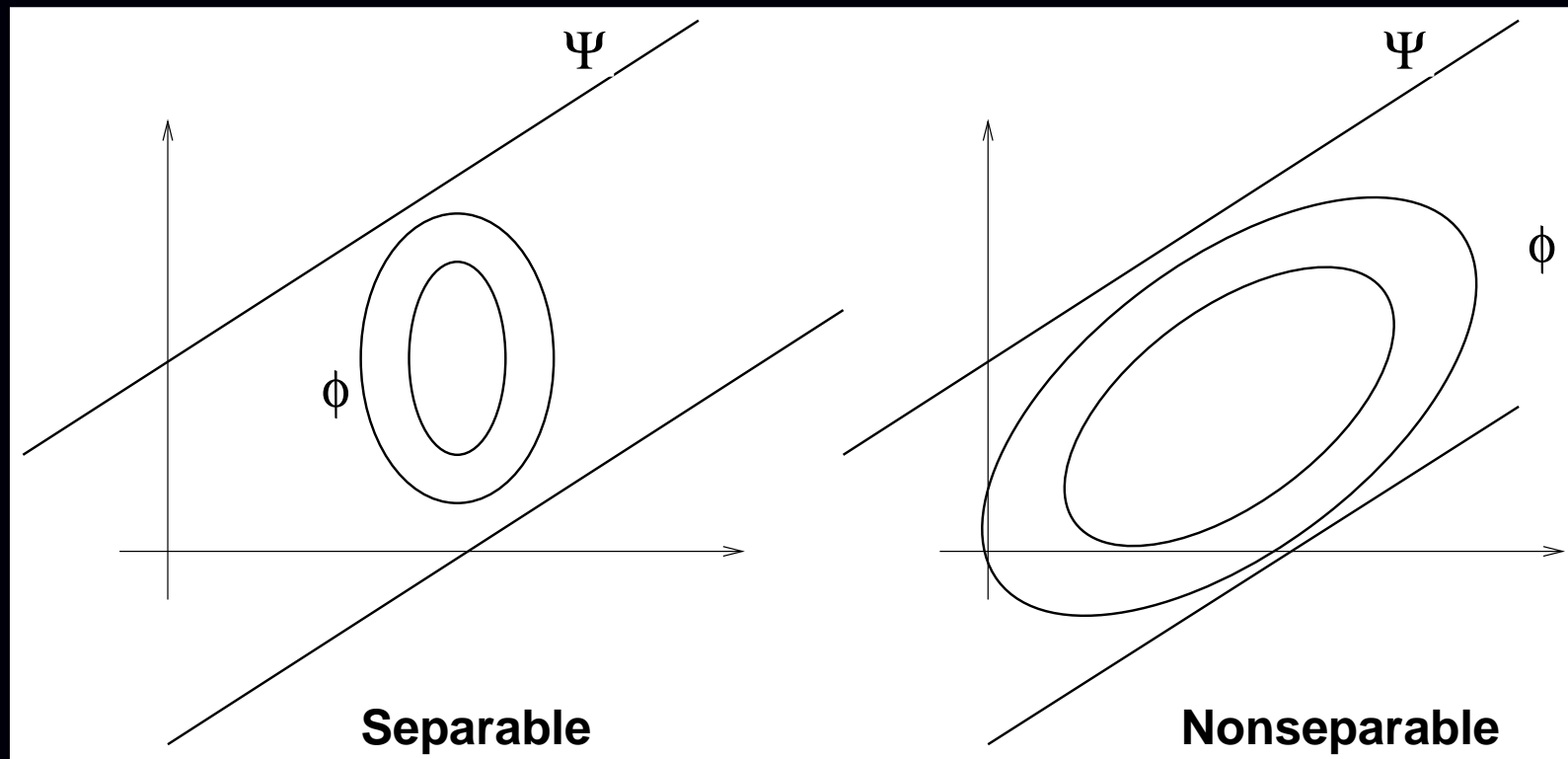
$$\Psi(\mathbf{x}) \leq \phi(\mathbf{x}; \mathbf{x}^{(n)}), \quad \text{where} \quad \phi(\mathbf{x}; \mathbf{x}^{(n)}) = \sum_{j=1}^{n_p} \phi_j(x_j; \mathbf{x}^{(n)})$$

M-step separates into 1D minimization problems (fully parallelizable):

$$\mathbf{x}^{(n+1)} = \arg \min_{\mathbf{x} \geq \mathbf{0}} \phi(\mathbf{x}; \mathbf{x}^{(n)}) \implies x_j^{(n+1)} = \arg \min_{x_j \geq 0} \phi_j(x_j; \mathbf{x}^{(n)}), \quad j = 1, \dots, n_p$$

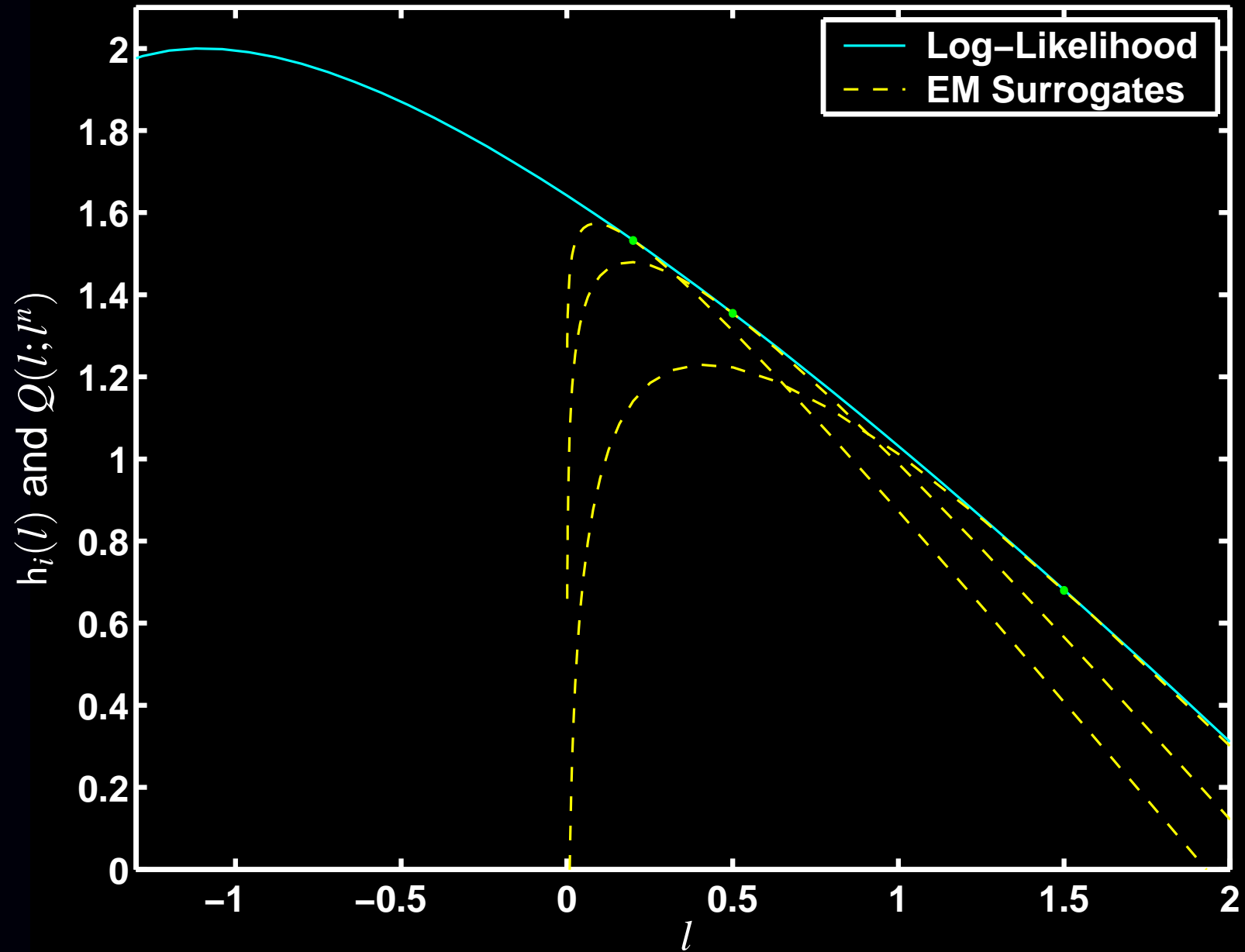
Why do EM / ISRA / convex-algorithm / etc. converge so slowly?

Separable vs Nonseparable



Separable surrogates (e.g., EM) have high curvature \therefore slow convergence.
Nonseparable surrogates can have lower curvature \therefore faster convergence.
Harder to minimize? Use paraboloids (quadratic surrogates).

High Curvature of EM Surrogate



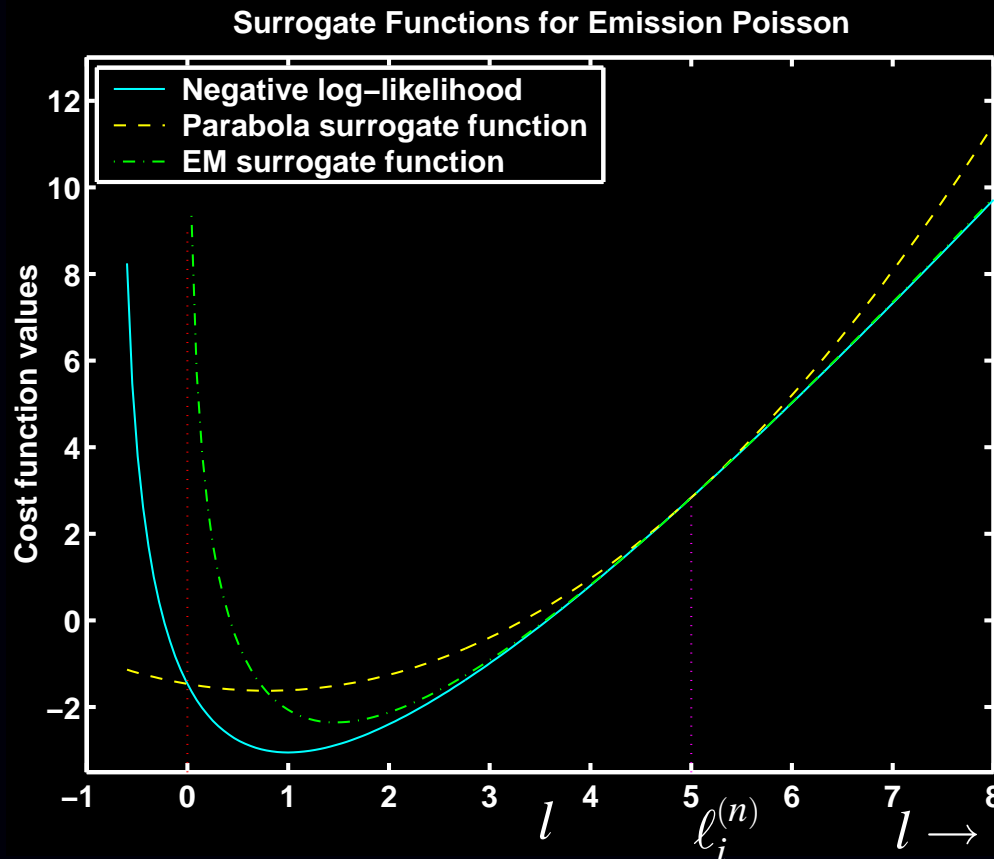
1D Parabola Surrogate Function

Find parabola $q_i^{(n)}(l)$ of the form:

$$q_i^{(n)}(l) = h_i(\ell_i^{(n)}) + \dot{h}_i(\ell_i^{(n)})(l - \ell_i^{(n)}) + c_i^{(n)} \frac{1}{2}(l - \ell_i^{(n)})^2, \quad \text{where } \ell_i^{(n)} \triangleq [\mathbf{Ax}^{(n)}]_i$$

Satisfies tangent condition. Choose curvature to ensure “lies above” condition:

$$c_i^{(n)} \triangleq \min \left\{ c \geq 0 : q_i^{(n)}(l) \geq h_i(l), \quad \forall l \geq 0 \right\}.$$



Lower
curvature!

Paraboloidal Surrogate

Combining 1D parabola surrogates yields *paraboloidal surrogate*:

$$\Psi(\mathbf{x}) = \sum_{i=1}^{n_d} h_i([\mathbf{A}\mathbf{x}]_i) \leq \phi(\mathbf{x}; \mathbf{x}^{(n)}) = \sum_{i=1}^{n_d} q_i^{(n)}([\mathbf{A}\mathbf{x}]_i)$$

$$\text{Rewriting: } \phi(\boldsymbol{\delta} + \mathbf{x}^{(n)}; \mathbf{x}^{(n)}) = \Psi(\mathbf{x}^{(n)}) + \nabla \Psi(\mathbf{x}^{(n)}) \boldsymbol{\delta} + \frac{1}{2} \boldsymbol{\delta}' \mathbf{A}' \text{diag} \left\{ c_i^{(n)} \right\} \mathbf{A} \boldsymbol{\delta}$$

Advantages

- Surrogate $\phi(\mathbf{x}; \mathbf{x}^{(n)})$ is *quadratic*, unlike Poisson log-likelihood
⇒ easier to minimize
- Not separable (unlike EM surrogate)
- Not self-similar (unlike EM surrogate)
- Small curvatures ⇒ fast convergence
- Intrinsically monotone global convergence
- Fairly simple to derive / implement

Quadratic minimization

- Coordinate descent
 - + fast converging
 - + Nonnegativity easy
 - precomputed column-stored system matrix
- Gradient-based quadratic minimization methods
 - Nonnegativity inconvenient

Example: PSCD for PET Transmission Scans

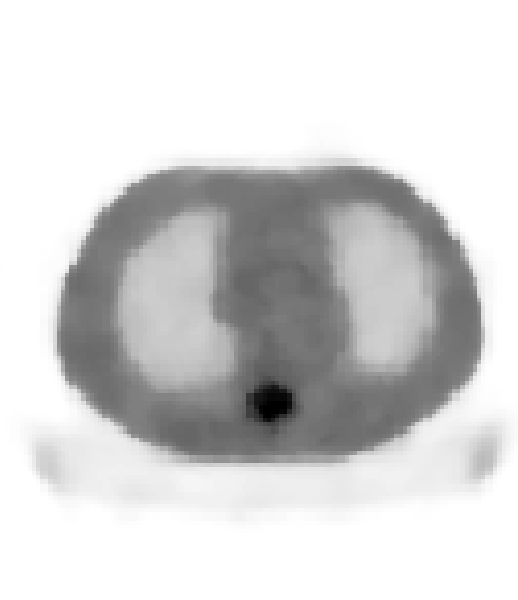
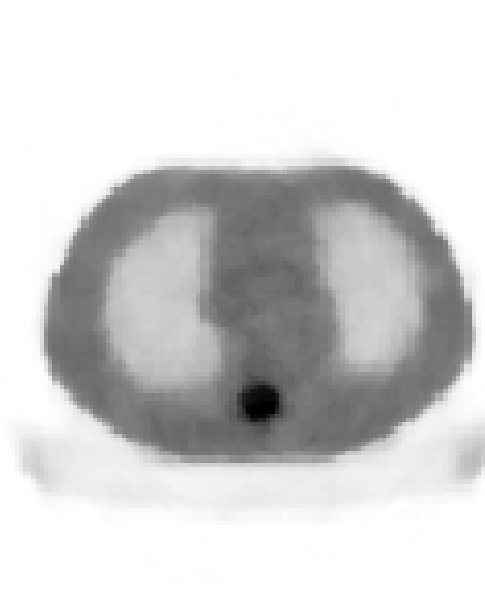
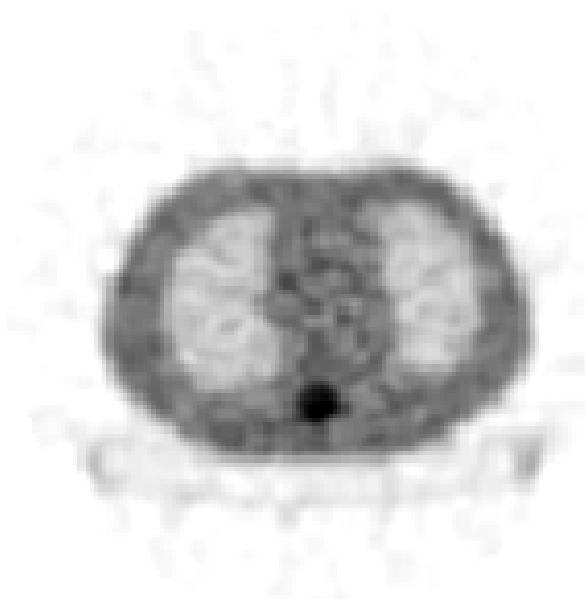
FBP

PL-OSTR-16

PL-PSCD

4 iterations

10 iterations



- square-pixel basis
- strip-integral system model
- shifted-Poisson statistical model
- edge-preserving convex regularization (Huber)
- nonnegativity constraint
- inscribed circle support constraint
- paraboloidal surrogate coordinate descent (PSCD) algorithm

Separable Paraboloidal Surrogate

To derive a parallelizable algorithm apply another De Pierro trick:

$$[\mathbf{Ax}]_i = \sum_{j=1}^{n_p} \pi_{ij} \left[\frac{a_{ij}}{\pi_{ij}} (x_j - x_j^{(n)}) + \ell_i^{(n)} \right], \quad \ell_i^{(n)} = [\mathbf{Ax}^{(n)}]_i.$$

Provided $\pi_{ij} \geq 0$ and $\sum_{j=1}^{n_p} \pi_{ij} = 1$, since parabola q_i is convex:

$$q_i^{(n)}([\mathbf{Ax}]_i) = q_i^{(n)} \left(\sum_{j=1}^{n_p} \pi_{ij} \left[\frac{a_{ij}}{\pi_{ij}} (x_j - x_j^{(n)}) + \ell_i^{(n)} \right] \right) \leq \sum_{j=1}^{n_p} \pi_{ij} q_i^{(n)} \left(\frac{a_{ij}}{\pi_{ij}} (x_j - x_j^{(n)}) + \ell_i^{(n)} \right)$$

$$\therefore \phi(\mathbf{x}; \mathbf{x}^{(n)}) = \sum_{i=1}^{n_d} q_i^{(n)}([\mathbf{Ax}]_i) \leq \tilde{\phi}(\mathbf{x}; \mathbf{x}^{(n)}) \triangleq \sum_{i=1}^{n_d} \sum_{j=1}^{n_p} \pi_{ij} q_i^{(n)} \left(\frac{a_{ij}}{\pi_{ij}} (x_j - x_j^{(n)}) + \ell_i^{(n)} \right)$$

Separable Paraboloidal Surrogate:

$$\tilde{\phi}(\mathbf{x}; \mathbf{x}^{(n)}) = \sum_{j=1}^{n_p} \phi_j(x_j; \mathbf{x}^{(n)}), \quad \phi_j(x_j; \mathbf{x}^{(n)}) \triangleq \sum_{i=1}^{n_d} \pi_{ij} q_i^{(n)} \left(\frac{a_{ij}}{\pi_{ij}} (x_j - x_j^{(n)}) + \ell_i^{(n)} \right)$$

Parallelizable M-step (cf gradient descent!):

$$x_j^{(n+1)} = \arg \min_{x_j \geq 0} \phi_j(x_j; \mathbf{x}^{(n)}) = \left[x_j^{(n)} - \frac{1}{d_j^{(n)}} \frac{\partial}{\partial x_j} \Psi(\mathbf{x}^{(n)}) \right]_+, \quad d_j^{(n)} = \sum_{i=1}^{n_d} \frac{a_{ij}^2}{\pi_{ij}} c_i^{(n)}$$

Natural choice is $\pi_{ij} = |a_{ij}|/|a|_i$, $|a|_i = \sum_{j=1}^{n_p} |a_{ij}|$

Example: Poisson ML Transmission Problem

Transmission negative log-likelihood (for i th ray):

$$h_i(l) = (b_i e^{-l} + r_i) - y_i \log(b_i e^{-l} + r_i).$$

Optimal (smallest) parabola surrogate curvature (Erdođan, T-MI, Sep. 1999):

$$c_i^{(n)} = c(\ell_i^{(n)}, h_i), \quad c(l, h) = \begin{cases} \left[2 \frac{h(0) - h(l) + \dot{h}(l)l}{l^2} \right]_+, & l > 0 \\ [\ddot{h}(l)]_+, & l = 0. \end{cases}$$

Separable Paraboloidal Surrogate (SPS) Algorithm:

Precompute $|a|_i = \sum_{j=1}^{n_p} a_{ij}$, $i = 1, \dots, n_d$

$$\ell_i^{(n)} = [\mathbf{A}\mathbf{x}^{(n)}]_i, \quad (\text{forward projection})$$

$$\bar{y}_i^{(n)} = b_i e^{-\ell_i^{(n)}} + r_i \quad (\text{predicted means})$$

$$\dot{h}_i^{(n)} = 1 - y_i / \bar{y}_i^{(n)} \quad (\text{slopes})$$

$$c_i^{(n)} = c(\ell_i^{(n)}, h_i) \quad (\text{curvatures})$$

$$x_j^{(n+1)} = \left[x_j^{(n)} - \frac{1}{d_j^{(n)}} \frac{\partial}{\partial x_j} \Psi(\mathbf{x}^{(n)}) \right]_+ = \left[x_j^{(n)} - \frac{\sum_{i=1}^{n_d} a_{ij} \dot{h}_i^{(n)}}{\sum_{i=1}^{n_d} a_{ij} |a|_i c_i^{(n)}} \right]_+, \quad j = 1, \dots, n_p$$

Monotonically decreases cost function each iteration.

No logarithm!

The MAP-EM M-step “Problem”

Add a penalty function to our surrogate for the negative log-likelihood:

$$\Psi(\mathbf{x}) = \ell(\mathbf{x}) + \beta R(\mathbf{x})$$
$$\phi(\mathbf{x}; \mathbf{x}^{(n)}) = \sum_{j=1}^{n_p} \phi_j(x_j; \mathbf{x}^{(n)}) + \beta R(\mathbf{x})$$

$$\text{M-step: } \mathbf{x}^{(n+1)} = \arg \min_{\mathbf{x} \geq \mathbf{0}} \phi(\mathbf{x}; \mathbf{x}^{(n)}) = \arg \min_{\mathbf{x} \geq \mathbf{0}} \sum_{j=1}^{n_p} \phi_j(x_j; \mathbf{x}^{(n)}) + \beta R(\mathbf{x}) = ?$$

For nonseparable penalty functions, the M-step is coupled \therefore difficult.

Suboptimal solutions

- Generalized EM (GEM) algorithm (coordinate descent on ϕ)
Monotonic, but inherits slow convergence of EM.
- One-step late (OSL) algorithm (use outdated gradients) (Green, T-MI, 1990)

$$\frac{\partial}{\partial x_j} \phi(\mathbf{x}; \mathbf{x}^{(n)}) = \frac{\partial}{\partial x_j} \phi_j(x_j; \mathbf{x}^{(n)}) + \beta \frac{\partial}{\partial x_j} R(\mathbf{x}) \stackrel{?}{\approx} \frac{\partial}{\partial x_j} \phi_j(x_j; \mathbf{x}^{(n)}) + \beta \frac{\partial}{\partial x_j} R(\mathbf{x}^{(n)})$$

Nonmonotonic. Known to diverge, depending on β .

Temporarily simple, but *avoid!*

Contemporary solution

- Use separable surrogate for penalty function too (De Pierro, T-MI, Dec. 1995)
Ensures monotonicity. Obviates all reasons for using OSL!

De Pierro's MAP-EM Algorithm

Apply separable paraboloidal surrogates to penalty function:

$$R(\mathbf{x}) \leq R_{\text{SPS}}(\mathbf{x}; \mathbf{x}^{(n)}) = \sum_{j=1}^{n_p} R_j(x_j; \mathbf{x}^{(n)})$$

Overall separable surrogate: $\phi(\mathbf{x}; \mathbf{x}^{(n)}) = \sum_{j=1}^{n_p} \phi_j(x_j; \mathbf{x}^{(n)}) + \beta \sum_{j=1}^{n_p} R_j(x_j; \mathbf{x}^{(n)})$

The M-step becomes fully parallelizable:

$$x_j^{(n+1)} = \arg \min_{x_j \geq 0} \phi_j(x_j; \mathbf{x}^{(n)}) - \beta R_j(x_j; \mathbf{x}^{(n)}), \quad j = 1, \dots, n_p.$$

Consider quadratic penalty $R(\mathbf{x}) = \sum_k \psi([\mathbf{C}\mathbf{x}]_k)$, where $\psi(t) = t^2/2$.

If $\gamma_{kj} \geq 0$ and $\sum_{j=1}^{n_p} \gamma_{kj} = 1$ then

$$[\mathbf{C}\mathbf{x}]_k = \sum_{j=1}^{n_p} \gamma_{kj} \left[\frac{c_{kj}}{\gamma_{kj}} (x_j - x_j^{(n)}) + [\mathbf{C}\mathbf{x}^{(n)}]_k \right].$$

Since ψ is convex:

$$\begin{aligned} \psi([\mathbf{C}\mathbf{x}]_k) &= \psi \left(\sum_{j=1}^{n_p} \gamma_{kj} \left[\frac{c_{kj}}{\gamma_{kj}} (x_j - x_j^{(n)}) + [\mathbf{C}\mathbf{x}^{(n)}]_k \right] \right) \\ &\leq \sum_{j=1}^{n_p} \gamma_{kj} \psi \left(\frac{c_{kj}}{\gamma_{kj}} (x_j - x_j^{(n)}) + [\mathbf{C}\mathbf{x}^{(n)}]_k \right) \end{aligned}$$

De Pierro's Algorithm Continued

So $R(\mathbf{x}) \leq R(\mathbf{x}; \mathbf{x}^{(n)}) \triangleq \sum_{j=1}^{n_p} R_j(x_j; \mathbf{x}^{(n)})$ where

$$R_j(x_j; \mathbf{x}^{(n)}) \triangleq \sum_k \gamma_{kj} \Psi \left(\frac{c_{kj}}{\gamma_{kj}} (x_j - x_j^{(n)}) + [\mathbf{C}\mathbf{x}^{(n)}]_k \right)$$

M-step: Minimizing $\phi_j(x_j; \mathbf{x}^{(n)}) + \beta R_j(x_j; \mathbf{x}^{(n)})$ yields the iteration:

$$x_j^{(n+1)} = \frac{x_j^{(n)} \sum_{i=1}^{n_d} a_{ij} y_i / \bar{y}_i^{(n)}}{B_j + \sqrt{B_j^2 + \left(x_j^{(n)} \sum_{i=1}^{n_d} a_{ij} y_i / \bar{y}_i^{(n)} \right) \left(\beta \sum_k c_{kj}^2 / \gamma_{kj} \right)}}$$

$$\text{where } B_j \triangleq \frac{1}{2} \left[\sum_{i=1}^{n_d} a_{ij} + \beta \sum_k \left(c_{kj} [\mathbf{C}\mathbf{x}^{(n)}]_k - \frac{c_{kj}^2}{\gamma_{kj}} x_j^{(n)} \right) \right], \quad j = 1, \dots, n_p$$

and $\bar{y}_i^{(n)} = [\mathbf{A}\mathbf{x}^{(n)}]_i + r_i$.

Advantages: Intrinsically monotone, nonnegativity, fully parallelizable.
Requires only a couple % more computation per iteration than ML-EM

Disadvantages: Slow convergence (like EM) due to separable surrogate

Ordered Subsets Algorithms

aka *block iterative* or *incremental gradient* algorithms

The gradient appears in essentially every algorithm:

$$\ell(\mathbf{x}) = \sum_{i=1}^{n_d} h_i([\mathbf{A}\mathbf{x}]_i) \implies \frac{\partial}{\partial x_j} \ell(\mathbf{x}) = \sum_{i=1}^{n_d} a_{ij} \dot{h}_i([\mathbf{A}\mathbf{x}]_i).$$

This is a *backprojection* of a sinogram of the derivatives $\{\dot{h}_i([\mathbf{A}\mathbf{x}]_i)\}$.

Intuition: with half the angular sampling, this backprojection would be fairly similar

$$\frac{1}{n_d} \sum_{i=1}^{n_d} a_{ij} \dot{h}_i(\cdot) \approx \frac{1}{|\mathcal{S}|} \sum_{i \in \mathcal{S}} a_{ij} \dot{h}_i(\cdot),$$

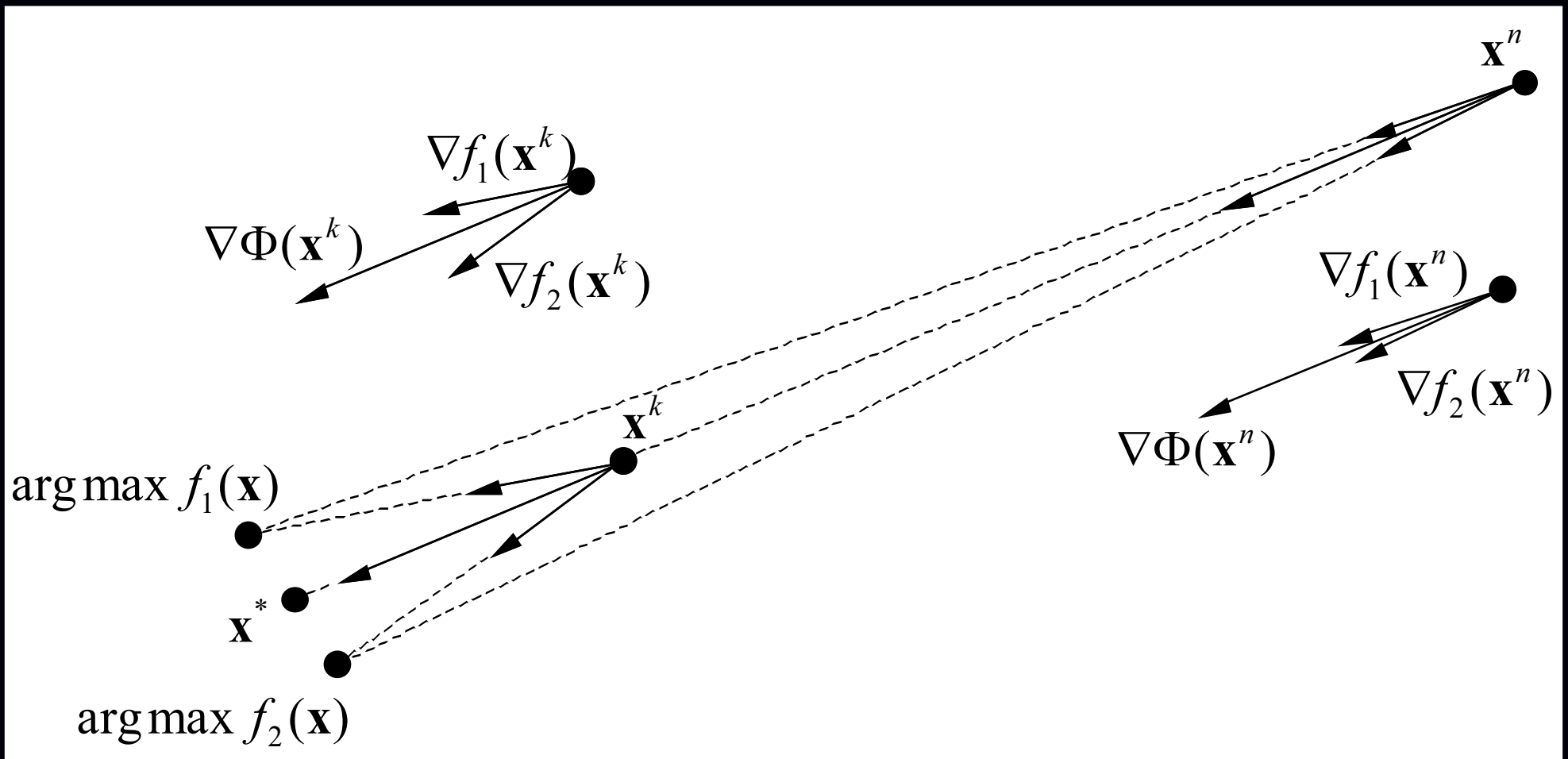
where \mathcal{S} is a subset of the rays.

To “OS-ize” an algorithm, replace all backprojections with partial sums.

Recall typical iteration:

$$\mathbf{x}^{(n+1)} = \mathbf{x}^{(n)} - \mathbf{D}(\mathbf{x}^{(n)}) \nabla \Psi(\mathbf{x}^{(n)}).$$

Geometric View of Ordered Subsets



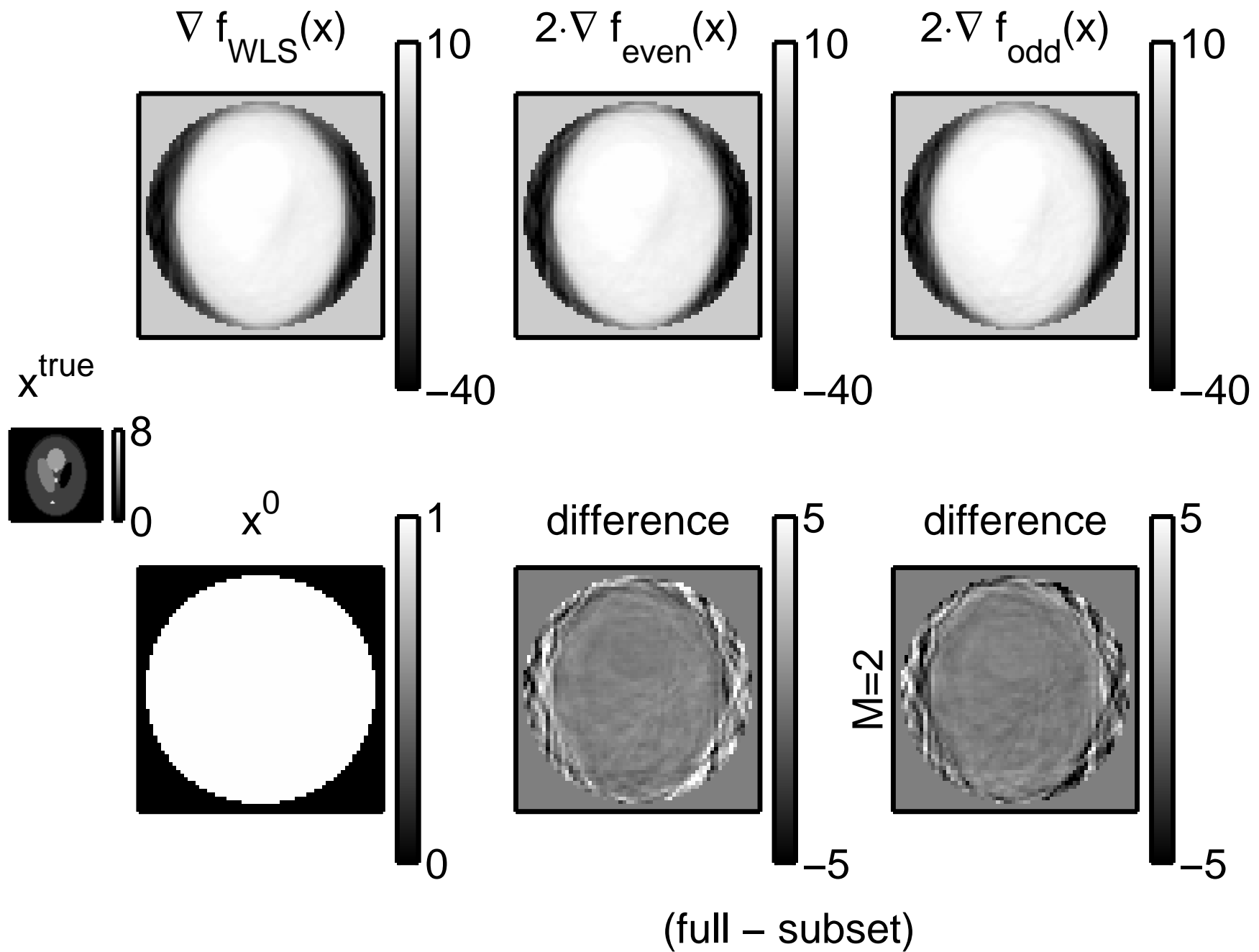
Two subset case: $\Psi(\mathbf{x}) = f_1(\mathbf{x}) + f_2(\mathbf{x})$ (e.g., odd and even projection views).

For $\mathbf{x}^{(n)}$ far from \mathbf{x}^* , even partial gradients should point roughly towards \mathbf{x}^* .

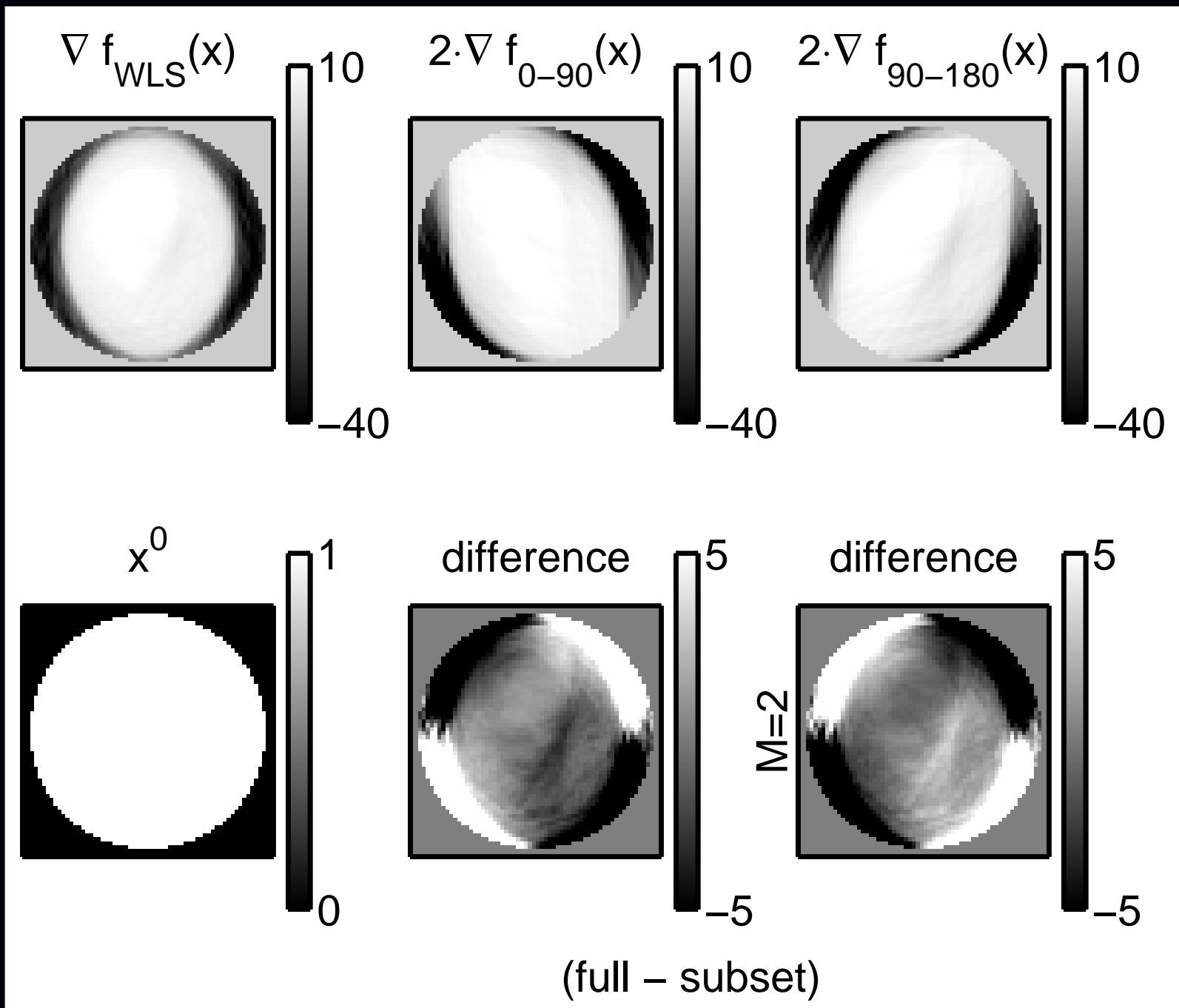
For $\mathbf{x}^{(n)}$ near \mathbf{x}^* , however, $\nabla\Psi(\mathbf{x}) \approx \mathbf{0}$, so $\nabla f_1(\mathbf{x}) \approx -\nabla f_2(\mathbf{x}) \implies$ cycles!

Issues. "Subset gradient balance": $\nabla\Psi(\mathbf{x}) \approx M\nabla f_k(\mathbf{x})$. Choice of ordering.

Incremental Gradients (WLS, 2 Subsets)



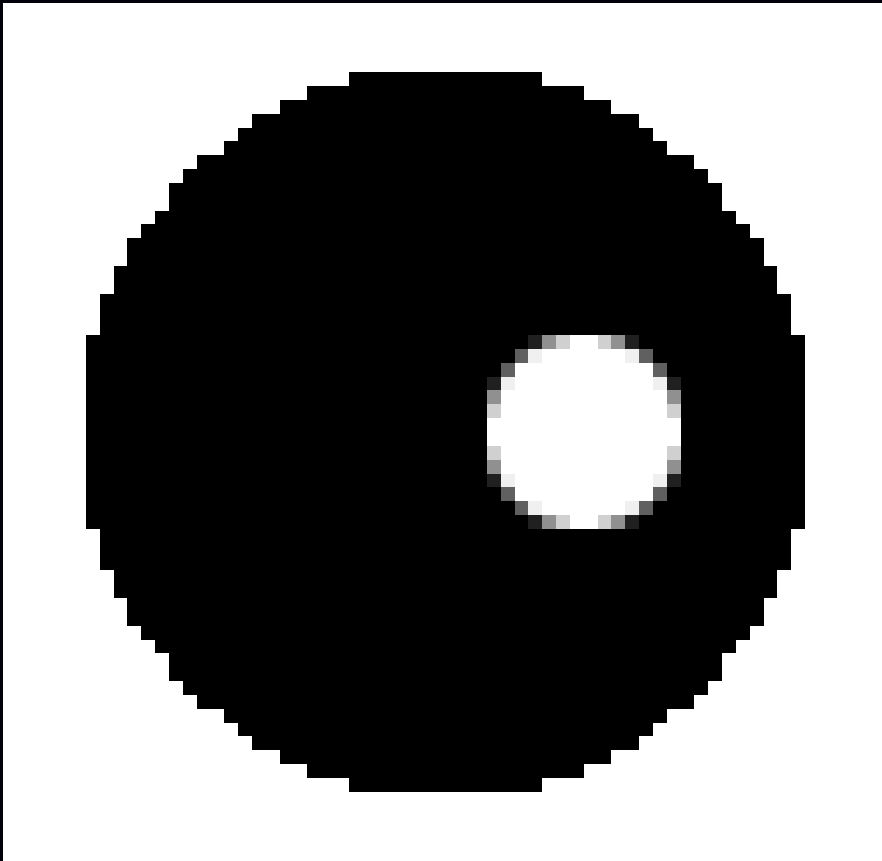
Subset Gradient Imbalance



Problems with OS-EM

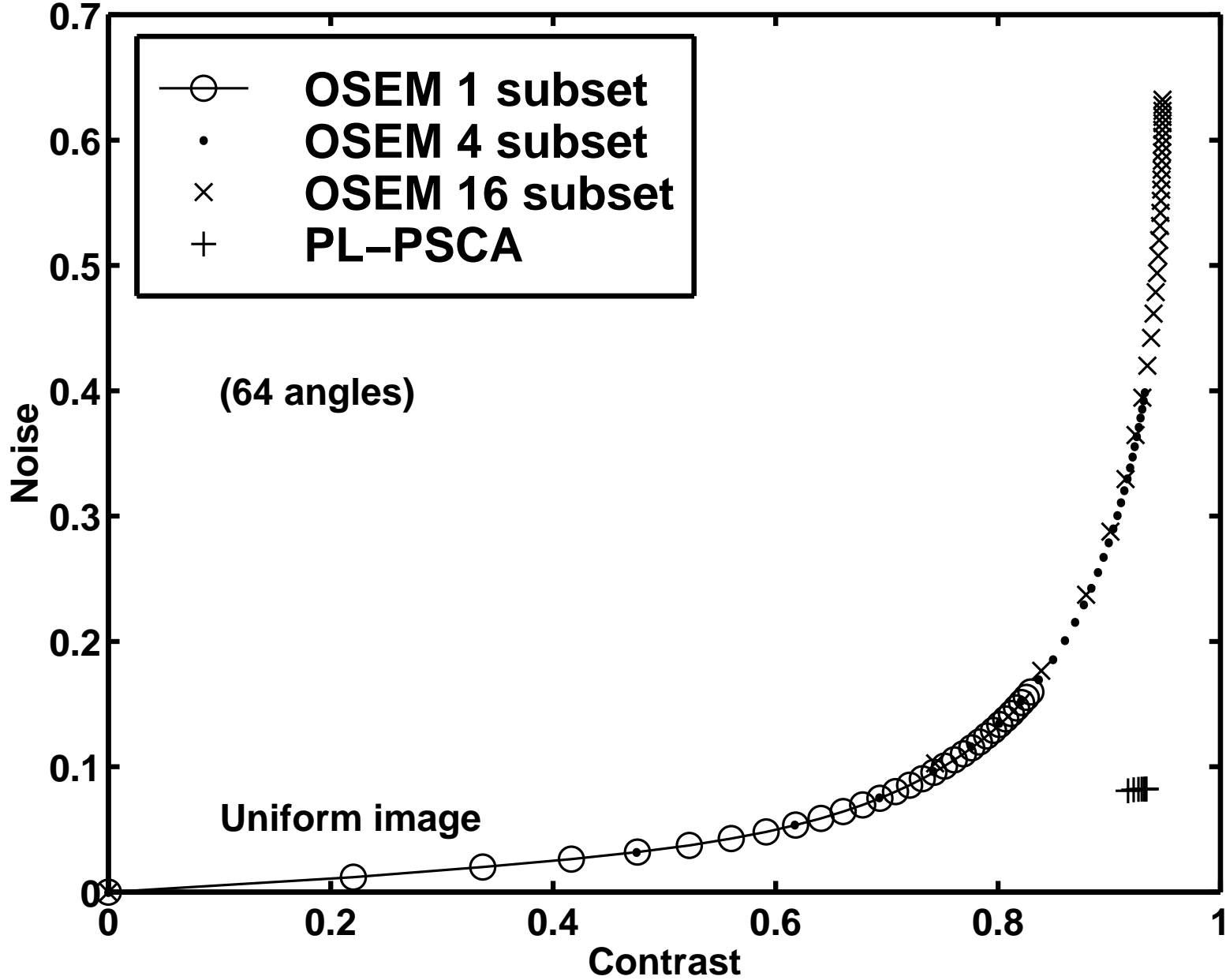
- Non-monotone
- Does not converge (may cycle)
- Byrne's "rescaled block iterative" (RBI) approach converges only for consistent (noiseless) data
- \therefore unpredictable
 - What resolution after n iterations?
Object-dependent, spatially nonuniform
 - What variance after n iterations?
 - ROI variance? (e.g., for Huesman's WLS kinetics)

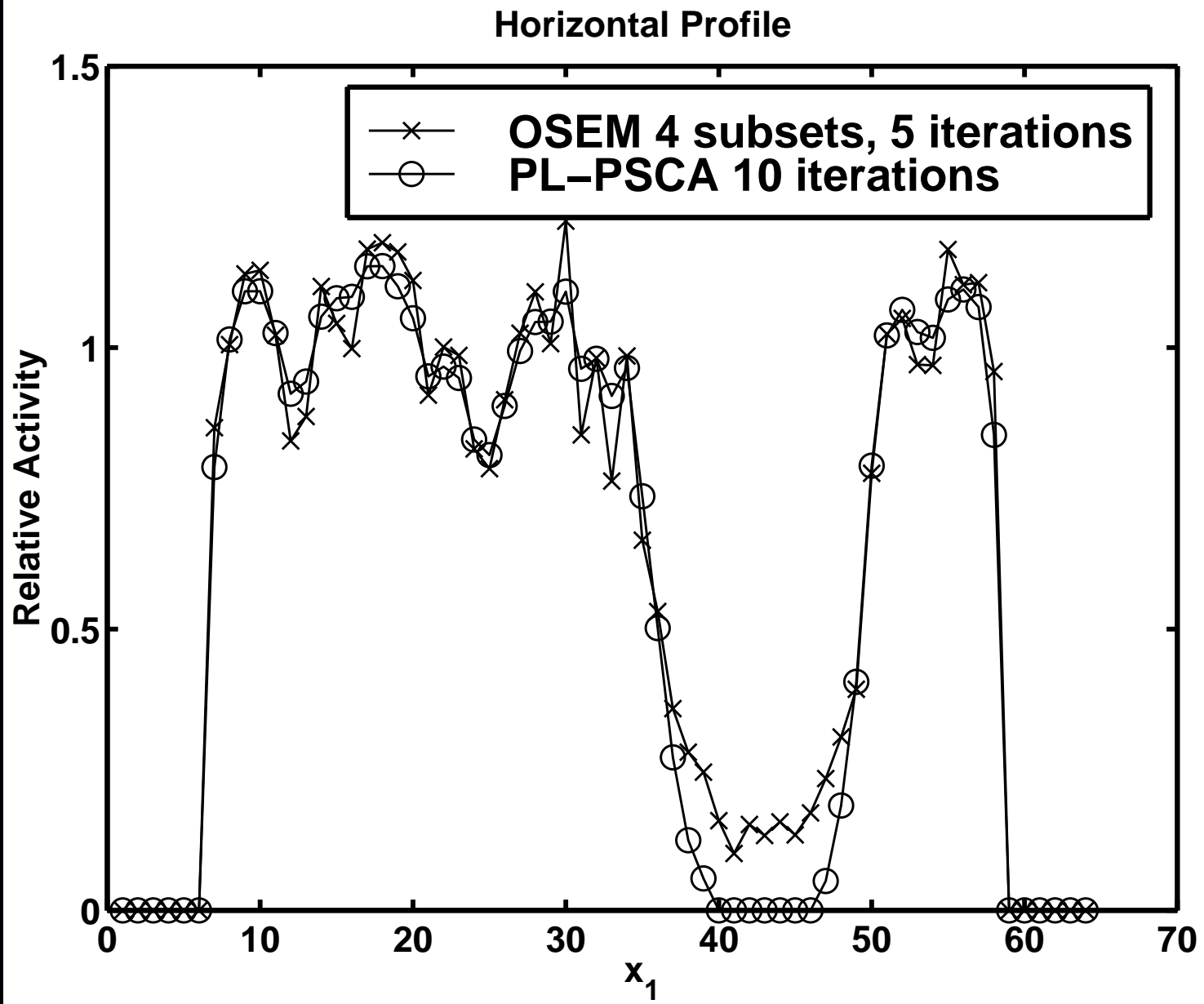
OSEM vs Penalized Likelihood



- 64×62 image
- 66×60 sinogram
- 10^6 counts
- 15% randoms/scatter
- uniform attenuation
- contrast in cold region
- within-region σ opposite side

Contrast-Noise Results





Making OS Methods Converge

- Relaxation
- Incrementalism

Relaxed block-iterative methods

$$\Psi(\mathbf{x}) = \sum_{m=1}^M \Psi_m(\mathbf{x})$$

$$\mathbf{x}^{(n+(m+1)/M)} = \mathbf{x}^{(n+m/M)} - \alpha_n D(\mathbf{x}^{(n+m/M)}) \nabla \Psi_m(\mathbf{x}^{(n+m/M)}), \quad m = 0, \dots, M-1$$

Relaxation of step sizes:

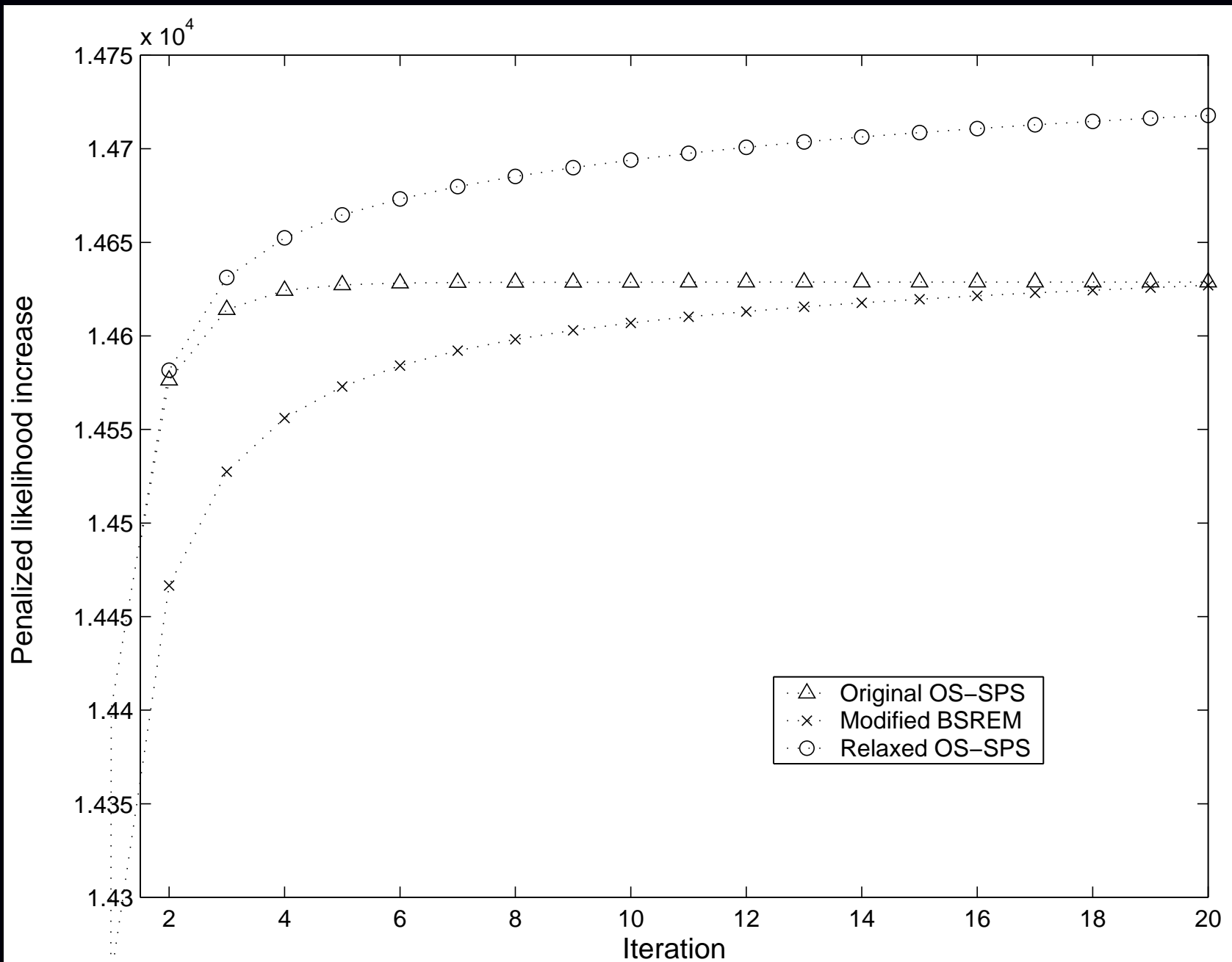
$$\alpha_n \rightarrow 0 \text{ as } n \rightarrow \infty, \quad \sum_n \alpha_n = \infty, \quad \sum_n \alpha_n^2 < \infty$$

- ART
- RAMLA, BSREM (De Pierro, T-MI, 1997, 2001)
- Ahn and Fessler, NSS/MIC 2001, T-MI 2003

Considerations

- Proper relaxation can induce convergence, *but* still lacks monotonicity.
- Choice of relaxation schedule requires experimentation.
- $\Psi_m(\mathbf{x}) = \ell_m(\mathbf{x}) + \frac{1}{M} R(\mathbf{x})$, so each Ψ_m includes part of the likelihood yet all of R

Relaxed OS-SPS



Incremental Methods

Incremental EM applied to emission tomography by Hsiao *et al.* as C-OSEM

Incremental optimization transfer (Ahn & Fessler, MIC 2004)

Find majorizing surrogate for each sub-objective function:

$$\begin{aligned}\phi_m(\mathbf{x}; \mathbf{x}) &= \Psi_m(\mathbf{x}), & \forall \mathbf{x} \\ \phi_m(\mathbf{x}; \bar{\mathbf{x}}) &\geq \Psi_m(\mathbf{x}), & \forall \mathbf{x}, \bar{\mathbf{x}}\end{aligned}$$

Define the following augmented cost function: $F(\mathbf{x}; \bar{\mathbf{x}}_1, \dots, \bar{\mathbf{x}}_M) = \sum_{m=1}^M \phi_m(\mathbf{x}; \bar{\mathbf{x}}_m)$.

Fact: by construction $\hat{\mathbf{x}} = \arg \min_{\mathbf{x}} \Psi(\mathbf{x}) = \arg \min_{\mathbf{x}} \min_{\bar{\mathbf{x}}_1, \dots, \bar{\mathbf{x}}_M} F(\mathbf{x}; \bar{\mathbf{x}}_1, \dots, \bar{\mathbf{x}}_M)$.

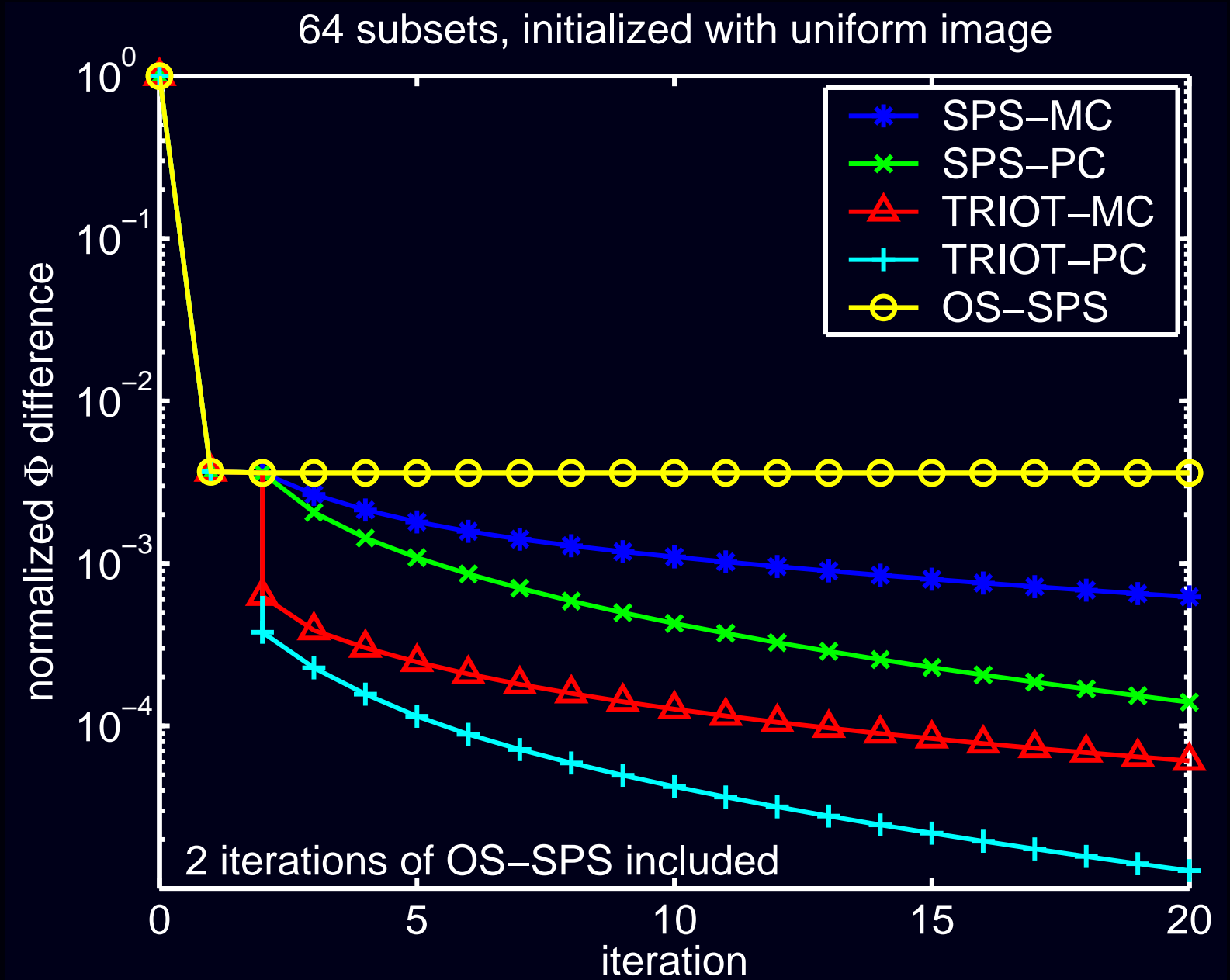
Alternating minimization: for $m = 1, \dots, M$:

$$\begin{aligned}\mathbf{x}^{\text{new}} &= \arg \min_{\mathbf{x}} F\left(\mathbf{x}; \bar{\mathbf{x}}_1^{(n+1)}, \dots, \bar{\mathbf{x}}_{m-1}^{(n+1)}, \bar{\mathbf{x}}_m^{(n)}, \bar{\mathbf{x}}_{m+1}^{(n)}, \dots, \bar{\mathbf{x}}_M^{(n)}\right) \\ \bar{\mathbf{x}}_m^{(n+1)} &= \arg \min_{\bar{\mathbf{x}}_m} F\left(\mathbf{x}^{\text{new}}; \bar{\mathbf{x}}_1^{(n+1)}, \dots, \bar{\mathbf{x}}_{m-1}^{(n+1)}, \bar{\mathbf{x}}_m, \bar{\mathbf{x}}_{m+1}^{(n)}, \dots, \bar{\mathbf{x}}_M^{(n)}\right) = \mathbf{x}^{\text{new}}.\end{aligned}$$

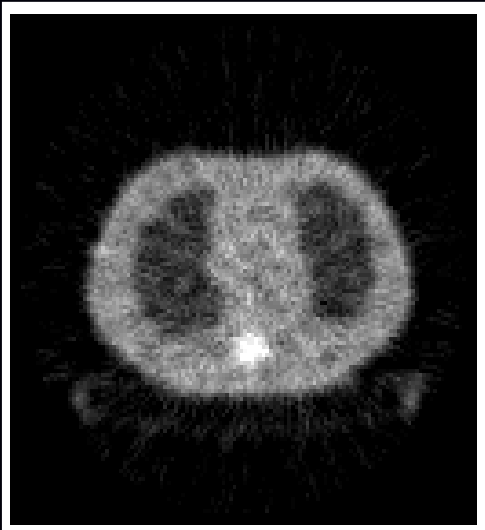
- Use all current information, but increment the surrogate for only one subset.
- Monotone in F , converges under reasonable assumptions on Ψ
- In contrast, OS-EM uses the information from *only* one subset at a time

TRIOT Example: Convergence Rate

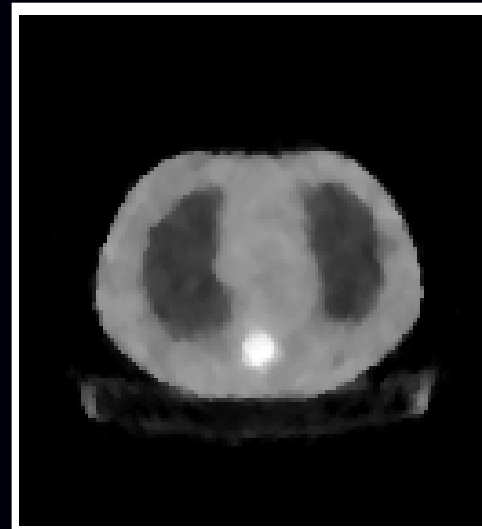
Transmission incremental optimization transfer (TRIOT)



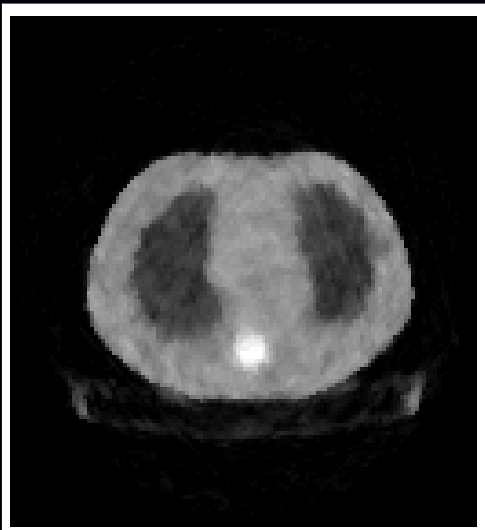
TRIOT Example: Attenuation Map Images



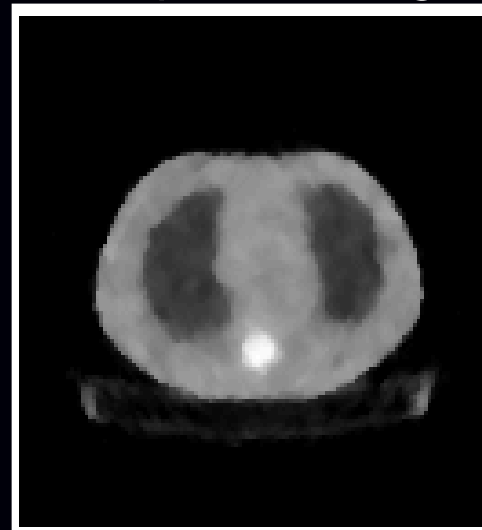
FBP



PL optimal image



OS-SPS



TRIOT-PC

OS-SPS: 64 subsets, 20 iterations, one point of the limit cycle

TRIOT-PC: 64 subsets, 20 iterations, after 2 iterations of OS-SPS)

OSTR aka Transmission OS-SPS

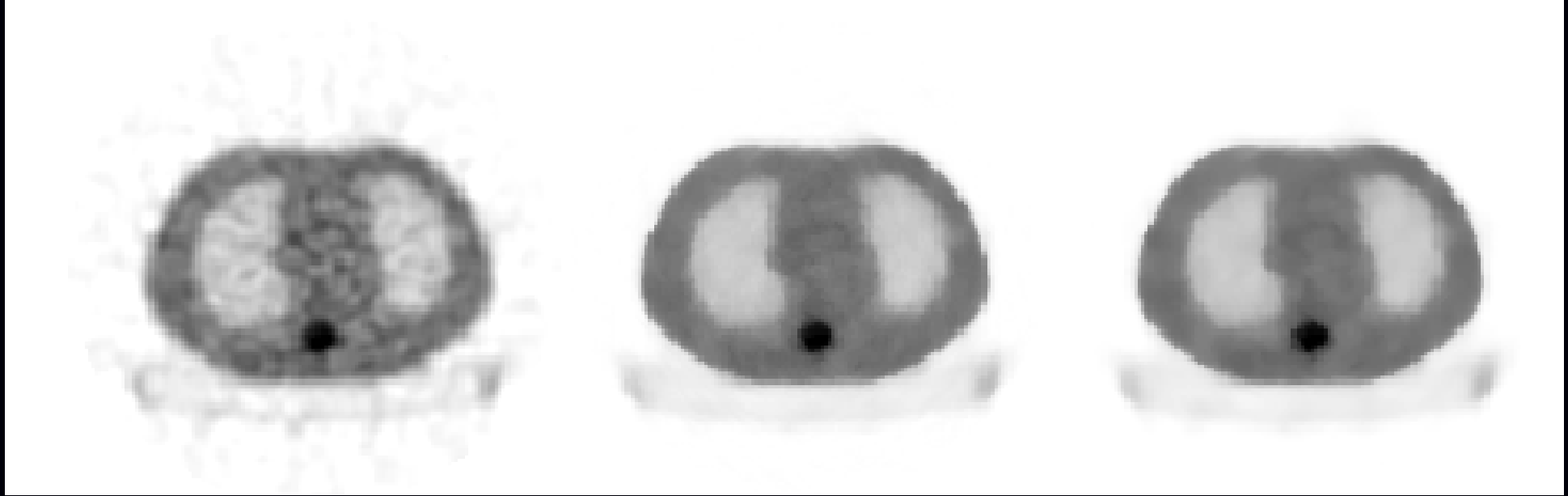
FBP

PL-OSTR-16

PL-PSCD

4 iterations

10 iterations



Ordered subsets version of separable paraboloidal surrogates
for PET transmission problem with nonquadratic convex *regularization*

Matlab m-file [http://www.eecs.umich.edu/~fessler
/code/transmission/tpl_osps.m](http://www.eecs.umich.edu/~fessler/code/transmission/tpl_osps.m)

Precomputed curvatures for OS-SPS

Separable Paraboloidal Surrogate (SPS) Algorithm:

$$x_j^{(n+1)} = \left[x_j^{(n)} - \frac{\sum_{i=1}^{n_d} a_{ij} \dot{h}_i([\mathbf{A}\mathbf{x}^{(n)}]_i)}{\sum_{i=1}^{n_d} a_{ij} |a|_i c_i^{(n)}} \right]_+, \quad j = 1, \dots, n_p$$

Ordered-subsets abandons monotonicity, so why use optimal curvatures $c_i^{(n)}$?

Precomputed curvature:

$$c_i = \ddot{h}_i(\hat{l}_i), \quad \hat{l}_i = \arg \min_l h_i(l)$$

Precomputed denominator (saves one backprojection each iteration!):

$$d_j = \sum_{i=1}^{n_d} a_{ij} |a|_i c_i, \quad j = 1, \dots, n_p.$$

OS-SPS algorithm with M subsets:

$$x_j^{(n+1)} = \left[x_j^{(n)} - \frac{\sum_{i \in \mathcal{S}^{(n)}} a_{ij} \dot{h}_i([\mathbf{A}\mathbf{x}^{(n)}]_i)}{d_j / M} \right]_+, \quad j = 1, \dots, n_p$$

Summary of Algorithms

- General-purpose optimization algorithms
- Optimization transfer for image reconstruction algorithms
- Separable surrogates \implies high curvatures \implies slow convergence
- Ordered subsets accelerate *initial* convergence
require relaxation or incrementalism for true convergence
- Principles apply to emission and transmission reconstruction
- Still work to be done...

Matlab/Freemat “image reconstruction toolbox” online:
<http://www.eecs.umich.edu/~fessler/code>

An Open Problem

Still no algorithm with all of the following properties:

- Nonnegativity easy
- Fast converging
- Intrinsically monotone global convergence
- Accepts any type of system matrix
- Parallelizable

Part 4. Performance Characteristics

- Spatial resolution properties
- Noise properties
- Detection properties

Spatial Resolution Properties

Choosing β can be painful, so ...

For true minimization methods:

$$\hat{\mathbf{x}} = \arg \min_{\mathbf{x}} \Psi(\mathbf{x})$$

the *local impulse response* is approximately (Fessler and Rogers, T-MI, 1996):

$$l_j(\mathbf{x}) = \lim_{\delta \rightarrow 0} \frac{E[\hat{\mathbf{x}} | \mathbf{x} + \delta \mathbf{e}_j] - E[\hat{\mathbf{x}} | \mathbf{x}]}{\delta} \approx [-\nabla^{20} \Psi]^{-1} \nabla^{11} \Psi \frac{\partial}{\partial x_j} \bar{\mathbf{y}}(\mathbf{x}).$$

Depends only on chosen **cost function** and **statistical model**.

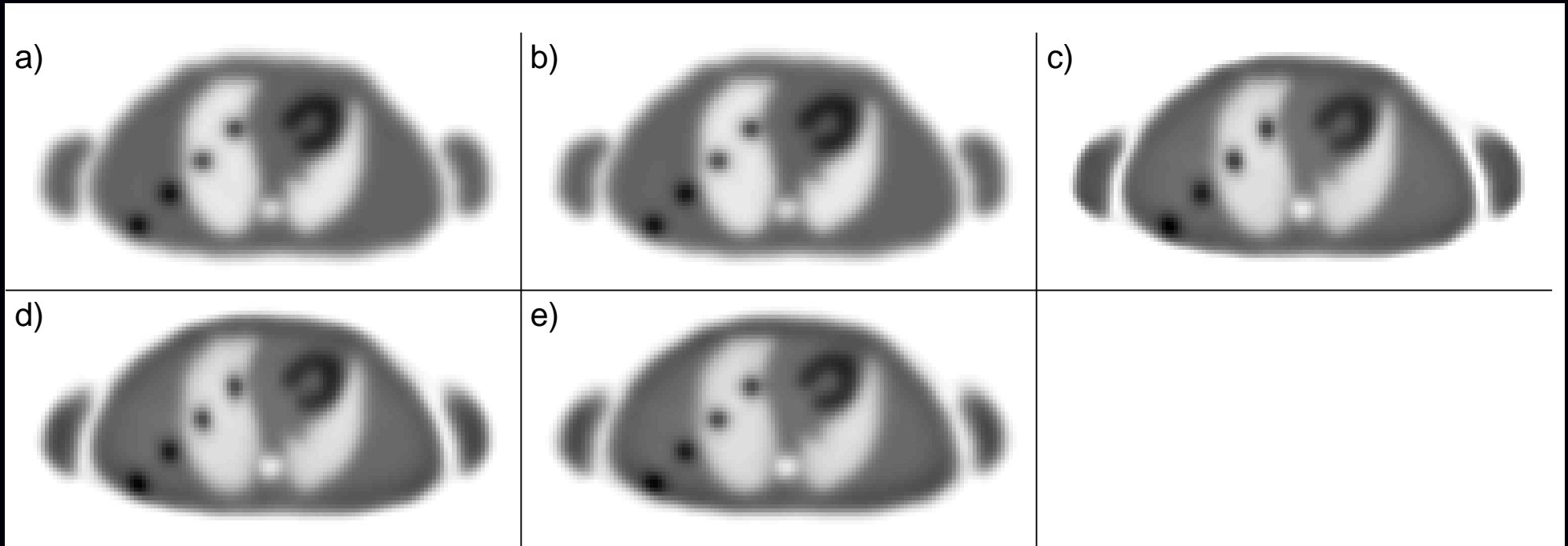
Independent of optimization algorithm (if iterated “to convergence”).

- Enables prediction of resolution properties (provided Ψ is minimized)
- Useful for designing regularization penalty functions with desired resolution properties. For penalized likelihood:

$$l_j(\mathbf{x}) \approx [\mathbf{A}'\mathbf{W}\mathbf{A} + \beta\mathbf{R}]^{-1} \mathbf{A}'\mathbf{W}\mathbf{A}\mathbf{x}^{\text{true}}.$$

- Helps choose β for desired spatial resolution

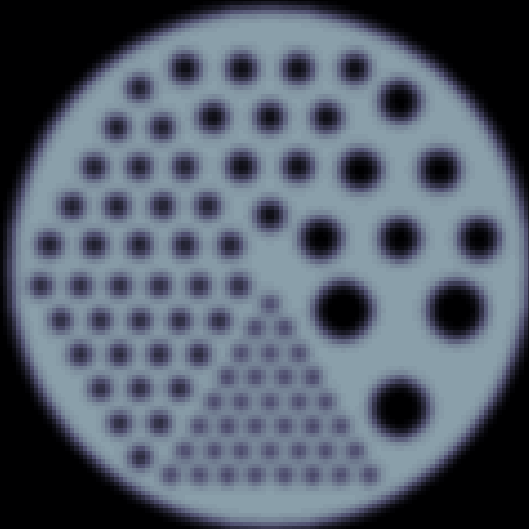
Modified Penalty Example, PET



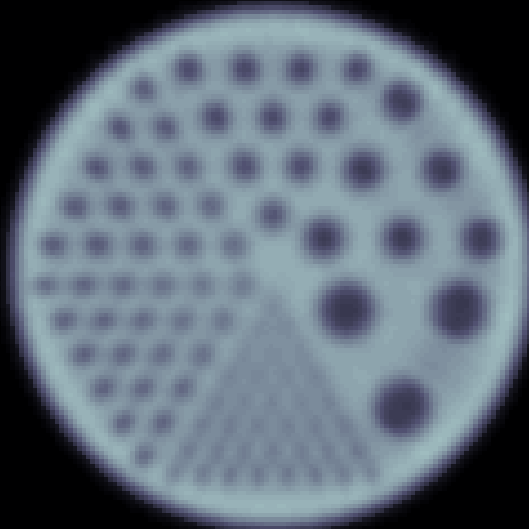
- a) filtered backprojection
- b) Penalized unweighted least-squares
- c) PWLS with conventional regularization
- d) PWLS with certainty-based penalty [36]
- e) PWLS with modified penalty [139]

Modified Penalty Example, SPECT - Noiseless

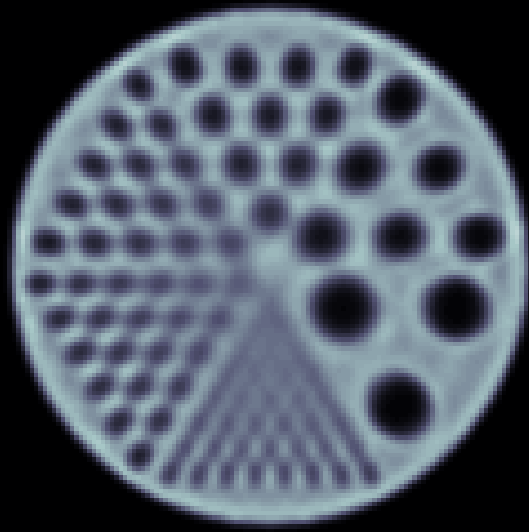
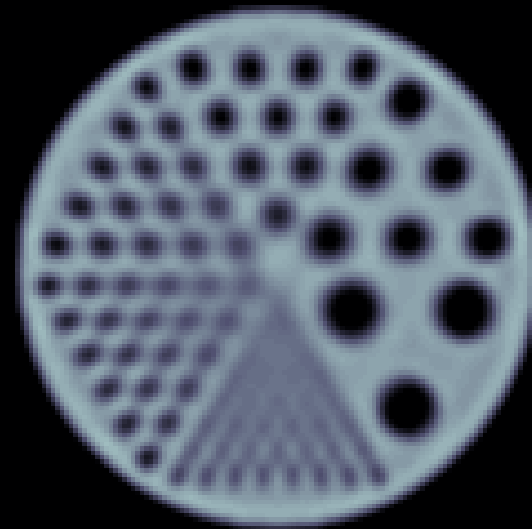
Target filtered object



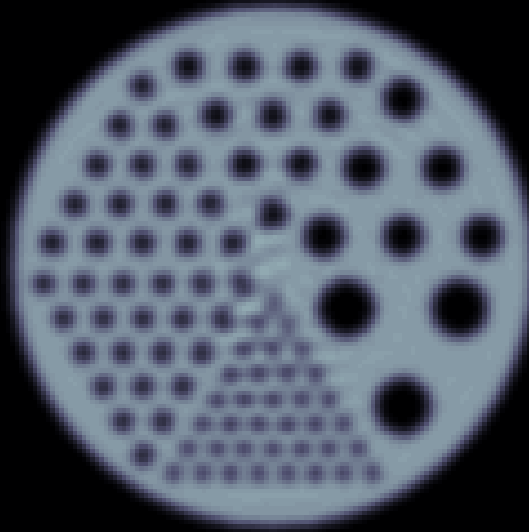
FBP



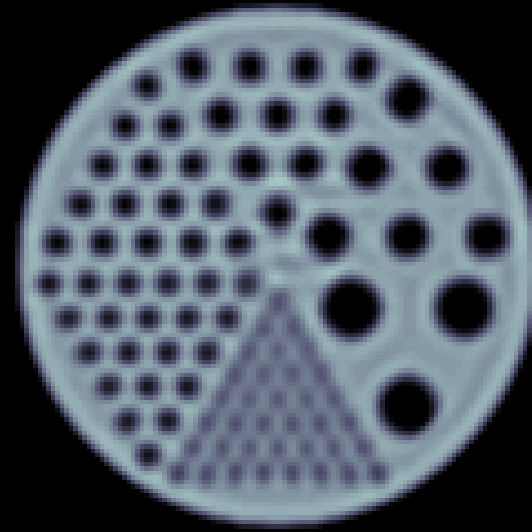
Conventional PWLS



Truncated EM



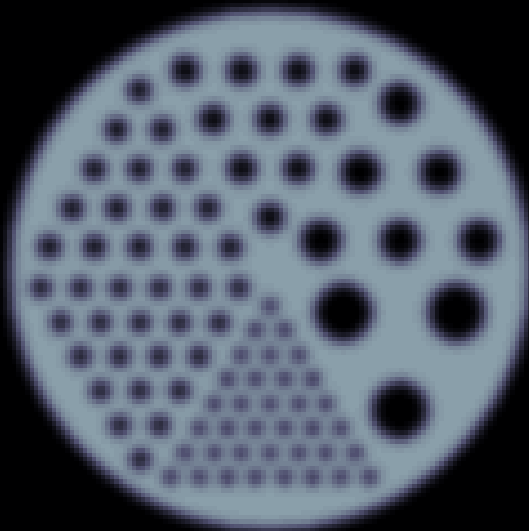
Post-filtered EM



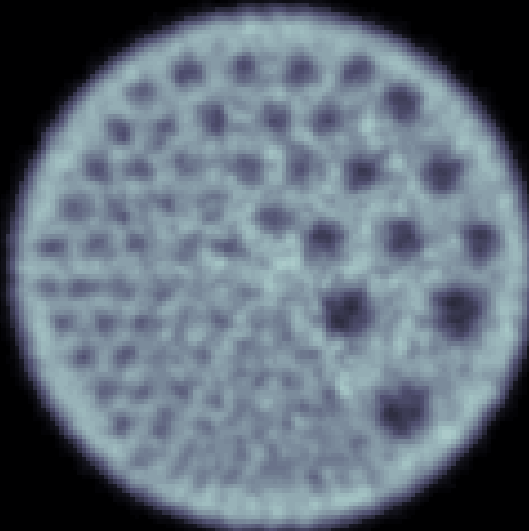
Modified Regularization

Modified Penalty Example, SPECT - Noisy

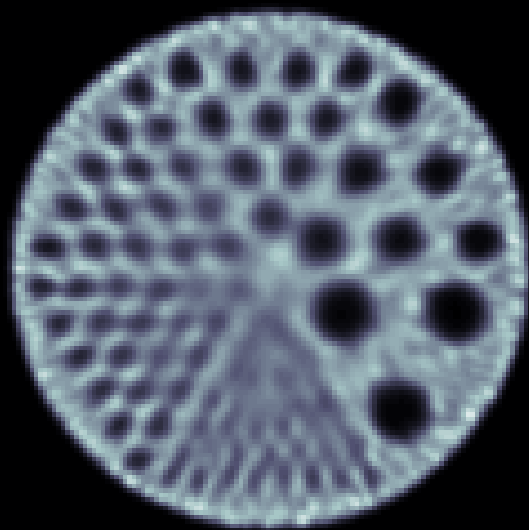
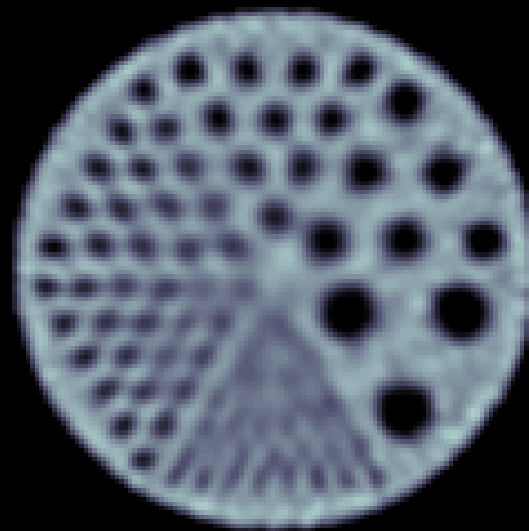
Target filtered object



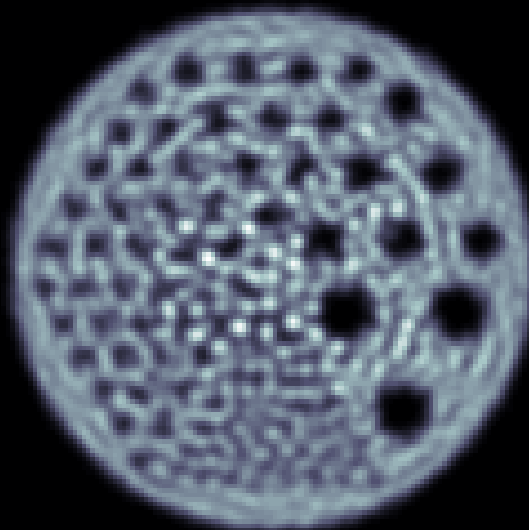
FBP



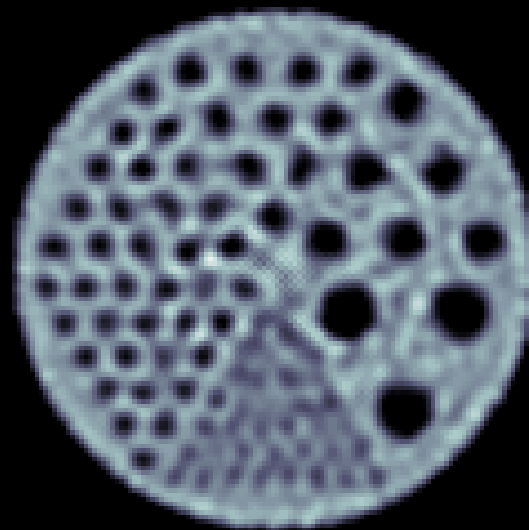
Conventional PWLS



Truncated EM

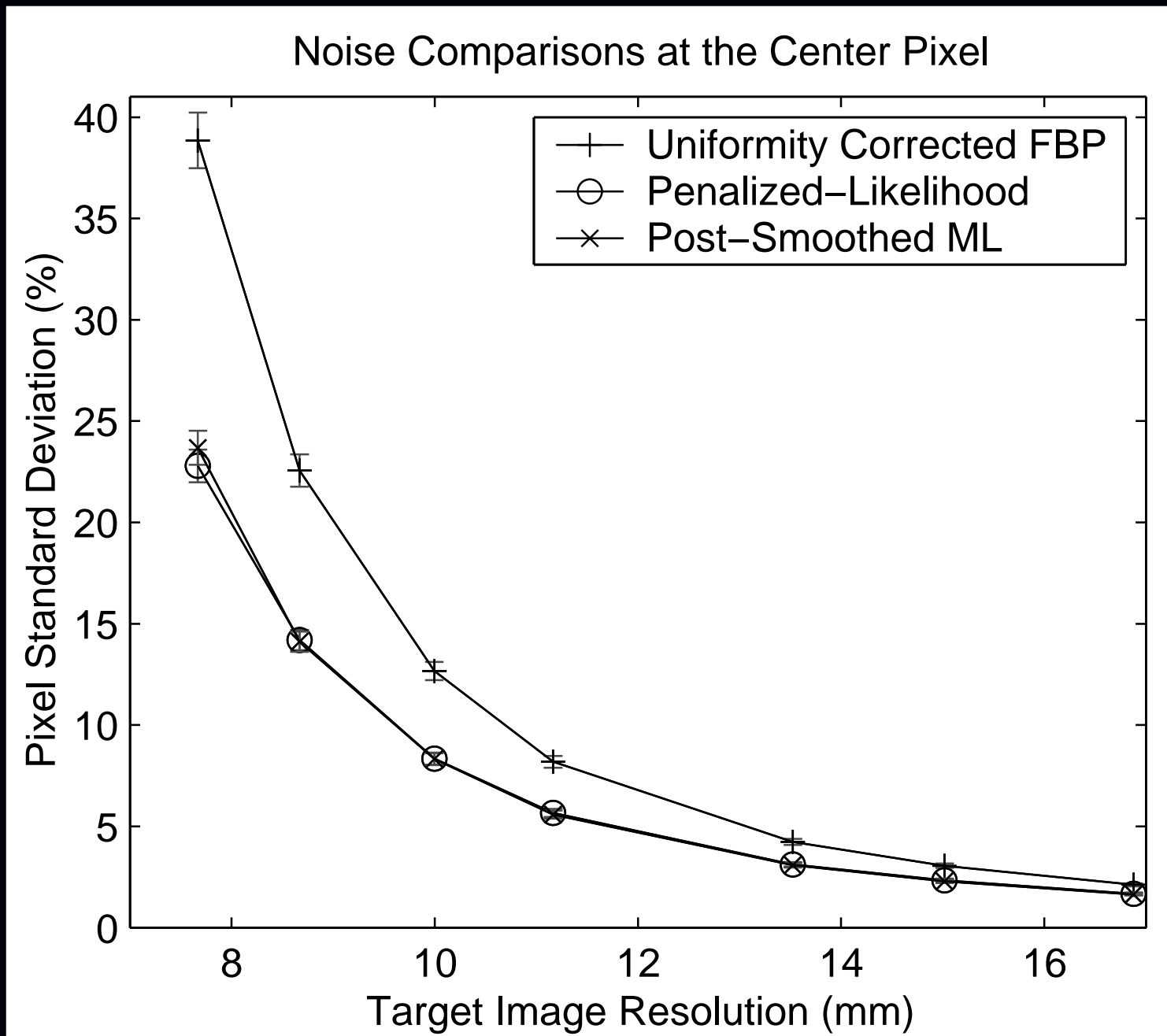


Post-filtered EM



Modified Regularization

Regularized vs Post-filtered, with Matched PSF



Reconstruction Noise Properties

For unconstrained (converged) minimization methods, the estimator is *implicit*:

$$\hat{\mathbf{x}} = \hat{\mathbf{x}}(\mathbf{y}) = \arg \min_x \Psi(\mathbf{x}, \mathbf{y}).$$

What is $\text{Cov}\{\hat{\mathbf{x}}\}$?

New simpler derivation.

Denote the column gradient by $g(\mathbf{x}, \mathbf{y}) \triangleq \nabla_x \Psi(\mathbf{x}, \mathbf{y})$.

Ignoring constraints, the gradient is zero at the minimizer: $g(\hat{\mathbf{x}}(\mathbf{y}), \mathbf{y}) = \mathbf{0}$.

First-order Taylor series expansion:

$$\begin{aligned} g(\hat{\mathbf{x}}, \mathbf{y}) &\approx g(\mathbf{x}^{\text{true}}, \mathbf{y}) + \nabla_x g(\mathbf{x}^{\text{true}}, \mathbf{y})(\hat{\mathbf{x}} - \mathbf{x}^{\text{true}}) \\ &= g(\mathbf{x}^{\text{true}}, \mathbf{y}) + \nabla_x^2 \Psi(\mathbf{x}^{\text{true}}, \mathbf{y})(\hat{\mathbf{x}} - \mathbf{x}^{\text{true}}). \end{aligned}$$

Equating to zero:

$$\hat{\mathbf{x}} \approx \mathbf{x}^{\text{true}} - [\nabla_x^2 \Psi(\mathbf{x}^{\text{true}}, \mathbf{y})]^{-1} \nabla_x \Psi(\mathbf{x}^{\text{true}}, \mathbf{y}).$$

If the Hessian $\nabla^2 \Psi$ is weakly dependent on \mathbf{y} , then

$$\boxed{\text{Cov}\{\hat{\mathbf{x}}\} \approx [\nabla_x^2 \Psi(\mathbf{x}^{\text{true}}, \bar{\mathbf{y}})]^{-1} \text{Cov}\{\nabla_x \Psi(\mathbf{x}^{\text{true}}, \mathbf{y})\} [\nabla_x^2 \Psi(\mathbf{x}^{\text{true}}, \bar{\mathbf{y}})]^{-1} .}$$

If we further linearize w.r.t. the data: $g(\mathbf{x}, \mathbf{y}) \approx g(\mathbf{x}, \bar{\mathbf{y}}) + \nabla_y g(\mathbf{x}, \bar{\mathbf{y}})(\mathbf{y} - \bar{\mathbf{y}})$, then

$$\text{Cov}\{\hat{\mathbf{x}}\} \approx [\nabla_x^2 \Psi]^{-1} (\nabla_x \nabla_y \Psi) \text{Cov}\{\mathbf{y}\} (\nabla_x \nabla_y \Psi)' [\nabla_x^2 \Psi]^{-1} .$$

Covariance Continued

Covariance approximation:

$$\text{Cov}\{\hat{\mathbf{x}}\} \approx [\nabla_{\mathbf{x}}^2 \Psi(\mathbf{x}^{\text{true}}, \bar{\mathbf{y}})]^{-1} \text{Cov}\{\nabla_{\mathbf{x}} \Psi(\mathbf{x}^{\text{true}}, \mathbf{y})\} [\nabla_{\mathbf{x}}^2 \Psi(\mathbf{x}^{\text{true}}, \bar{\mathbf{y}})]^{-1}$$

Depends only on chosen **cost function** and **statistical model**.
Independent of optimization algorithm.

- Enables prediction of noise properties
- Can make variance images
- Useful for computing ROI variance (e.g., for weighted kinetic fitting)
- Good variance prediction for quadratic regularization in nonzero regions
- Inaccurate for nonquadratic penalties, or in nearly-zero regions

Qi and Huesman's Detection Analysis

SNR of MAP reconstruction $>$ SNR of FBP reconstruction (T-MI, Aug. 2001)

quadratic regularization

SKE/BKE task

prewhitened observer

non-prewhitened observer

Open issues

Choice of regularizer to optimize detectability?

Active work in several groups.

(e.g., 2004 MIC poster by Yendiki & Fessler.)

References

- [1] S. Webb. *From the watching of shadows: the origins of radiological tomography*. A. Hilger, Bristol, 1990.
- [2] H. H. Barrett and K. J. Myers. *Foundations of image science*. Wiley, New York, 2003.
- [3] J. Kay. The EM algorithm in medical imaging. *Stat. Meth. Med. Res.*, 6(1):55–75, January 1997.
- [4] J. A. Fessler. Statistical image reconstruction methods for transmission tomography. In M. Sonka and J. Michael Fitzpatrick, editors, *Handbook of Medical Imaging, Volume 2. Medical Image Processing and Analysis*, pages 1–70. SPIE, Bellingham, 2000.
- [5] R. M. Leahy and J. Qi. Statistical approaches in quantitative positron emission tomography. *Statistics and Computing*, 10(2):147–65, April 2000.
- [6] M. Defrise. A short reader's guide to 3D tomographic reconstruction. *Computerized Medical Imaging and Graphics*, 25(2):113–6, March 2001.
- [7] S. Vandenberghe, Y. D'Asseler, R. V. Walle, T. Kauppinen, M. Koole, L. Bouwens, K. V. Laere, I. Lemahieu, and R. A. Dierckx. Iterative reconstruction algorithms in nuclear medicine. *Computerized Medical Imaging and Graphics*, 25(2):105–11, March 2001.
- [8] G. L. Zeng. Image reconstruction, a tutorial. *Computerized Medical Imaging and Graphics*, 25(2):97–103, March 2001.
- [9] R. M. Lewitt and S. Matej. Overview of methods for image reconstruction from projections in emission computed tomography. *Proc. IEEE*, 91(10):1588–611, October 2003.
- [10] R. N. Bracewell. Strip integration in radio astronomy. *Aust. J. Phys.*, 9:198–217, 1956.
- [11] G. Hounsfield. A method of apparatus for examination of a body by radiation such as x-ray or gamma radiation, 1972. US Patent 1283915. British patent 1283915, London. Issued to EMI Ltd. Filed Aug. 1968. See [1, Ch. 5].
- [12] G. Muehllehner and R. A. Wetzel. Section imaging by computer calculation. *J. Nuc. Med.*, 12(2):76–85, 1971.
- [13] D. E. Kuhl, R. Q. Edwards, A. R. Ricci, and M. Reivich. Quantitative section scanning using orthogonal tangent correction. *J. Nuc. Med.*, 14(4):196–200, April 1973.
- [14] R. Gordon, R. Bender, and G. T. Herman. Algebraic reconstruction techniques (ART) for the three-dimensional electron microscopy and X-ray photography. *J. Theor. Biol.*, 29:471–81, 1970.
- [15] R. Gordon and G. T. Herman. Reconstruction of pictures from their projections. *Comm. ACM*, 14:759–68, 1971.
- [16] G. T. Herman, A. Lent, and S. W. Rowland. ART: mathematics and applications (a report on the mathematical foundations and on the applicability to real data of the algebraic reconstruction techniques). *J. Theor. Biol.*, 42:1–32, 1973.
- [17] R. Gordon. A tutorial on ART (algebraic reconstruction techniques). *IEEE Trans. Nuc. Sci.*, 21(3):78–93, June 1974.
- [18] R. Richardson. Bayesian-based iterative method of image restoration. *J. Opt. Soc. Am.*, 62(1):55–9, January 1972.
- [19] L. Lucy. An iterative technique for the rectification of observed distributions. *The Astronomical J.*, 79(6):745–54, June 1974.
- [20] A. J. Rockmore and A. Macovski. A maximum likelihood approach to emission image reconstruction from projections. *IEEE Trans. Nuc. Sci.*, 23:1428–32, 1976.
- [21] A. J. Rockmore and A. Macovski. A maximum likelihood approach to transmission image reconstruction from projections. *IEEE Trans. Nuc. Sci.*, 24(3):1929–35, June 1977.
- [22] A. P. Dempster, N. M. Laird, and D. B. Rubin. Maximum likelihood from incomplete data via the EM algorithm. *J. Royal Stat. Soc. Ser. B*, 39(1):1–38, 1977.
- [23] L. A. Shepp and Y. Vardi. Maximum likelihood reconstruction for emission tomography. *IEEE Trans. Med. Imag.*, 1(2):113–22, October 1982.
- [24] K. Lange and R. Carson. EM reconstruction algorithms for emission and transmission tomography. *J. Comp. Assisted Tomo.*, 8(2):306–16, April 1984.
- [25] S. Geman and D. E. McClure. Bayesian image analysis: an application to single photon emission tomography. In *Proc. of Stat. Comp. Sect. of Amer. Stat. Assoc.*, pages 12–8, 1985.
- [26] H. M. Hudson and R. S. Larkin. Accelerated image reconstruction using ordered subsets of projection data. *IEEE Trans. Med. Imag.*, 13(4):601–9, December 1994.
- [27] M. Goitein. Three-dimensional density reconstruction from a series of two-dimensional projections. *Nucl. Instr. Meth.*, 101(3):509–18, June 1972.
- [28] T. F. Budinger and G. T. Gullberg. Three dimensional reconstruction in nuclear medicine emission imaging. *IEEE Trans. Nuc. Sci.*, 21(3):2–20, June 1974.
- [29] R. H. Huesman, G. T. Gullberg, W. L. Greenberg, and T. F. Budinger. *RECLBL library users manual*. Lawrence Berkeley Laboratory, Berkeley, CA, 1977.
- [30] R. H. Huesman. A new fast algorithm for the evaluation of regions of interest and statistical uncertainty in computed tomography. *Phys. Med. Biol.*, 29(5):543–52, May 1984.
- [31] D. W. Wilson and B. M. W. Tsui. Noise properties of filtered-backprojection and ML-EM reconstructed emission tomographic images. *IEEE Trans. Nuc. Sci.*, 40(4):1198–1203, August 1993.

- [32] D. W. Wilson and B. M. W. Tsui. Spatial resolution properties of FB and ML-EM reconstruction methods. In *Proc. IEEE Nuc. Sci. Symp. Med. Im. Conf.*, volume 2, pages 1189–93, 1993.
- [33] H. H. Barrett, D. W. Wilson, and B. M. W. Tsui. Noise properties of the EM algorithm: I. Theory. *Phys. Med. Biol.*, 39(5):833–46, May 1994.
- [34] D. W. Wilson, B. M. W. Tsui, and H. H. Barrett. Noise properties of the EM algorithm: II. Monte Carlo simulations. *Phys. Med. Biol.*, 39(5):847–72, May 1994.
- [35] J. A. Fessler. Mean and variance of implicitly defined biased estimators (such as penalized maximum likelihood): Applications to tomography. *IEEE Trans. Im. Proc.*, 5(3):493–506, March 1996.
- [36] J. A. Fessler and W. L. Rogers. Spatial resolution properties of penalized-likelihood image reconstruction methods: Space-invariant tomographs. *IEEE Trans. Im. Proc.*, 5(9):1346–58, September 1996.
- [37] W. Wang and G. Gindi. Noise analysis of regularized EM SPECT reconstruction. In *Proc. IEEE Nuc. Sci. Symp. Med. Im. Conf.*, volume 3, pages 1933–7, 1996.
- [38] C. K. Abbey, E. Clarkson, H. H. Barrett, S. P. Mueller, and F. J. Rybicki. Approximate distributions for maximum likelihood and maximum a posteriori estimates under a Gaussian noise model. In J. Duncan and G. Gindi, editors, *Information Processing in Medical Im.*, pages 167–75. Springer-Verlag, Berlin, 1997.
- [39] W. Wang and G. Gindi. Noise analysis of MAP-EM algorithms for emission tomography. *Phys. Med. Biol.*, 42(11):2215–32, November 1997.
- [40] S. J. Glick and E. J. Soares. Noise characteristics of SPECT iterative reconstruction with a mis-matched projector-backprojector pair. *IEEE Trans. Nuc. Sci.*, 45(4):2183–8, August 1998.
- [41] E. J. Soares, C. L. Byrne, T-S. Pan, S. J. Glick, and M. A. King. Modeling the population covariance matrices of block-iterative expectation-maximization reconstructed images. In *Proc. SPIE 3034, Med. Im. 1997: Im. Proc.*, pages 415–25, 1997.
- [42] J. Qi and R. H. Huesman. Theoretical study of lesion detectability of MAP reconstruction using computer observers. *IEEE Trans. Med. Imag.*, 20(8):815–22, August 2001.
- [43] D. Brasse, P. E. Kinahan, R. Clackdoyle, M. Defrise, C. Comtat, and D. W. Townsend. Fast fully 3-D image reconstruction in PET using planograms. *IEEE Trans. Med. Imag.*, 23(4):413–25, April 2004.
- [44] J. A. Fessler, I. Elbakri, P. Sukovic, and N. H. Clinthorne. Maximum-likelihood dual-energy tomographic image reconstruction. In *Proc. SPIE 4684, Medical Imaging 2002: Image Proc.*, volume 1, pages 38–49, 2002.
- [45] B. De Man, J. Nuyts, P. Dupont, G. Marchal, and P. Suetens. An iterative maximum-likelihood polychromatic algorithm for CT. *IEEE Trans. Med. Imag.*, 20(10):999–1008, October 2001.
- [46] I. A. Elbakri and J. A. Fessler. Statistical image reconstruction for polyenergetic X-ray computed tomography. *IEEE Trans. Med. Imag.*, 21(2):89–99, February 2002.
- [47] I. A. Elbakri and J. A. Fessler. Segmentation-free statistical image reconstruction for polyenergetic X-ray computed tomography with experimental validation. *Phys. Med. Biol.*, 48(15):2543–78, August 2003.
- [48] P. E. Kinahan, J. A. Fessler, and J. S. Karp. Statistical image reconstruction in PET with compensation for missing data. *IEEE Trans. Nuc. Sci.*, 44(4):1552–7, August 1997.
- [49] J. A. Fessler and B. P. Sutton. Nonuniform fast Fourier transforms using min-max interpolation. *IEEE Trans. Sig. Proc.*, 51(2):560–74, February 2003.
- [50] B. P. Sutton, D. C. Noll, and J. A. Fessler. Fast, iterative image reconstruction for MRI in the presence of field inhomogeneities. *IEEE Trans. Med. Imag.*, 22(2):178–88, February 2003.
- [51] B. P. Sutton, D. C. Noll, and J. A. Fessler. Dynamic field map estimation using a spiral-in / spiral-out acquisition. *Mag. Res. Med.*, 51(6):1194–204, June 2004.
- [52] B. W. Silverman. Some aspects of the spline smoothing approach to non-parametric regression curve fitting. *J. Royal Stat. Soc. Ser. B*, 47(1):1–52, 1985.
- [53] R. Van de Walle, H. H. Barrett, K. J. Myers, M. I. Altbach, B. Desplanques, A. F. Gmitro, J. Cornelis, and I. Lemahieu. Reconstruction of MR images from data acquired on a general non-regular grid by pseudoinverse calculation. *IEEE Trans. Med. Imag.*, 19(12):1160–7, December 2000.
- [54] M. Bertero, C. De Mol, and E. R. Pike. Linear inverse problems with discrete data, I: General formulation and singular system analysis. *Inverse Prob.*, 1(4):301–30, November 1985.
- [55] K. M. Hanson and G. W. Wecksung. Local basis-function approach to computed tomography. *Appl. Optics*, 24(23):4028–39, December 1985.
- [56] E. J. Mazur and R. Gordon. Interpolative algebraic reconstruction techniques without beam partitioning for computed tomography. *Med. Biol. Eng. Comput.*, 33(1):82–6, January 1995.
- [57] Y. Censor. Finite series expansion reconstruction methods. *Proc. IEEE*, 71(3):409–19, March 1983.
- [58] D. L. Snyder. Utilizing side information in emission tomography. *IEEE Trans. Nuc. Sci.*, 31(1):533–7, February 1984.
- [59] R. E. Carson, M. V. Green, and S. M. Larson. A maximum likelihood method for calculation of tomographic region-of-interest (ROI) values. *J. Nuc. Med.*, 26:P20, 1985.

- [60] R. E. Carson and K. Lange. The EM parametric image reconstruction algorithm. *J. Am. Stat. Ass.*, 80(389):20–2, March 1985.
- [61] R. E. Carson. A maximum likelihood method for region-of-interest evaluation in emission tomography. *J. Comp. Assisted Tomo.*, 10(4):654–63, July 1986.
- [62] A. R. Formiconi. Least squares algorithm for region-of-interest evaluation in emission tomography. *IEEE Trans. Med. Imag.*, 12(1):90–100, March 1993.
- [63] B. W. Reutter, G. T. Gullberg, and R. H. Huesman. Kinetic parameter estimation from attenuated SPECT projection measurements. *IEEE Trans. Nuc. Sci.*, 45(6):3007–13, December 1998.
- [64] D. J. Rossi and A. S. Willsky. Reconstruction from projections based on detection and estimation of objects—Parts I & II: Performance analysis and robustness analysis. *IEEE Trans. Acoust. Sp. Sig. Proc.*, 32(4):886–906, August 1984.
- [65] S. P. Müller, M. F. Kijewski, S. C. Moore, and B. L. Holman. Maximum-likelihood estimation: a mathematical model for quantitation in nuclear medicine. *J. Nuc. Med.*, 31(10):1693–701, October 1990.
- [66] P. C. Chiao, W. L. Rogers, N. H. Clinthorne, J. A. Fessler, and A. O. Hero. Model-based estimation for dynamic cardiac studies using ECT. *IEEE Trans. Med. Imag.*, 13(2):217–26, June 1994.
- [67] Z. P. Liang, F. E. Boada, R. T. Constable, E. M. Haacke, P. C. Lauterbur, and M. R. Smith. Constrained reconstruction methods in MR imaging. *Reviews of Magnetic Resonance in Medicine*, 4:67–185, 1992.
- [68] G. S. Cunningham and A. Lehovich. 4D reconstructions from low-count SPECT data using deformable models with smooth interior intensity variations. In *Proc. SPIE 3979: Medical Imaging 2000: Image Proc.*, 2000.
- [69] A. Yendiki and J. A. Fessler. A comparison of rotation- and blob-based system models for 3D SPECT with depth-dependent detector response. *Phys. Med. Biol.*, 49(11):2157–68, June 2004.
- [70] R. M. Lewitt. Multidimensional digital image representations using generalized Kaiser-Bessel window functions. *J. Opt. Soc. Am. A*, 7(10):1834–46, October 1990.
- [71] R. M. Lewitt. Alternatives to voxels for image representation in iterative reconstruction algorithms. *Phys. Med. Biol.*, 37(3):705–16, March 1992.
- [72] G. L. Zeng and G. T. Gullberg. Unmatched projector/backprojector pairs in an iterative reconstruction algorithm. *IEEE Trans. Med. Imag.*, 19(5):548–55, May 2000.
- [73] C. Kamphuis, F. J. Beekman, P. P. van Rijk, and M. A. Viergever. Dual matrix ordered subsets reconstruction for accelerated 3D scatter compensation in single-photon emission tomography. *Eur. J. Nuc. Med.*, 25(1):8–18, January 1998.
- [74] F. J. Beekman, H. W. A. M. de Jong, and S. van Geloven. Efficient fully 3D iterative SPECT reconstruction with Monte Carlo based scatter compensation. *IEEE Trans. Med. Imag.*, 21(8):867–77, August 2002.
- [75] R. Griesse and A. Walther. Evaluating gradients in optimal control: continuous adjoints versus automatic differentiation. *J. Optim. Theory Appl.*, 122(1):63–86, July 2004.
- [76] C. W. Stearns and J. A. Fessler. 3D PET reconstruction with FORE and WLS-OS-EM. In *Proc. IEEE Nuc. Sci. Symp. Med. Im. Conf.*, volume 2, pages 912–5, 2002.
- [77] M. Yavuz and J. A. Fessler. Objective functions for tomographic reconstruction from randoms-precorrected PET scans. In *Proc. IEEE Nuc. Sci. Symp. Med. Im. Conf.*, volume 2, pages 1067–71, 1996.
- [78] M. Yavuz and J. A. Fessler. New statistical models for randoms-precorrected PET scans. In J. Duncan and G. Gindi, editors, *Information Processing in Medical Im.*, volume 1230 of *Lecture Notes in Computer Science*, pages 190–203. Springer-Verlag, Berlin, 1997.
- [79] M. Yavuz and J. A. Fessler. Statistical image reconstruction methods for randoms-precorrected PET scans. *Med. Im. Anal.*, 2(4):369–78, December 1998.
- [80] M. Yavuz and J. A. Fessler. Penalized-likelihood estimators and noise analysis for randoms-precorrected PET transmission scans. *IEEE Trans. Med. Imag.*, 18(8):665–74, August 1999.
- [81] D. L. Snyder, A. M. Hammoud, and R. L. White. Image recovery from data acquired with a charge-coupled-device camera. *J. Opt. Soc. Am. A*, 10(5):1014–23, May 1993.
- [82] D. L. Snyder, C. W. Helstrom, A. D. Lanterman, M. Faisal, and R. L. White. Compensation for readout noise in CCD images. *J. Opt. Soc. Am. A*, 12(2):272–83, February 1995.
- [83] U. Engeland, T. Striker, and H. Luig. Count-rate statistics of the gamma camera. *Phys. Med. Biol.*, 43(10):2939–47, October 1998.
- [84] J. A. Fessler. Penalized weighted least-squares image reconstruction for positron emission tomography. *IEEE Trans. Med. Imag.*, 13(2):290–300, June 1994.
- [85] C. Comtat, P. E. Kinahan, M. Defrise, C. Michel, and D. W. Townsend. Fast reconstruction of 3D PET data with accurate statistical modeling. *IEEE Trans. Nuc. Sci.*, 45(3):1083–9, June 1998.
- [86] B. R. Whiting. Signal statistics in x-ray computed tomography. In *Proc. SPIE 4682, Medical Imaging 2002: Med. Phys.*, pages 53–60, 2002.
- [87] B. R. Whiting, L. J. Montagnino, and D. G. Politte. Modeling X-ray computed tomography sinograms, 2001. submitted to mp.
- [88] I. A. Elbakri and J. A. Fessler. Efficient and accurate likelihood for iterative image reconstruction in X-ray computed tomography. In *Proc. SPIE 5032, Medical*

Imaging 2003: Image Proc., pages 1839–50, 2003.

- [89] A. O. Hero, J. A. Fessler, and M. Usman. Exploring estimator bias-variance tradeoffs using the uniform CR bound. *IEEE Trans. Sig. Proc.*, 44(8):2026–41, August 1996.
- [90] Y. C. Eldar. Minimum variance in biased estimation: bounds and asymptotically optimal estimators. *IEEE Trans. Sig. Proc.*, 52(7):1915–30, July 2004.
- [91] E. Mumcuoglu, R. Leahy, S. Cherry, and E. Hoffman. Accurate geometric and physical response modeling for statistical image reconstruction in high resolution PET scanners. In *Proc. IEEE Nuc. Sci. Symp. Med. Im. Conf.*, volume 3, pages 1569–73, 1996.
- [92] J. Qi, R. M. Leahy, E. U. Mumcuoglu, S. R. Cherry, A. Chatziioannou, and T. H. Farquhar. High resolution 3D Bayesian image reconstruction for microPET. In *Proc. Intl. Mtg. on Fully 3D Image Recon. in Rad. and Nuc. Med.*, 1997.
- [93] G. Christ. Exact treatment of the dual-energy method in CT using polyenergetic X-ray spectra. *Phys. Med. Biol.*, 29(12):1511–25, December 1984.
- [94] Z. Liang. Compensation for attenuation, scatter, and detector response in SPECT reconstruction via iterative FBP methods. *Med. Phys.*, 20(4):1097–106, July 1993.
- [95] X. L. Xu, J. S. Liow, and S. C. Strother. Iterative algebraic reconstruction algorithms for emission computed tomography: a unified framework and its application to positron emission tomography. *Med. Phys.*, 20(6):1675–84, November 1993.
- [96] J. W. Wallis and T. R. Miller. Rapidly converging iterative reconstruction algorithms in single-photon emission computed tomography. *J. Nuc. Med.*, 34(10):1793–1800, October 1993.
- [97] P. J. Green. Iteratively reweighted least squares for maximum likelihood estimation, and some robust and resistant alternatives. *J. Royal Stat. Soc. Ser. B*, 46(2):149–92, 1984.
- [98] J. M. M. Anderson, B. A. Mair, M. Rao, and C. H. Wu. A weighted least-squares method for PET. In *Proc. IEEE Nuc. Sci. Symp. Med. Im. Conf.*, volume 2, pages 1292–6, 1995.
- [99] J. M. M. Anderson, B. A. Mair, M. Rao, and C-H. Wu. Weighted least-squares reconstruction methods for positron emission tomography. *IEEE Trans. Med. Imag.*, 16(2):159–65, April 1997.
- [100] P. J. Huber. *Robust statistics*. Wiley, New York, 1981.
- [101] C. Bouman and K. Sauer. A generalized Gaussian image model for edge-preserving MAP estimation. *IEEE Trans. Im. Proc.*, 2(3):296–310, July 1993.
- [102] E. Tanaka. Improved iterative image reconstruction with automatic noise artifact suppression. *IEEE Trans. Med. Imag.*, 11(1):21–7, March 1992.
- [103] B. W. Silverman, M. C. Jones, J. D. Wilson, and D. W. Nychka. A smoothed EM approach to indirect estimation problems, with particular reference to stereology and emission tomography. *J. Royal Stat. Soc. Ser. B*, 52(2):271–324, 1990.
- [104] T. R. Miller, J. W. Wallis, C. S. Butler, M. I. Miller, and D. L. Snyder. Improved brain SPECT by maximum-likelihood reconstruction. *J. Nuc. Med. (Abs. Book)*, 33(5):964, May 1992.
- [105] F. J. Beekman, E. T. P. Slijpen, and W. J. Niessen. Selection of task-dependent diffusion filters for the post-processing of SPECT images. *Phys. Med. Biol.*, 43(6):1713–30, June 1998.
- [106] D. S. Lalush and B. M. W. Tsui. Performance of ordered subset reconstruction algorithms under conditions of extreme attenuation and truncation in myocardial SPECT. *J. Nuc. Med.*, 41(4):737–44, April 2000.
- [107] E. T. P. Slijpen and F. J. Beekman. Comparison of post-filtering and filtering between iterations for SPECT reconstruction. *IEEE Trans. Nuc. Sci.*, 46(6):2233–8, December 1999.
- [108] R. H. Huesman. The effects of a finite number of projection angles and finite lateral sampling of projections on the propagation of statistical errors in transverse section reconstruction. *Phys. Med. Biol.*, 22(3):511–21, May 1977.
- [109] D. L. Snyder and M. I. Miller. The use of sieves to stabilize images produced with the EM algorithm for emission tomography. *IEEE Trans. Nuc. Sci.*, 32(5):3864–71, October 1985.
- [110] D. L. Snyder, M. I. Miller, L. J. Thomas, and D. G. Politte. Noise and edge artifacts in maximum-likelihood reconstructions for emission tomography. *IEEE Trans. Med. Imag.*, 6(3):228–38, September 1987.
- [111] T. R. Miller and J. W. Wallis. Clinically important characteristics of maximum-likelihood reconstruction. *J. Nuc. Med.*, 33(9):1678–84, September 1992.
- [112] A. Tikhonov and V. Arsenin. *Solution of ill-posed problems*. Wiley, New York, 1977.
- [113] I. Csiszár. Why least squares and maximum entropy? An axiomatic approach to inference for linear inverse problems. *Ann. Stat.*, 19(4):2032–66, 1991.
- [114] D. L. Donoho, I. M. Johnstone, A. S. Stern, and J.C. Hoch. Does the maximum entropy method improve sensitivity. *Proc. Natl. Acad. Sci.*, 87(13):5066–8, July 1990.
- [115] D. L. Donoho, I. M. Johnstone, J. C. Hoch, and A. S. Stern. Maximum entropy and the nearly black object. *J. Royal Stat. Soc. Ser. B*, 54(1):41–81, 1992.

- [116] R. T. Constable and R. M. Henkelman. Why MEM does not work in MR image reconstruction. *Mag. Res. Med.*, 14(1):12–25, April 1990.
- [117] A. R. De Pierro. A modified expectation maximization algorithm for penalized likelihood estimation in emission tomography. *IEEE Trans. Med. Imag.*, 14(1):132–137, March 1995.
- [118] A. H. Delaney and Y. Bresler. A fast and accurate Fourier algorithm for iterative parallel-beam tomography. *IEEE Trans. Im. Proc.*, 5(5):740–53, May 1996.
- [119] S. J. Lee, A. Rangarajan, and G. Gindi. A comparative study of the effects of using higher order mechanical priors in SPECT reconstruction. In *Proc. IEEE Nuc. Sci. Symp. Med. Im. Conf.*, volume 4, pages 1696–1700, 1994.
- [120] S.-J. Lee, A. Rangarajan, and G. Gindi. Bayesian image reconstruction in SPECT using higher order mechanical models as priors. *IEEE Trans. Med. Imag.*, 14(4):669–80, December 1995.
- [121] S. Geman and D. Geman. Stochastic relaxation, Gibbs distributions, and Bayesian restoration of images. *IEEE Trans. Patt. Anal. Mach. Int.*, 6(6):721–41, November 1984.
- [122] B. W. Silverman, C. Jennison, J. Stander, and T. C. Brown. The specification of edge penalties for regular and irregular pixel images. *IEEE Trans. Patt. Anal. Mach. Int.*, 12(10):1017–24, October 1990.
- [123] V. E. Johnson, W. H. Wong, X. Hu, and C. T. Chen. Image restoration using Gibbs priors: Boundary modeling, treatment of blurring, and selection of hyperparameter. *IEEE Trans. Patt. Anal. Mach. Int.*, 13(5):413–25, May 1991.
- [124] V. E. Johnson. A model for segmentation and analysis of noisy images. *J. Am. Stat. Ass.*, 89(425):230–41, March 1994.
- [125] S. Alenius and U. Ruotsalainen. Bayesian image reconstruction for emission tomography based on median root prior. *Eur. J. Nuc. Med.*, 24(3):258–65, 1997.
- [126] S. Alenius, U. Ruotsalainen, and J. Astola. Using local median as the location of the prior distribution in iterative emission tomography image reconstruction. *IEEE Trans. Nuc. Sci.*, 45(6):3097–104, December 1998.
- [127] W. Chlewicki, F. Hermansen, and S. B. Hansen. Noise reduction and convergence of Bayesian algorithms with blobs based on the huber function and median root prior. *Phys. Med. Biol.*, 49(20):4717–30, October 2004.
- [128] V. Y. Panin, G. L. Zeng, and G. T. Gullberg. Total variation regulated EM algorithm. *IEEE Trans. Nuc. Sci.*, 46(6):2202–10, December 1999.
- [129] P. Kisilev, M. Zibulevsky, and Y. Zeevi. Wavelet representation and total variation regularization in emission tomography. In *Proc. IEEE Intl. Conf. on Image Processing*, volume 1, pages 702–5, 2001.
- [130] C. R. Vogel and M. E. Oman. Fast numerical methods for total variation minimization in image reconstruction. In *Proc. SPIE 2563, Adv. Signal Proc. Alg.*, pages 359–67, 1995.
- [131] M. Lassas and S. Siltanen. Can one use total variation prior for edge-preserving Bayesian inversion? *Inverse Prob.*, 20(5):1537–1564, October 2004.
- [132] I.-T. Hsiao, A. Rangarajan, and G. Gindi. A new convex edge-preserving median prior with applications to tomography. *IEEE Trans. Med. Imag.*, 22(5):580–5, May 2003.
- [133] M. Nikolova. Thresholding implied by truncated quadratic regularization. *IEEE Trans. Sig. Proc.*, 48(12):3437–50, December 2000.
- [134] A. Antoniadis and J. Fan. Regularization and wavelet approximations. *J. Am. Stat. Ass.*, 96(455):939–55, September 2001.
- [135] D. F. Yu and J. A. Fessler. Edge-preserving tomographic reconstruction with nonlocal regularization. In *Proc. IEEE Intl. Conf. on Image Processing*, volume 1, pages 29–33, 1998.
- [136] D. F. Yu and J. A. Fessler. Edge-preserving tomographic reconstruction with nonlocal regularization. *IEEE Trans. Med. Imag.*, 21(2):159–73, February 2002.
- [137] J. Ye, Y. Bresler, and P. Moulin. A self-referencing level-set method for image reconstruction from sparse Fourier samples. In *Proc. IEEE Intl. Conf. on Image Processing*, volume 2, pages 33–6, 2001.
- [138] M. J. Black and A. Rangarajan. On the unification of line processes, outlier rejection, and robust statistics with applications in early vision. *Intl. J. Comp. Vision*, 19(1):57–91, July 1996.
- [139] J. W. Stayman and J. A. Fessler. Regularization for uniform spatial resolution properties in penalized-likelihood image reconstruction. *IEEE Trans. Med. Imag.*, 19(6):601–15, June 2000.
- [140] J. W. Stayman and J. A. Fessler. Nonnegative definite quadratic penalty design for penalized-likelihood reconstruction. In *Proc. IEEE Nuc. Sci. Symp. Med. Im. Conf.*, volume 2, pages 1060–3, 2001.
- [141] J. W. Stayman and J. A. Fessler. Compensation for nonuniform resolution using penalized-likelihood reconstruction in space-variant imaging systems. *IEEE Trans. Med. Imag.*, 23(3):269–84, March 2004.
- [142] C. T. Chen, X. Ouyang, W. H. Wong, and X. Hu. Improvement of PET image reconstruction using high-resolution anatomic images. In *Proc. IEEE Nuc. Sci. Symp. Med. Im. Conf.*, volume 3, page 2062, 1991. (Abstract.)
- [143] R. Leahy and X. H. Yan. Statistical models and methods for PET image reconstruction. In *Proc. of Stat. Comp. Sect. of Amer. Stat. Assoc.*, pages 1–10, 1991.

- [144] J. A. Fessler, N. H. Clinthorne, and W. L. Rogers. Regularized emission image reconstruction using imperfect side information. *IEEE Trans. Nuc. Sci.*, 39(5):1464–71, October 1992.
- [145] I. G. Zubal, M. Lee, A. Rangarajan, C. R. Harrell, and G. Gindi. Bayesian reconstruction of SPECT images using registered anatomical images as priors. *J. Nuc. Med. (Abs. Book)*, 33(5):963, May 1992.
- [146] G. Gindi, M. Lee, A. Rangarajan, and I. G. Zubal. Bayesian reconstruction of functional images using anatomical information as priors. *IEEE Trans. Med. Imag.*, 12(4):670–80, December 1993.
- [147] X. Ouyang, W. H. Wong, V. E. Johnson, X. Hu, and C-T. Chen. Incorporation of correlated structural images in PET image reconstruction. *IEEE Trans. Med. Imag.*, 13(4):627–40, December 1994.
- [148] S. J. Lee, G. R. Gindi, I. G. Zubal, and A. Rangarajan. Using ground-truth data to design priors in Bayesian SPECT reconstruction. In Y. Bizais, C. Barillot, and R. D. Paola, editors, *Information Processing in Medical Im.* Kluwer, 1995.
- [149] J. E. Bowsher, V. E. Johnson, T. G. Turkington, R. J. Jaszczak, C. E. Floyd, and R. E. Coleman. Bayesian reconstruction and use of anatomical a priori information for emission tomography. *IEEE Trans. Med. Imag.*, 15(5):673–86, October 1996.
- [150] S. Sastry and R. E. Carson. Multimodality Bayesian algorithm for image reconstruction in positron emission tomography: a tissue composition model. *IEEE Trans. Med. Imag.*, 16(6):750–61, December 1997.
- [151] R. Piramuthu and A. O. Hero. Side information averaging method for PML emission tomography. In *Proc. IEEE Intl. Conf. on Image Processing*, volume 2, pages 671–5, 1998.
- [152] C. Comtat, P. E. Kinahan, J. A. Fessler, T. Beyer, D. W. Townsend, M. Defrise, and C. Michel. Reconstruction of 3d whole-body PET data using blurred anatomical labels. In *Proc. IEEE Nuc. Sci. Symp. Med. Im. Conf.*, volume 3, pages 1651–5, 1998.
- [153] A. O. Hero, R. Piramuthu, S. R. Titus, and J. A. Fessler. Minimax emission computed tomography using high resolution anatomical side information and B-spline models. *IEEE Trans. Info. Theory*, 45(3):920–38, April 1999.
- [154] D. F. Yu and J. A. Fessler. Mean and variance of singles photon counting with deadtime. *Phys. Med. Biol.*, 45(7):2043–56, July 2000.
- [155] D. F. Yu and J. A. Fessler. Mean and variance of coincidence photon counting with deadtime. *Nucl. Instr. Meth. Phys. Res. A.*, 488(1-2):362–74, August 2002.
- [156] J. Qi and R. H. Huesman. Propagation of errors from the sensitivity image in list mode reconstruction. *IEEE Trans. Med. Imag.*, 23(9):1094–9, September 2004.
- [157] J. Qi and R. H. Huesman. Effect of errors in the system matrix on iterative image reconstruction. In *Proc. IEEE Nuc. Sci. Symp. Med. Im. Conf.*, volume 5, pages 2854–8, 2004.
- [158] Y. S. Shim and Z. H. Cho. SVD pseudoinversion image reconstruction. *IEEE Trans. Acoust. Sp. Sig. Proc.*, 29(4):904–9, August 1981.
- [159] U. Raff, D. N. Stroud, and W. R. Hendee. Improvement of lesion detection in scintigraphic images by SVD techniques for resolution recovery. *IEEE Trans. Med. Imag.*, 5(1):35–44, March 1986.
- [160] D. A. Fish, J. Grochmalicki, and E. R. Pike. Scanning SVD method for restoration of images with space-variant blur. *J. Opt. Soc. Am. A*, 13(3):464–9, March 1996.
- [161] A. Caponnetto and M. Bertero. Tomography with a finite set of projections: singular value decomposition and resolution. *Inverse Prob.*, 13(5):1191–1205, October 1997.
- [162] A. K. Louis. Incomplete data problems in x-ray computerized tomography. I. Singular value decomposition of the limited angle transform. *Numerische Mathematik*, 48(3):251–62, 1986.
- [163] F. Natterer. Numerical treatment of ill-posed problems. In G Talenti, editor, *Inverse Prob.*, volume 1225, pages 142–67. Berlin, Springer, 1986. Lecture Notes in Math.
- [164] R. C. Liu and L. D. Brown. Nonexistence of informative unbiased estimators in singular problems. *Ann. Stat.*, 21(1):1–13, March 1993.
- [165] J. Ory and R. G. Pratt. Are our parameter estimators biased? The significance of finite-different regularization operators. *Inverse Prob.*, 11(2):397–424, April 1995.
- [166] I. M. Johnstone. On singular value decompositions for the Radon Transform and smoothness classes of functions. Technical Report 310, Dept. of Statistics, Stanford, January 1989.
- [167] M. F. Smith, C. E. Floyd, R. J. Jaszczak, and R. E. Coleman. Reconstruction of SPECT images using generalized matrix inverses. *IEEE Trans. Med. Imag.*, 11(2):165–75, June 1992.
- [168] M. Lavielle. A stochastic algorithm for parametric and non-parametric estimation in the case of incomplete data. *Signal Processing*, 42(1):3–17, 1995.
- [169] W. H. Press, B. P. Flannery, S. A. Teukolsky, and W. T. Vetterling. *Numerical recipes in C*. Cambridge Univ. Press, New York, 1988.
- [170] K. Sauer and C. Bouman. Bayesian estimation of transmission tomograms using local optimization operations. In *Proc. IEEE Nuc. Sci. Symp. Med. Im. Conf.*, volume 3, pages 2089–93, 1991.
- [171] K. Sauer and C. Bouman. Bayesian estimation of transmission tomograms using segmentation based optimization. *IEEE Trans. Nuc. Sci.*, 39(4):1144–52, August

1992.

- [172] D. P. Bertsekas and S. K. Mitter. A descent numerical method for optimization problems with nondifferentiable cost functionals. *SIAM J. Control*, 1:637–52, 1973.
- [173] W. C. Davidon. Variable metric methods for minimization. Technical Report ANL-5990, AEC Research and Development Report, Argonne National Laboratory, USA, 1959.
- [174] H. F. Khalfan, R. H. Byrd, and R. B. Schnabel. A theoretical and experimental study of the symmetric rank-one update. *SIAM J. Optim.*, 3(1):1–24, 1993.
- [175] C. Zhu, R. H. Byrd, P. Lu, and J. Nocedal. Algorithm 778: L-BFGS-B: Fortran subroutines for large-scale bound-constrained optimization. *ACM Trans. Math. Software*, 23(4):550–60, December 1997.
- [176] T. G. Kolda, D. P. O’Leary, and L. Nazareth. BFGS with update skipping and varying memory. *SIAM J. Optim.*, 8(4):1060–83, 1998.
- [177] K. Lange. *Numerical analysis for statisticians*. Springer-Verlag, New York, 1999.
- [178] B. T. Polyak. *Introduction to optimization*. Optimization Software Inc, New York, 1987.
- [179] D. P. Bertsekas. *Constrained optimization and Lagrange multiplier methods*. Academic-Press, New York, 1982.
- [180] R. H. Byrd, P. Lu, J. Nocedal, and C. Zhu. A limited memory algorithm for bound constrained optimization. *SIAM J. Sci. Comp.*, 16:1190–1208, 1995.
- [181] L. Kaufman. Reduced storage, Quasi-Newton trust region approaches to function optimization. *SIAM J. Optim.*, 10(1):56–69, 1999.
- [182] M. Hanke, J. G. Nagy, and C. Vogel. Quasi-Newton approach to nonnegative image restorations. *Linear Algebra and its Applications*, 316(1):223–36, September 2000.
- [183] J. L. Morales and J. Nocedal. Automatic preconditioning by limited memory Quasi-Newton updating. *SIAM J. Optim.*, 10(4):1079–96, 2000.
- [184] R. R. Meyer. Sufficient conditions for the convergence of monotonic mathematical programming algorithms. *J. Comput. System. Sci.*, 12(1):108–21, 1976.
- [185] L. Kaufman. Implementing and accelerating the EM algorithm for positron emission tomography. *IEEE Trans. Med. Imag.*, 6(1):37–51, March 1987.
- [186] N. H. Clinthorne, T. S. Pan, P. C. Chiao, W. L. Rogers, and J. A. Stamos. Preconditioning methods for improved convergence rates in iterative reconstructions. *IEEE Trans. Med. Imag.*, 12(1):78–83, March 1993.
- [187] J. A. Fessler and S. D. Booth. Conjugate-gradient preconditioning methods for shift-variant PET image reconstruction. *IEEE Trans. Im. Proc.*, 8(5):688–99, May 1999.
- [188] E. U. Mumcuoglu, R. Leahy, S. R. Cherry, and Z. Zhou. Fast gradient-based methods for Bayesian reconstruction of transmission and emission PET images. *IEEE Trans. Med. Imag.*, 13(3):687–701, December 1994.
- [189] E. Ü Mumcuoğlu, R. M. Leahy, and S. R. Cherry. Bayesian reconstruction of PET images: methodology and performance analysis. *Phys. Med. Biol.*, 41(9):1777–1807, September 1996.
- [190] J. A. Fessler and A. O. Hero. Space-alternating generalized expectation-maximization algorithm. *IEEE Trans. Sig. Proc.*, 42(10):2664–77, October 1994.
- [191] J. A. Fessler and A. O. Hero. Penalized maximum-likelihood image reconstruction using space-alternating generalized EM algorithms. *IEEE Trans. Im. Proc.*, 4(10):1417–29, October 1995.
- [192] J. A. Fessler, E. P. Ficaro, N. H. Clinthorne, and K. Lange. Grouped-coordinate ascent algorithms for penalized-likelihood transmission image reconstruction. *IEEE Trans. Med. Imag.*, 16(2):166–75, April 1997.
- [193] J. A. Fessler and A. O. Hero. Space-alternating generalized EM algorithms for penalized maximum-likelihood image reconstruction. Technical Report 286, Comm. and Sign. Proc. Lab., Dept. of EECS, Univ. of Michigan, Ann Arbor, MI, 48109-2122, February 1994.
- [194] J. A. Browne and A. R. De Pierro. A row-action alternative to the EM algorithm for maximizing likelihoods in emission tomography. *IEEE Trans. Med. Imag.*, 15(5):687–99, October 1996.
- [195] C. L. Byrne. Block-iterative methods for image reconstruction from projections. *IEEE Trans. Im. Proc.*, 5(5):792–3, May 1996.
- [196] C. L. Byrne. Convergent block-iterative algorithms for image reconstruction from inconsistent data. *IEEE Trans. Im. Proc.*, 6(9):1296–304, September 1997.
- [197] C. L. Byrne. Accelerating the EML algorithm and related iterative algorithms by rescaled block-iterative methods. *IEEE Trans. Im. Proc.*, 7(1):100–9, January 1998.
- [198] M. E. Daube-Witherspoon and G. Muehllehner. An iterative image space reconstruction algorithm suitable for volume ECT. *IEEE Trans. Med. Imag.*, 5(2):61–66, June 1986.
- [199] J. M. Ollinger. Iterative reconstruction-reprojection and the expectation-maximization algorithm. *IEEE Trans. Med. Imag.*, 9(1):94–8, March 1990.
- [200] A. R. De Pierro. On the relation between the ISRA and the EM algorithm for positron emission tomography. *IEEE Trans. Med. Imag.*, 12(2):328–33, June 1993.
- [201] P. J. Green. Bayesian reconstructions from emission tomography data using a modified EM algorithm. *IEEE Trans. Med. Imag.*, 9(1):84–93, March 1990.
- [202] P. J. Green. On use of the EM algorithm for penalized likelihood estimation. *J. Royal Stat. Soc. Ser. B*, 52(3):443–452, 1990.
- [203] K. Sauer and C. Bouman. A local update strategy for iterative reconstruction from projections. *IEEE Trans. Sig. Proc.*, 41(2):534–48, February 1993.

- [204] K. G. Murty. *Linear complementarity, linear and nonlinear programming*. Helderman Verlag, Berlin, 1988.
- [205] C. A. Bouman, K. Sauer, and S. S. Saquib. Tractable models and efficient algorithms for Bayesian tomography. In *Proc. IEEE Conf. Acoust. Speech Sig. Proc.*, volume 5, pages 2907–10, 1995.
- [206] C. A. Bouman and K. Sauer. A unified approach to statistical tomography using coordinate descent optimization. *IEEE Trans. Im. Proc.*, 5(3):480–92, March 1996.
- [207] J. A. Fessler. Hybrid Poisson/polynomial objective functions for tomographic image reconstruction from transmission scans. *IEEE Trans. Im. Proc.*, 4(10):1439–50, October 1995.
- [208] H. Erdođan and J. A. Fessler. Monotonic algorithms for transmission tomography. *IEEE Trans. Med. Imag.*, 18(9):801–14, September 1999.
- [209] C. A. Johnson, J. Seidel, and A. Sofer. Interior point methodology for 3-D PET reconstruction. *IEEE Trans. Med. Imag.*, 19(4):271–85, April 2000.
- [210] K. Lange and J. A. Fessler. Globally convergent algorithms for maximum a posteriori transmission tomography. *IEEE Trans. Im. Proc.*, 4(10):1430–8, October 1995.
- [211] J. A. Fessler, N. H. Clinthorne, and W. L. Rogers. On complete data spaces for PET reconstruction algorithms. *IEEE Trans. Nuc. Sci.*, 40(4):1055–61, August 1993.
- [212] J. A. Fessler and H. Erdođan. A paraboloidal surrogates algorithm for convergent penalized-likelihood emission image reconstruction. In *Proc. IEEE Nuc. Sci. Symp. Med. Im. Conf.*, volume 2, pages 1132–5, 1998.
- [213] T. Hebert and R. Leahy. A Bayesian reconstruction algorithm for emission tomography using a Markov random field prior. In *Proc. SPIE 1092, Med. Im. III: Im. Proc.*, pages 458–66, 1989.
- [214] T. Hebert and R. Leahy. A generalized EM algorithm for 3-D Bayesian reconstruction from Poisson data using Gibbs priors. *IEEE Trans. Med. Imag.*, 8(2):194–202, June 1989.
- [215] T. J. Hebert and R. Leahy. Statistic-based MAP image reconstruction from Poisson data using Gibbs priors. *IEEE Trans. Sig. Proc.*, 40(9):2290–303, September 1992.
- [216] E. Tanaka. Utilization of non-negativity constraints in reconstruction of emission tomograms. In S L Bacharach, editor, *Information Processing in Medical Im.*, pages 379–93. Martinus-Nijhoff, Boston, 1985.
- [217] R. M. Lewitt and G. Muehlelehner. Accelerated iterative reconstruction for positron emission tomography based on the EM algorithm for maximum likelihood estimation. *IEEE Trans. Med. Imag.*, 5(1):16–22, March 1986.
- [218] T. Hebert, R. Leahy, and M. Singh. Three-dimensional maximum-likelihood reconstruction for an electronically collimated single-photon-emission imaging system. *J. Opt. Soc. Am. A*, 7(7):1305–13, July 1990.
- [219] S. Holte, P. Schmidlin, A. Lindén, G. Rosenqvist, and L. Eriksson. Iterative image reconstruction for emission tomography: A study of convergence and quantitation problems. *IEEE Trans. Nuc. Sci.*, 37(2):629–635, April 1990.
- [220] D. P. Bertsekas. A new class of incremental gradient methods for least squares problems. *SIAM J. Optim.*, 7(4):913–26, November 1997.
- [221] R. Neal and G. E. Hinton. A view of the EM algorithm that justifies incremental, sparse and other variants. In M. I. Jordan, editor, *Learning in Graphical Models*, pages 255–68. Kluwer, Dordrecht, 1998.
- [222] A. Nedic and D. Bertsekas. Convergence rate of incremental subgradient algorithms. In S. Uryasev and P. M. Pardalos, editors, *Stochastic Optimization: Algorithms and Applications*, pages 263–304. Kluwer, New York, 2000.
- [223] A. Nedic, D. Bertsekas, and V. Borkar. Distributed asynchronous incremental subgradient methods. In D. Butnariu Y. Censor S. Reich, editor, *Inherently Parallel Algorithms in Feasibility and Optimization and Their Applications*. Elsevier, Amsterdam, 2000.
- [224] A. Nedic and D. P. Bertsekas. Incremental subgradient methods for nondifferentiable optimization. *SIAM J. Optim.*, 12(1):109–38, 2001.
- [225] V. M. Kibardin. Decomposition into functions in the minimization problem. *Avtomatika i Telemekhanika*, 9:66–79, September 1979. Translation: p. 1311-23 in Plenum Publishing Co. "Adaptive Systems".
- [226] H. Kudo, H. Nakazawa, and T. Saito. Convergent block-iterative method for general convex cost functions. In *Proc. Intl. Mtg. on Fully 3D Image Recon. in Rad. and Nuc. Med*, pages 247–250, 1999.
- [227] A. R. De Pierro and M. E. B. Yamagishi. Fast EM-like methods for maximum 'a posteriori' estimates in emission tomography. *IEEE Trans. Med. Imag.*, 20(4):280–8, April 2001.
- [228] S. Ahn and J. A. Fessler. Globally convergent image reconstruction for emission tomography using relaxed ordered subsets algorithms. *IEEE Trans. Med. Imag.*, 22(5):613–26, May 2003.
- [229] S. Ahn and J. A. Fessler. Globally convergent ordered subsets algorithms: Application to tomography. In *Proc. IEEE Nuc. Sci. Symp. Med. Im. Conf.*, volume 2, pages 1064–8, 2001.

- [230] P. Khurd, I-T. Hsiao, A. Rangarajan, and G. Gindi. A globally convergent regularized ordered-subset EM algorithm for list-mode reconstruction. *IEEE Trans. Nuc. Sci.*, 51(3):719–25, June 2004.
- [231] S. Ahn, J. A. Fessler, D. Blatt, and A. O. Hero. Convergent incremental optimization transfer algorithms: Application to tomography. *IEEE Trans. Med. Imag.*, 25(3):283–96, March 2006.
- [232] S. Ahn, J. A. Fessler, D. Blatt, and A. O. Hero. Incremental surrogates algorithms: Application to transmission tomography. In *Proc. IEEE Nuc. Sci. Symp. Med. Im. Conf.*, volume 5, pages 2835–9, 2004.
- [233] H. Erdoğ̃an and J. A. Fessler. Ordered subsets algorithms for transmission tomography. *Phys. Med. Biol.*, 44(11):2835–51, November 1999.
- [234] J. W. Stayman and J. A. Fessler. Spatially-variant roughness penalty design for uniform resolution in penalized-likelihood image reconstruction. In *Proc. IEEE Intl. Conf. on Image Processing*, volume 2, pages 685–9, 1998.
- [235] J. Nuyts and J. A. Fessler. A penalized-likelihood image reconstruction method for emission tomography, compared to post-smoothed maximum-likelihood with matched spatial resolution. *IEEE Trans. Med. Imag.*, 22(9):1042–52, September 2003.
- [236] J. Qi and R. M. Leahy. Resolution and noise properties of MAP reconstruction for fully 3D PET. In *Proc. Intl. Mtg. on Fully 3D Image Recon. in Rad. and Nuc. Med.*, pages 35–9, 1999.
- [237] T. H. Farquhar, J. Llacer, C. K. Hoh, J. Czernin, S. S. Gambhir, M. A. Seltzer, D. H. Silverman, J. Qi, C. Hsu, and E. J. Hoffman. ROC and localization ROC analyses of lesion detection in whole-body FDG PET: effects of acquisition mode, attenuation correction and reconstruction algorithm. *J. Nuc. Med.*, 40(12):2043–52, December 1999.
- [238] P. Bonetto, J. Qi, and R. M. Leahy. Covariance approximation for fast and accurate computation of channelized Hotelling observer statistics. *IEEE Trans. Nuc. Sci.*, 47(4):1567–72, August 2000.
- [239] J. Qi. Theoretical evaluation of the detectability of random lesions in Bayesian emission reconstruction. In *Information Processing in Medical Im.*, pages 354–65, 2003.
- [240] P. K. Khurd and G. R. Gindi. LROC model observers for emission tomographic reconstruction. In *Proc. SPIE 5372, Medical Imaging 2004: Image Perception, Observer Performance, and Technology Assessment*, pages 509–20, 2004.
- [241] J. Qi and R. H. Huesman. Fast approach to evaluate MAP reconstruction for lesion detection and localization. In *Proc. SPIE 5372, Medical Imaging 2004: Image Perception, Observer Performance, and Technology Assessment*, pages 273–82, 2004.
- [242] J. Qi. Analysis of lesion detectability in Bayesian emission reconstruction with nonstationary object variability. *IEEE Trans. Med. Imag.*, 23(3):321–9, March 2004.

The literature on image reconstruction is enormous and growing. Many valuable publications are not included in this list, which is not intended to be comprehensive.

Slides and lecture notes available from:

<http://www.eecs.umich.edu/~fessler>